Doctoral Dissertation

Microstructure Control of Cu Alloy Sheets by Cryogenic High-Speed Rolling

（極低温高速圧延による銅合金板の材質制御）

LEE SANGMIN

June 2020

Graduate School of Engineering

Osaka University

Contents

Chapter 1

General introduction

1.1 Background

1.1.1 Copper and copper alloys

Copper and copper alloys constitute one of the major groups of industrial metals. They are widely used because of their excellent electrical and thermal conductivities, outstanding resistance to corrosion, ease of fabrication, and comparable strength and fatigue resistance. They are generally non-magnetic. They can be readily soldered and brazed, and many coppers and copper alloys can be welded by various gas, arc, and resistance methods. For decorative parts, standard alloys having specific colors are readily available. Copper alloys can be polished and buffed to almost any desired texture and luster. They can be plated, coated with organic substances, or chemically colored to extend the variety of available finishes further [1.1].

Pure copper is used extensively for cables and wires, harness, electrical contacts, and a wide variety of other parts that are required to transit an electrical current. Coppers and certain brasses, bronzes, and cupronickels are used extensively for automobile radiators, heat exchangers, home heating systems, panels for absorbing solar energy, and various other applications requiring rapid conduction of heat across or along a metal section. Because of their outstanding ability to resist corrosion, coppers, brasses, some bronzes, and cupronickels are used for pipes, valves, and fittings in systems carrying potable water, process water, or other aqueous fluids.

In the point of the metallurgy, copper and copper alloys used to be studied to investigate the effects of stacking fault energy (SFE) on the deformation behavior of FCC metals because deformation twinning is known to the dominant deformation mode when SFE is less than 25mJ/m^2 [1.2]. SFE of Cu (=78mJ/m^2) decreases with the addition of alloy components, such as Si, Zn, and Al. The SFE of Cu and Cu alloys are shown in Table. 1.1 and Fig. 1.1. The change in SFE significantly affects the microstructure change by

plastic deformation, which is an important factor in determining the mechanical and electrical properties of copper and copper alloy.

Table 1.1 Stacking fault energy of Cu and Cu alloys. [1.2]

Cu alloy(wt%)	SFE (mJ/m^2)
Cu	78
Cu-6Zn	50
Cu-8Zn	38
Cu-10Zn	36
Cu-16Zn	23
Cu-20Zn	18
Cu-24Zn	16
Cu-30Zn	14
Cu-2Al	27
Cu-4.5Al	7
Cu-8Al	4
Cu-2.5Si	5
Cu-4Si	2.4

1.1.2 Deformation of FCC metals and alloys

When the FCC metals and alloys in plastically deformed, the competition of two deformation mechanisms decide to their microstructure evolution, which are crystallographic slip and twinning, the SFE mainly determines each deformation mechanism, and the microstructure changes also show a significant difference, as shown in Fig. 1.2 [1.3]. First, in the case of the slip-based microstructure (high SFE), the dislocation cell structure is developed at initial plastic deformation, as shown in Fig. 1.2(a). As the strain increases, dense dislocation walls form to compensate for the difference in orientation caused by different slip systems on the grain boundaries. Inside of this wall consists of the dislocation cells with the same slip system. As the strain further increases, the fraction of the cell block becomes smaller, and the misorientation between nearby cell blocks increases. This structure is called a micro band, and it develops

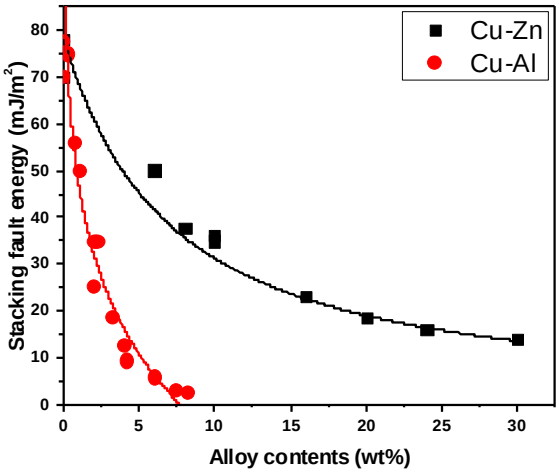

Fig. 1.1.Change in stacking fault energy of Cu-Zn and Cu-Al alloy as a function of amount of alloy components. [1.2]

as a lamellar structure with the increasing reduction in thickness. Finally, the shear band is formed crossing the rolling plane.

Meanwhile, the twinning-based microstructure, which the SFE of material is low, is shown in Fig. 1.2(b). In the early stage of deformation, deformation twinning occurs inside the grain boundaries, which is thin and lamellar shaped. As the strain increases, the fraction of the deformation twin increases, and the density also increases. As the deformation progresses further, a shear band is formed obliquely on the rolled plane of the twin-matrix lamellar structure. Consequently, the shear band erodes the lamellar structure, and its inside is composed of fine-sized sub-grains.

Fig. 1.3 shows the schematics of slip and twinning during the plastic deformation of FCC materials on the atomic scale [1.4]. A lattice of FCC consists of a "..ABCABC.." stacking sequence of close-packed planes, as shown in Fig. 1.3(a). When this structure is loaded by shear stress, between which there is an angle θ and the $[\bar{1}2\bar{1}]$ direction, a shift of all atoms in B plane and C over the atoms in plane A along $[\bar{2}11]$ direction leads to a local "..ABCA/CABC.." stacking sequence, including a stacking fault, as shown in Fig. 1.3(c). And then, there are two choices for the leading partial: one is the slip that if the SFE is high enough, as shown in Fig. 1(b1). In this case, small shear stress should make the atoms in planes B and C shift over the atoms in plane A along $[\bar{1}2\bar{1}]$ direction turning back to the original stacking sequence. The other case is the twinning, when the SFE is low, the shear stress may make the atoms in plane C move

to the atoms in plane B along $[\bar{2}11]$ direction resulting in a local "..ABCA/CBCA.." stacking sequence associating with the formation of a two-layer twin, as shown in Fig. 1(b2).

In contrast to slip, although twinning is not typical for many FCC metals and alloys, experimentally, a lot of FCC alloys such as Cu-Al alloys [1.5, 1.6], Cu-Zn alloys [1.7, 1.8], and TWIP ("twinning induced plasticity") steels [1.9] show deformation twinning even at room temperature.

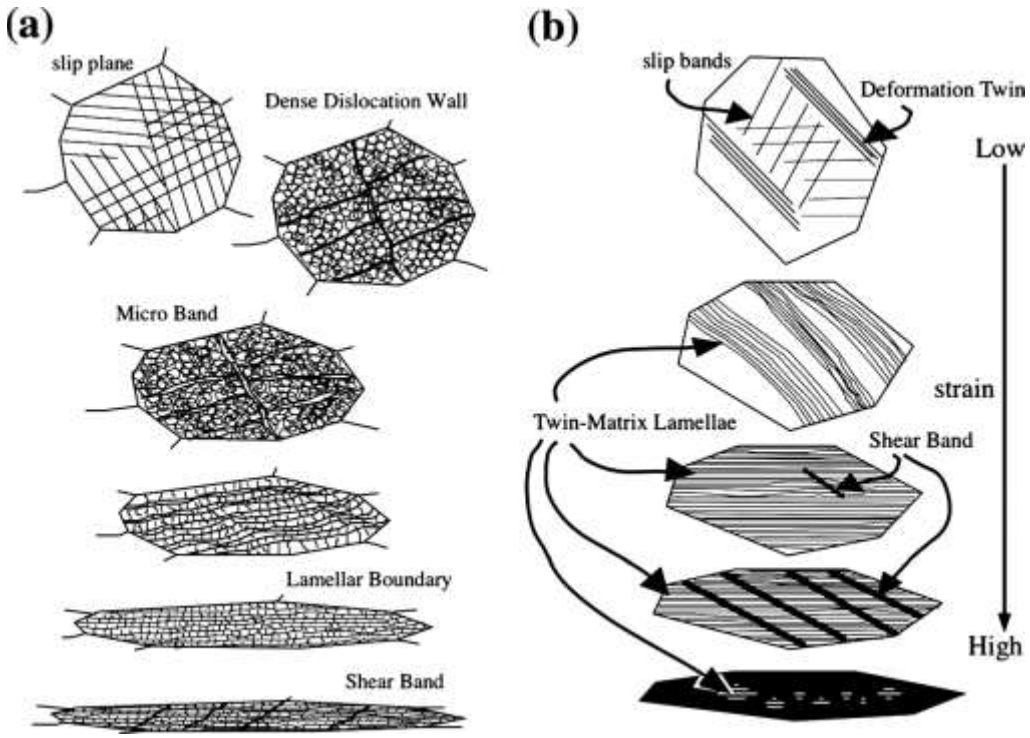

Fig. 1.2. Schematic illustrations of microstructural evolution in cold-rolled FCC metals and alloys observed from transverse direction (a) Slip-based microstructure, (b) twinning-based microstructure [Higashida and Morikawa, 1.3]

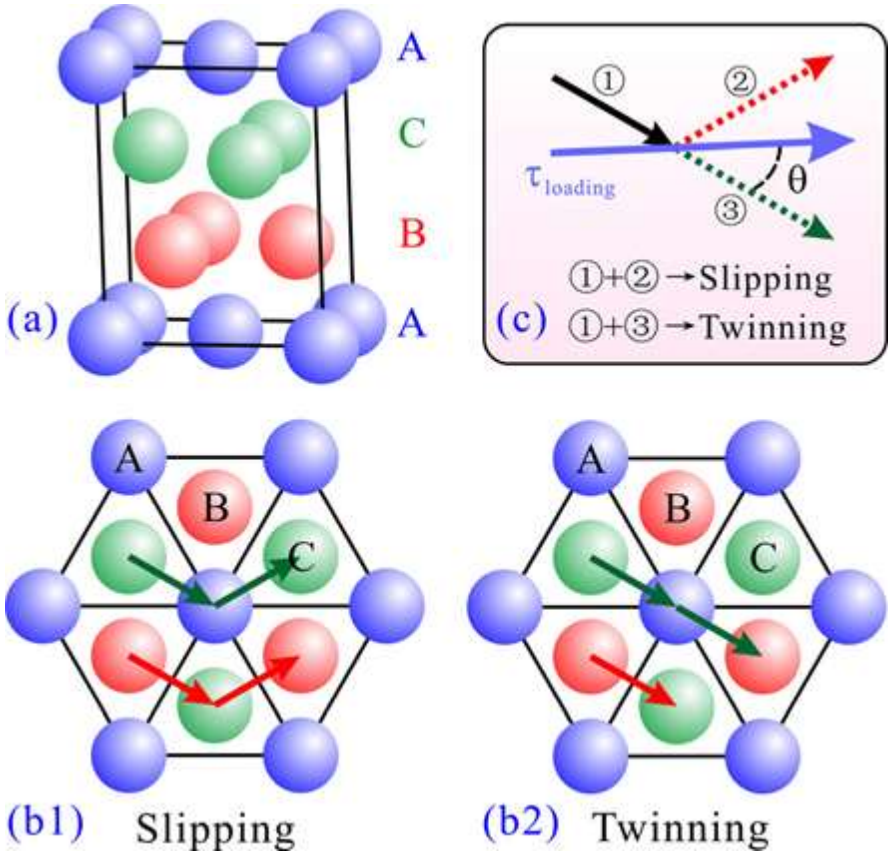

Fig. 1.3. (a) A representative of the three-dimensional geometry for FCC metals, (b1) slipping, (b2) twinning, and (c) direction of slip and twinning [Cai et al., 1.4]

1.1.3 Deformation twinning in FCC metals and alloys

Cottrell and Bilby [1.10] and Thompson and Millard [1.11] devised the concept of the pole mechanism to explain particular models for twinning in BCC and HCP, respectively. The theory of the formers showed when applied to an analogous dissociation in FCC would produce only a monolayer of stacking fault. Later, it was found that deformation twinning is readily activated in FCC materials of sufficiently low stacking fault energy.

Venables[1.12] suggested a modified mechanism to allow continuous growth from a single stacking fault. Stacking fault models seem physically more realistic for FCC structures since wide faults are formed in many alloys. The prismatic glide mechanism for FCC twinning was shown in Fig. 1.4. The mechanism could be explained in six steps, which is as follows [1.13].

1. Fig. 1.4(a) shows the dislocation with a Burgers vector AC lying in plane *b* except for a long jog N_1N_2 lying in the plane *a*. The part of the dislocation in *a* now dissociate into a Shockley and a Frank partial,

$$\mathrm{AC} = \mathrm{A}\alpha + \alpha\mathrm{C} \tag{1.1}$$

2. Under the action of stress, the glide Shockley partial αC moves away from the sessile Frank partial Aα on the plane *a*, leaving an intrinsic fault, as shown in Fig. 1.4(b).
3. And then, after it attains the unstable semicircular configuration, it winds rapidly around N_1 and N_2 to reach the position, like the following in Fig. 1.4(c). In this configuration, two segments of the αC dislocation delineating the fault meet along with *RS* at a separation of only one inter-planar distance.
4. These two parts of αC are opposites since their line directions, originally parallel, are now antiparallel, and considerable stress would be required to force them past each other. It is important to note that the right-hand element of the Shockley partial has moved downwards in wrapping itself around the pole dislocation so that it is the lower dislocation of the dipole along with *RS*. This element has a Burgers vector of -αC when the positive line direction looks outwards from N_2, whilst the upper element of the dipole, looking outward from N_1, has a Burgers vector of +αC, as shown in Fig. 1.4(d)
5. The end element of the partial αC recombines with the sessile partial Aα along the length RN_2, and the reformed dislocation with Burgers vector AC then glides to the next plane α and repeats the dissociation. When the second layer of fault expands, two different segments of its twinning partial will again meet on successive planes along with *RS*, but each will be displaced by one plane from the initial pair. One of these segments, which were on the central plane, will annihilate the partial twinning left there by the expansion of the first faulted layer, thus joining the two layers into a continuous fault, and the final configuration (Fig. 1.4(e)) is now a double-helical layer of fault terminated by twinning partials SRN_1 and SRN_2 at a separation of two atomic layers. The recombination and glide are represented in the figure as the operation of a dislocation source T_2, and an equivalent source operates at the node N_1.
6. When the two partials attain a critical separation, they may pass one another under the action of the

static stress field, and the twin can thicken further by the pole mechanism alone, as shown in Fig. 1.4(f). The final configuration is identical with that obtained when a partial dislocation in a stress field favoring twin formation glides on a K_1 plane one interplanar distance below the super jog until it encounters the pole dislocation, about which is wraps itself

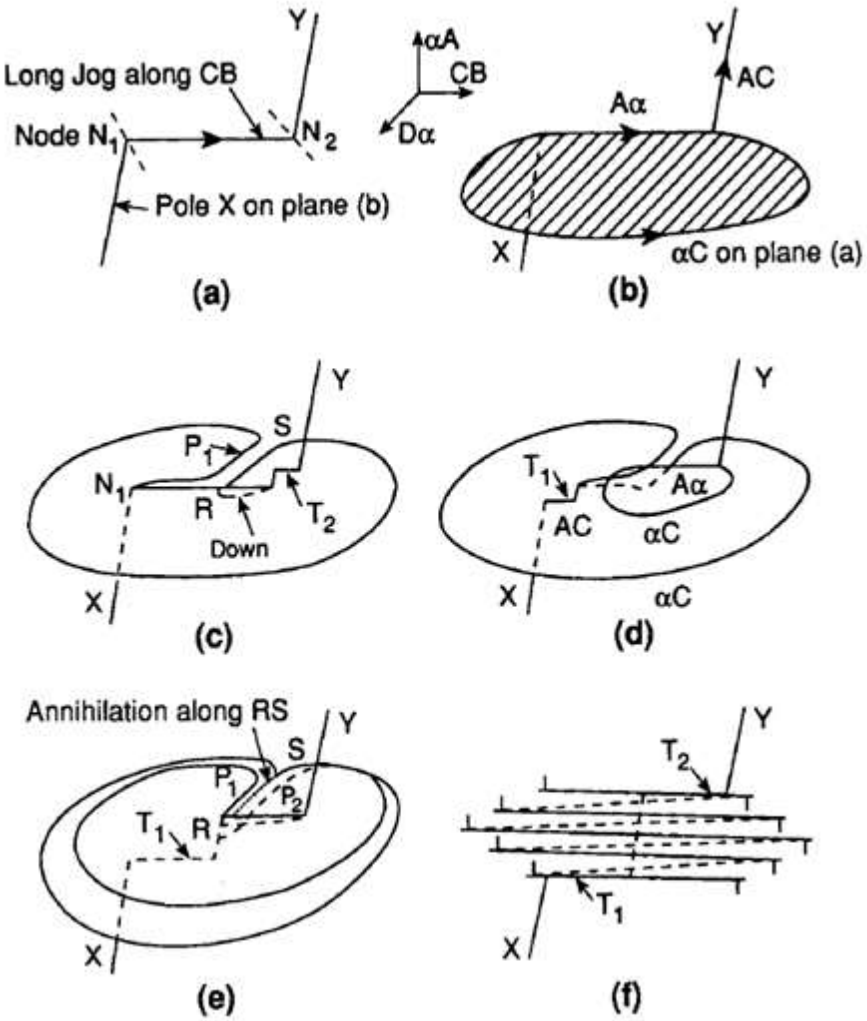

Fig. 1.4 Prismatic glide mechanism for FCC twinning [Venables, 1.12]

Since the proposal of Venables, Slleeswyk[1.14], Hirth[1.15], Fujita and Mori [1.16], Mahajan and Chin[1.17], Narita and Takamura[1.18], Suzuki and Barrett[1.19], et al. published the deformation twinning theories with modifying and fitting at the complexed situation.

Table. 1.2 Zerilli-Armstrong parameters for Cu [Vohringer and Metallk, 1.26]

Parameters	Cu
σ_G(MPa)	46.5
C_1	890
C_2(MPa)	0.28×10^{-3}
$C_3(k^{-1})$	1.15×10^{-4}
k_s (MPa $mm^{1/2}$)	5

Meanwhile, Meyers et al. [1.20] suggested a constitutive description of the slip – twinning transition. The onset of twinning occurs when the slip (τ_s) becomes equal to the twinning stress, (τ_T), that is

$$\tau_S = \tau_T \tag{1.2}$$

It will be assumed that there is a CRSS for twinning that is independent of the stress state. In the case of polycrystalline with randomly distributed orientation, upper eq.(1.2) can be written,

$$\frac{\sigma_S}{M_S} = \frac{\sigma_T}{M_T} \tag{1.3}$$

Then, if the orientation factors of slip (M_S) and twinning (M_T) are assumed to be equal to each other, the upper equation can be simplified as follows

$$\sigma_s = \sigma_T \tag{1.4}$$

In the cases of FCC metals, it is difficult to apply the constitutive equation for twinning. Attempts were made at obtaining the activation energy and dislocation velocity exponent *m* from Jassby and Vreeland [1.21], Greenman et al. [1.22], Kleintges, and Haasen [1.23], and Suzuki and Ishi [1.24]. However, these investigations calculated that twinning occurs at low values of *m* and unacceptably high temperature and strain rate sensitivity, which was not matched with the actual cases. Therefore it was decided to use the twinning stress determined experimentally only.

Thornton and Mitchell [1.25] report a shear twinning stress for single crystal copper of 150MPa, and this value is adopted. The Hall-Petch slope for twinning is assumed to 21.6MPa $mm^{1/2}$ and was obtained by Vohringer [1.26]. The slip response was modeled by the Zerilli-Armstrong equation for FCC metals, with parameters given in Table 1.1. The resulting equation is

$$\sigma = \sigma_G + C_2 \exp\left[-\left(C_3 - C_4 \ln\frac{\dot{\epsilon}}{\dot{\epsilon_0}}\right)T\right] + k_s d^{-1/2} \tag{1.5}$$

where σ_G is the athermal component of stress, C_2, C_3, C_4 is the Zerilli and Armstrong constants [1.54, 1.55], $\dot{\epsilon}$ is the strain rate, $\dot{\epsilon_0}$ is a reference strain rate which was 10^{20} s^{-1} [1.26], T is the temperature, k_s is the Hall-Petch slope for slip, and d is the grain size. The slip-twinning transition of Cu as a function of grain size is shown in Fig. 1.5(a), using the assumption that twinning stress is 150MPa and eq. (1.5). The effect of grain size influences the occurrence of twinning in a significant way. The effect of plastic strain is more clearly seen in the slip-twinning transition plot of Fig. 1.5(b). These calculations were made for a constant grain size of 10 μm. A plastic strain of 0.3 is necessary to initiate twinning. Therefore, the strain rate of 5×10^3 s^{-1} and the strain of 0.8 is required to produce the twinning at room temperature.

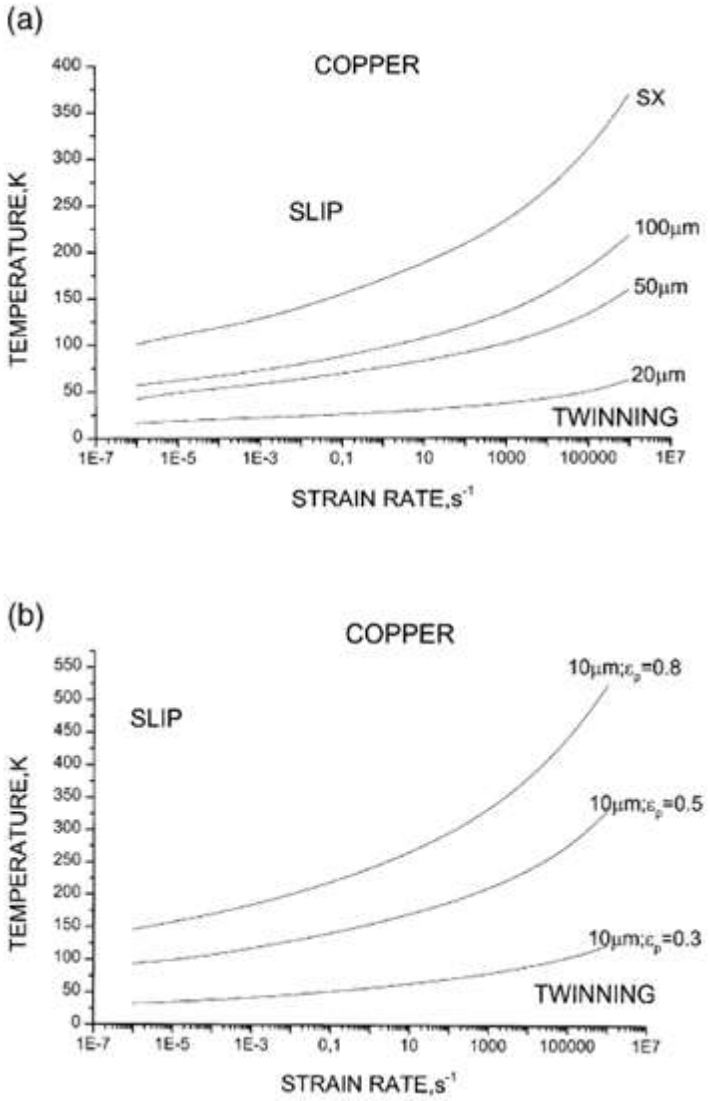

Fig. 1.5 (a) Calculated slip-twinning transition line for copper of different grain sizes. (b) Calculated slip-twinning transition line for copper (d = 10 μm), at strain of 0.3, 0.5, and 0.8. [Meyer et al., 1.20]

1.1.4 Contribution of deformation twins for mechanical and electrical properties

Strengthening by twins was known that the interaction of glide dislocations with TBs plays an important role. Christian and Mahajan [1.13] systemically reviewed that the presence of twins blocks the propagation of slip bands, implying that existing coherent twin boundaries behave more or less like grain

boundaries in acting as obstacles to strain propagation. For example, consider a case where a $(\bar{1}11)$ slip band interacts with a (111) twin, one may argue that $1/2[01\bar{1}]$ dislocations would propagate across the twin, whereas the motion of 1/2[110] and 1/2[101] dislocations would be blocked at the twin boundaries. However, these dislocations could also propagate across the twins if they were to undergo dislocation dissociation reactions, such as the following relationship,

$$\frac{1}{2}[101] \rightarrow \frac{1}{6}[1\bar{2}1] + \frac{1}{3}[111] \qquad (\#)$$

With this reaction, a non-slissile Frank dislocation will be left at the twin boundary. Other dislocation reactions are also possible in FCC metals.

In the twinning areas, many stacking faults embedded inside the twin/matrix (T/M) lamellar, as shown in Fig. 1.6(a) [1.27]. Since the stacking faults formed by the dissociation of full dislocation into partials are the embryos of deformation twins, external driving stress can readily catalyze the transformation from stacking faults to deformation twins in the case of low SFE. Since most of the dislocations exist in the T/M lamellas can act as effective obstacles to impede the motion of dislocations, as shown in Fig. 1.6(b) [1.27].

In addition, the electrical resistivity of twin boundaries is about one order of magnitude lower than that of the grain boundaries [1.27, 1.28]. Therefore, if the material contains a high density of twin boundaries,

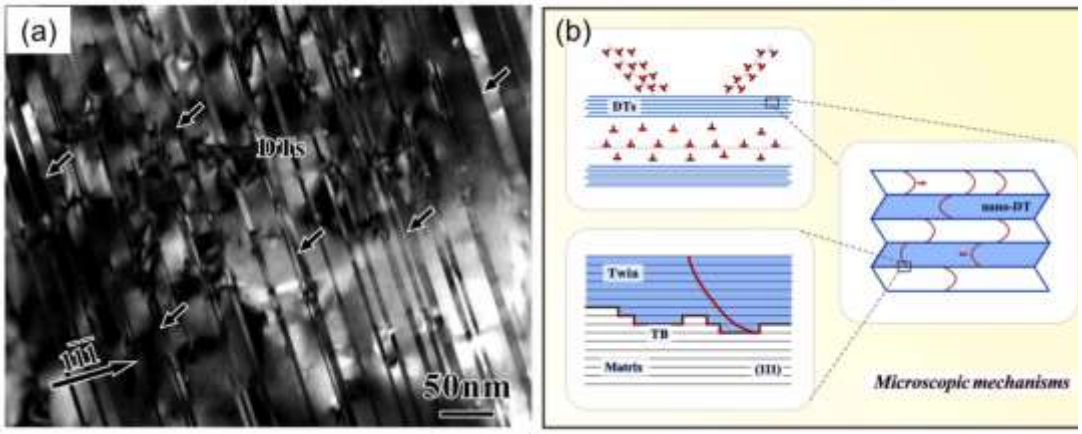

Fig. 1.6 (a) TEM microstructure of Cu-8 at.% Al at the strain of 0.49, bright field images along 110 zone axis (b) Illustrations of the cooperation between deformation twinning and dislocation slip at three different length scales [Liu et al., 1.27]

the material is supposed to be effectively strengthened without losing conductivity much. The facts are practically crucial for electrical conducting materials.

1.1.5 Effect of stacking fault energy on deformation twinning in Cu alloys

In face-centered cubic (FCC) materials with high stacking fault energy (SFE), dislocations move actively with cross slip, so that excellent ductility is observed and that low energy dislocation structures are formed by mutual trapping, rearrangement, and annihilation with low piling up at grain boundaries [1.29, 1.30]. On the other hand, FCC materials with low SFE show a rapid increase in dislocation density with plastic deformation, which leads to higher strength with less ductility [1.29, 1.30]. This is because dislocations in low SFE materials are decomposed into partials. The very wide stacking fault ribbons between the partials make them difficult for cross-slip. Therefore, deformation twinning and shear banding are more frequently observed in the later stage of the deformation, leading to the grain refinement.

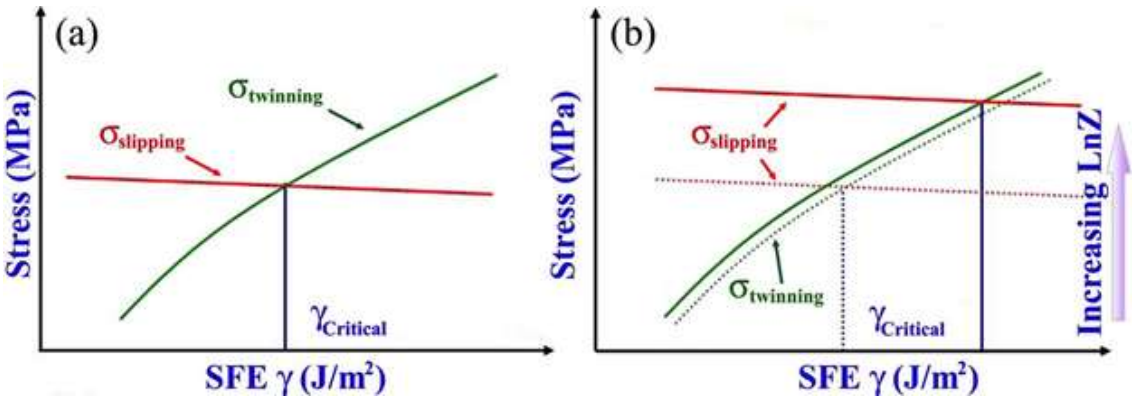

Fig. 1.7 (a) Effects of SFE on the slipping stress and twinning stress, (b) mutual effects of SFE and Ln Z on the slipping stress and twinning stress. [An et al., 1.43]

On the other hand, when materials are subjected to plastic deformation, dislocation slip and deformation twinning will be activated to accommodate the imposed plastic strain [1.20]. Extensive investigations have explicitly revealed that the preferred choice of two essential plasticity carriers is determined by the fundamental materials parameters, including microstructure such as SFE [1.13, 1.20], grain size [1.31 – 1.33] and crystallographic orientation [1.34, 1.35]. On the other hand, processing

parameters also influence it, such as stress [1.36], strain [1.37], strain rate [1.38 – 1.40], and temperature [1.40, 1.42].

1.1.6 Temperature and strain rate effect on deformation twinning in Cu alloys

Traditional crystal plasticity was reported that deformation twinning thermally activated, which implies that processing parameters, such as the strain rate and the temperature, importantly affect the microscopic process of deformation. An et al. [1.43] systemically reviewed about temperature and strain effect of deformation twinning in Cu alloys. According to dislocation theory, twinning stress remarkably decreases with a reduction of SFE, while slip stress is relatively insensitive to SFE [1.44, 1.45]. When the SFE is below a critical value, the deformation mechanism is primarily governed by twinning activities at room temperature and a low strain rate as schematically illustrated in Fig. 1.7.[1.43] In contrast, twinning stress is slightly vulnerable to strain rate and deformation temperature, whereas slip stress is highly susceptive [1.44, 1.45].

Generally, the mutual influences of strain rate and temperature on deformation behavior can be expressed through a single parameter Z (Zener–Hollomon parameter) [1.46] as

$$\mathrm{Z} = \dot{\varepsilon} \exp \frac{Q}{RT} \qquad (\#)$$

where $\dot{\varepsilon}$ is the strain rate, Q is the activation energy for diffusion, R is the gas constant, and T is the deformation temperature. The enhancement of ln Z by increasing and/or lowering T elevates the slipping stress by restricting the thermally activated mechanisms [1.45, 1.47]. Therefore, the critical value of SFE will increase and enable deformation twinning to be activated in materials with relatively higher SFE compared to that obtained under normal deformation conditions with a low strain rate at room temperature, as shown in Fig. 1.7(b).

1.1.7 Metal forming of Cu and Cu alloys in cryogenic temperature

In the cases of the rolling process, many studies have been conducted from the past. In particular, examples of the researches on cryogenic rolling of copper alloys are as follows. Bahmanpour et al. [1.48] reported that dynamic recovery and recrystallization are suppressed, grain refinement and deformation twinning are apparently promoted in cryo-rolling of pure copper and Cu-Al-Zn alloy. Even the dislocations rearranged themselves into dislocation cells, improvement in the ductility was observed. Roy et al. [1.49] reported that the dislocation density of alpha brass accumulated rolling pass by pass at cryogenic temperature. Wang et al. [1.50] proposed a cryogenic rolling using a specially designed liquid nitrogen cooling system that deformation twinning and shear banding were the primary deformation mechanisms of Cu-35%Zn alloy, which realized improvement in the balance between strength and ductility. However, these rolling methods did not include an increase in the strain rate.

On the other hand, the cryogenic severe plastic deformation (SPD) process has also been actively studied as a metalworking process. Cryogenic equal channel angular extrusion (ECAE) process was found to exhibit improved mechanical properties due to the formation of ultrafine grain and high dislocation density [1.51]. In addition, Tao and Lu and their collaborators [1.52] have developed an SPD process called the LNT-DPD, which represents liquid nitrogen temperature – dynamic plastic deformation, a metal forming process similar to forging. It has also been reported to improve mechanical properties through surface treatment through a cryogenic surface mechanical attrition treatment (SMAT) process [1.53]. However, such a cryogenic SPD process is strictly limited by the size of the specimen. In addition, these have critical limits of the practical application to an actual metal forming industry due to processing step, time, and cost problems.

As seen in Section 1.1.5, a high strain rate and low temperature are required to change Z. In this case, the decrease in temperature has the more significant effect than the increase in strain rate. From previous studies so far, there have been many attempts to try plastic deformation at cryogenic temperatures. However, in order to obtain the far larger Z, an increase in the strain rate will also be required.

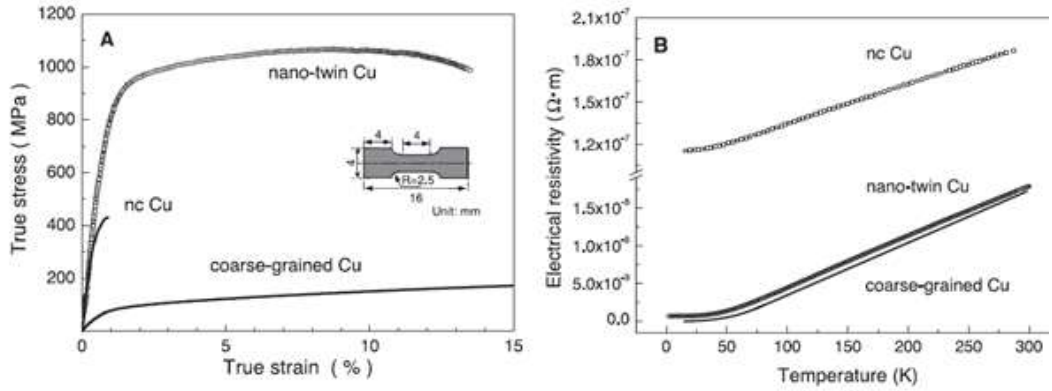

Fig. 1.8 (A) A typical tensile stress-strain curve for the as-deposited Cu sample with nano-twins in comparison with that for a coarse-grained polycrystalline Cu sample and a nano-crystalline (nc) Cu sample, (B) The measured temperature dependence of electrical resistivity for the as-electrodeposited nano-twin Cu sample and the coarse-grained sample as a function of temperature [Lu et al., 1.28]

1.2 Motivations and purpose of this thesis

With the development of technologies and industries, there is required for advanced metallic materials with higher mechanical properties. Especially in the case of Cu alloys for conducting materials in many applications, high electrical conductivity and high mechanical strength are often required simultaneously. It is well known that the mechanical properties of materials are highly dependent on their microstructure. However, pure Cu with high conductivities is very soft. Strengthening the metals to various approaches, including solid solution alloying, cold working, and grain refinement leads to a pronounced decrease in conductivity. For example, alloying pure Cu may increase the strength by two or three times, but the electrical conductivity of Cu alloys is only 10 to 40% that of pure Cu. Moreover, one of the disadvantages of copper alloys is their heavyweight. Therefore strengthening is more important because it can reduce cross-section and total weight of structural parts.

Facilitating deformation twinning by microstructure control could be the key to addressing this dilemma. As shown in Section 1.1.4, it is known that the twin boundaries improves the strength of the material and does not significantly affect the conductivity [1.27, 1.28]. L. Lu et al. [1.28] reported that an example of maximizing the potential of the twin boundaries. Pure copper was synthesized with a high density of nanoscale growth twins by a pulsed electrodeposition technique; then, the sample showed ultrahigh strength and high electrical conductivity could be realized, as shown in Fig. 1.8.

Therefore, the purpose of this thesis is as follows. The first one is to confirm whether the deformation twin can improve the properties in the actual rolling process. The next one is to propose a novel rolling process, which can be industrially utilized and can expect microstructure control. The last one is to apply to copper alloys with various SFEs and to analyze microstructure changes and mechanical properties quantitatively.

1.3 Outline of the thesis

This thesis is organized as follows,

Chapter 1. The motivations and purposes of this research work are described. Also, this outline of the thesis is given.

Chapter 2. Cu-15at% Al sheets were heavily processed by conventional multi-pass cold rolling up to 90% in reduction in thickness without annealing. In order to reveal the change in mechanical properties and the microstructure evolution, tensile test, hardness test, optical microscopy, and electron backscattering diffraction (EBSD) analysis were performed.

Chapter 3. A novel rolling process, named 'Cryogenic high-speed rolling (C-HSR)', was designed. In order to investigate the availability of microstructure control during rolling as expected, processing parameters were optimized.

Chapter 4. Cryogenic high-speed rolling (C-HSR) was applied to Cu-5mass% Zn sheets, which were relatively high stacking fault energy (SFE) Cu alloy. Mechanical properties and electrical conductivity were investigated. In order to discuss the reason why the C-HSR improved the properties comparing to low-speed cold rolling (LSR), EBSD analysis was carried out to investigate the microstructure evolution and texture.

Chapter 5. Cryogenic high-speed rolling (C-HSR) was carried out with Cu - *x* Al (*x*=3.1 and 6.8 mass%) alloy, which were intermediate and low stacking fault energy (SFE) Cu alloys, respectively. After the rolling, mechanical and electrical properties are investigated. Yield strength and electrical conductivity were predicted using the modified Hall-Petch equation and modified Mayada and Shatzkes (MS) model.

Chapter 6. Applications of cryogenic high-speed rolling are described

Chapter 7. The results of the present study are summarized

References

[1.1] ASM Metals Handbook (10th edition), Vol. 2, (1992) ASM International, Metals Park, Ohio.

[1.2] F. J. Humphreys and M. Hatherly, Recrystallization and Related Annealing Phenomena 2nd edition, (2004), Elsevier

[1.3] K. Higashida and T Morikawa, Tetsu-to-Hagane, 94 (2008) 576 [In Japanese]

[1.4] T. Cai, Z. J. Zhang, P. Zhang, J. B. Yang, and Z. F. Zhang, J. Appl. Phys. 116 (2014) 163512

[1.5] X. H. An, W. Z. Han, C. X. Huang, P. Zhang, G. Yang, S. D. Wu, and Z.F. Zhang, Appl. Phys. Lett. 92, (2008) 201915

[1.6] S. Qu, X. H. An, H. J. Yang, C. X. Huang, G. Yang, Q. S. Zang, Z. G. Wang, S. D. Wu, and Z. F. Zhang, Acta Mater. 57 (2009) 1586

[1.7] Z. J. Zhang, Q. Q. Duan, X. H. An, S. D. Wu, G. Yang, and Z. F. Zhang, Mater. Sci. Eng., A 528 (2011) 4259

[1.8] P. Zhang, X. H. An, Z. J. Zhang, S. D. Wu, S. X. Li, Z. F. Zhang, R. B. Figueiredo, N. Gao, and T. G. Langdon, Scr. Mater. 67 (2012) 871

[1.9] O. Grassel, L. Kruger, G. Frommeyer, and L. W. Meyer, Int. J. Plast. 16, (2000) 1391

[1.10] A. H. Cottrell and B. A. Bilby, Phil. Mag. 42 (1951) 573

[1.11] N. Thompson and D. J. Millard, Phil. Mag. 43, (1952) 422

[1.12] J. A. Venables, Phil. Mag. 6, (1961) 379

[1.13] J. W. Christian, and S. Mahajan, Prog. Mater. Sci. 39 (1995) 1

[1.14] A. W. Sleeswyk, Phil. Mag. 29, (1974) 407

[1.15] J. P. Hirth, Deformation Twinning (edited by R. E. Reed-Hill, J. P. Hirth and H. C. Rogers) Gordon and Breach, New York (1963) pp. 112

[1.16] T. Mori and H. Fujita, Acta Met. 28, (1980) 771

[1.17] S. Mahajan and G. Y. Chin, Acta Met. 21, (1973) 1353

[1.18] N. Narita and J. Takamura, Scripta Met. 9, (1974) 819

[1.19] H. Suzuki and C. S. Barrett, Acta Met. 6, (1958) 156

[1.20] M. A. Meyers, O. Vohringer, and V. A. Lubarda, Acta Mater. 49 (2001) 4025

[1.21] K. M. Jassby, and T. Vreeland Jr., Phil. Mag., 21, (1970) 1147

[1.22] W. F. Greeman, T. Vreeland Jr. and D. S. Wood, J. Appl. Phys., 89 (1967) 3595

[1.23] M. Kleintges, and P. Haasen, Scripta Met., 14 (1980) 999

[1.24] T. Suzuki, and T. Ishii, Trans. Jap. Inst., 9 (1968) 687

[1.25] P. R. Thornton, and T. E. Mitchell, Phil. Mag., 7 (1962) 361

[1.26] O. Vohringer, Z. Metallk., 67 (1976) 51. [in German]

[1.27] R. Liu, Z. J. Zhang, L. L. Li, X. H. An, and Z. F. Zhang, Scientific Reports 5 (2015) 9550

[1.28] L. Lu, Y. Shen, X. Chen, L. Qian, K. Lu, Science, 304 (2004) 422

[1.29] S. Qu, X.H. An, H. J. Yang, C. X. Huang, G. Yang, Q. S. Zang, Z. G. Wang, S. D. Wu, Z. F. Zhang, Acta Mater., 57 (2009) 1586

[1.30] N. R. Tao, Z. B. Wang, W. P. Tong, M. L. Sui, J. Lu, K. Lu K, Acta Mater., 50 (2002) 4603

[1.31] M. A. Meyers, U. R. Andrade, A. H. Chokshi, Metallurgical and Materials Transactions A. 26 (1995) 2881

[1.32] V. Caballero, S. K. Varma, Journal of Materials Science, 34 (1999) 461

[1.33] E. El-Danaf, S. Kalidindi, R. Doherty R, Metallurgical and Materials Transactions A. 30 (1999) 1223

[1.34] T. S. Byun, Acta Materialia, 51 (2003) 3063

[1.35] C. S. Hong, N. R. Tao, K. Lu, X. Huang, Scripta Materialia, 61 (2009) 289

[1.36] Y. Cao, Y. B. Wang, X. Z. Liao, M. Kawasaki, S. P. Ringer, T. G. Langdon, et al., Applied Physics Letters, 101 (2012) 231903

[1.37] G. Laplanche, A. Kostka, O. M. Horst, G. Eggeler, E. P. George, Acta Materialia. 118 (2016) 152

[1.38] D. H. Warner, W. A. Curtin, S. Qu, Nat Mater., 6 (2007) 876

[1.39] L. E. Murr, M. A. Meyers, C. S. Niou, Y. J. Chen, S. Pappu, C. Kennedy, Acta Materialia, 45 (1997) 157

[1.40] Y. S. Li, Y. Zhang, N. R. Tao, K. Lu, Acta Materialia, 57 (2009) 761

[1.41] T. H. Blewitt, R. R. Coltman, J. K. Redman, Journal of Applied Physics, 28 (1957) 651

[1.42] B. Gludovatz, A. Hohenwarter, D. Catoor, E. H. Chang, E. P. George, R. O. Ritchie, Science, 345 (2014)1153

[1.43] X. H. An, S. D. Wu, Z.G. Wang, Z.F. Zhang, Prog. Mater. Sci., 101 (2019) 1

[1.44] A. H. Cottrell Dislocations and plastic flow in crystals. Oxford, UK, (1953) Oxford University Press

[1.45] J. P. Hirth, J. Lothe. Theory of dislocations (2nd). New York, USA (1982) John Wiley&Sons

[1.46] C. Zener, J. H. Hollomon, Journal of Applied Physics, 15 (1944) 22

[1.47] M. A. Meyers, K. K. Chawla, Mechanical Behavior of Materials (2nd Ed). Cambridge, (2009) UK, Cambridge University Press

[1.48] H. Bahmanpour, A. Kauffmann, M.S. Khoshkhoo, Mater. Sci. Eng. A, 529 (2011) 230

[1.49] B. Roy, N.K. Kumar, P.M.G. Nambissan, J. Das, AIP Adv., 4, (2014) 067101

[1.50] P. Wang, J. Jie, C. Liu, L. Guo, T. Li, Mater. Sci. Eng. A, 715 (2018) 236

[1.51] W. Wei, S. L. Wang, K. X. Wei, L. V. Alecandrov et al., J. Alloys and Compound 678 (2016) 506

[1.52] N. Tao, K. Lu, J. Mater. Sci. Technol., 23-6 (2007) 771

[1.53] B. Cai, X. Ma, J. Moering et al., Mater. Sci. Eng. A. 626 (2015) 144

[1.54] Zerilli, F. J. and Armstrong, R. W., J. Appl. Phys., 61 (1987) 1816.

[1.55] Zerilli, F. J. and Armstrong, R. W., J. Appl. Phys., 68 (1990) 915.

Chapter 2

Deformation Twinning and Change in Mechanical Properties of Cu-15at%Al in Multi-pass Cold Rolling

2.1 Introduction

In Cu-Al alloys, stacking fault energy (SFE) is low and further decreases with Al content. Deformation twins are formed by plastic deformation due to the extra low SFE. The strength and the elongation rises simultaneously by the deformation twinning [2.1]. Recently, it was reported that Cu-Al alloys processed by severe plastic deformation and annealing shows excellent tensile properties due to TWIP (Twinning Induced Plasticity) [2.2 ~ 2.4]. Tian et al. [2.5] aimed at optimization of balance between strength and elongation by heat treatment after 96% heavy rolling, resulted in yield strength of 520 MPa with uniform elongation of 15% after annealing at 673 K for 10 s. In this chapter, microstructural evolution and changes in mechanical properties with rolling without heat treatment were investigated. Cu-15at% Al sheets were processed by multi-pass cold rolling. It is very important for industrial application if mechanical properties are improved by only conventional cold rolling without annealing due to TWIP behavior.

2.2 Experimental procedure

The used materials were produced by casting and cold-rolled into 5mm-thick sheets. Chemical composition of the sheet is Cu-14.64at%Al as shown in Table 2.1. Heat treatment was carried out at 800^{o}C for 60 s and cooled in air (referred to as initial material). Microstructure after the heat treatment is

Table 2.1 Chemical composition of the alloy used

Al	Fe	Ni	Si	Cu	
6.79	0.03	0.001	0.006	bal.	mass%
14.64	0.03	0.001	0.012	bal.	at.%

shown in Fig. 2.1. Annealing twins were observed in equi-axed grains. The mean grain size was about 23μm.

Cold rolling was carried out on a 2-high mill with roll diameter of 310 mm at room temperature. The rolling speed was 5 m/min and roll surface was lubricated by #150 mechanic oil. The reduction in thickness was 10 to 20% per each pass. The maximum total reduction applied was 90%.

In order to observe the microstructure evolution and to measure change in mechanical properties of the materials, specimens were sampled at various reductions. Equivalent strain introduced by the rolling was estimated using the following equation,

$$\varepsilon_{eq} = -\frac{2}{\sqrt{3}} \ln \frac{h}{h_0} \tag{2.1}$$

where h_0 is the initial thickness (5mm) and h is the thickness of the specimen. The rolled specimens were mechanically polished until #2000 SiC paper and chemically etched by a solution with (HCl : C_2H_5OH : H_2O : $FeCl_3$ = 10ml : 50ml : 50ml : 5g), to observe microstructure. Optical microstructure was observed the normal direction (ND) – rolling direction (RD) plane perpendicular to transverse direction (TD) by a Keyence VHX-100 digital microscope.

EBSD analyses were carried out to obtain the orientation information of the deformation twins and matrix grains. Specimens were prepared by mechanical polishing until #4000 of SiC paper and 1μm and 0.3μm of Al_2O_3 powder, followed by electro-polishing in a solution (H_3PO_4 : C_2H_5OH : H_2O = 50ml : 50ml : 100ml), with a voltage of 5V at 0^oC. The operation voltage was 15 kV, the step size in the Kikuchi-pattern scanning was around 0.1~1.0μm. Single iteration clean-up of EBSD data was performed

to reduce the point of zero solutions. The distribution of grain size was measured on EBSD microstructure by using the TSL-OIM analysis software.

Vickers hardness test was conducted with indentation load of 1.96 N (0.2 kgf) and holding time of 15 s. Tensile test was performed on a Shimazu autograph AGI - 100 kN. The tensile specimens were cut by a wire cutting machine into a dog-bone shape with gauge length of 20mm and width of 5mm, which tensile axis was paralleled to the RD. The initial strain rate was 1.67×10^{-3} s^{-1}.

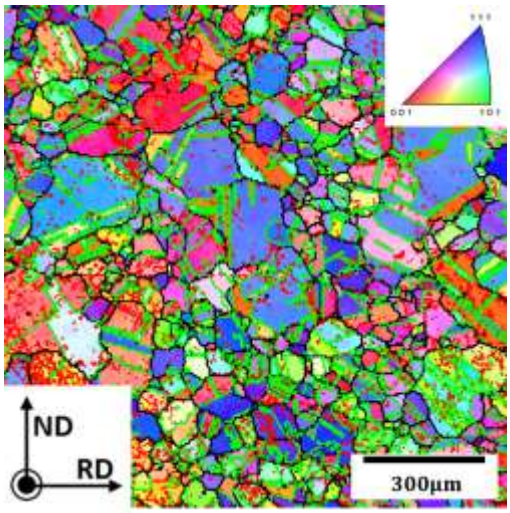

Fig. 2.1. Initial microstructure with low angle boundaries (red line), high angle boundaries (black line) and Σ3 boundaries (green line)

2.3 Results

2.3.1 S-S curve

Fig. 2.2 shows tensile true stress (σ) – strain (ε) curve and strain hardening rate (SHR, dσ / dε) of the initial material. Flow stress increases almost linearly up to strain of 0.6. SHR shows 4 stages (A-D) with increasing strain. In the case of true strain range from 0.05 to 0.4 (stage B), SHR shows upward trend which is explained primary twinning [2.7] or TWIP phenomenon [2.1]. In Stage C, the SHR curve shows a decreasing trend, which is explained by a decreasing of primary twinning or secondary twinning [2.7, 2.8]

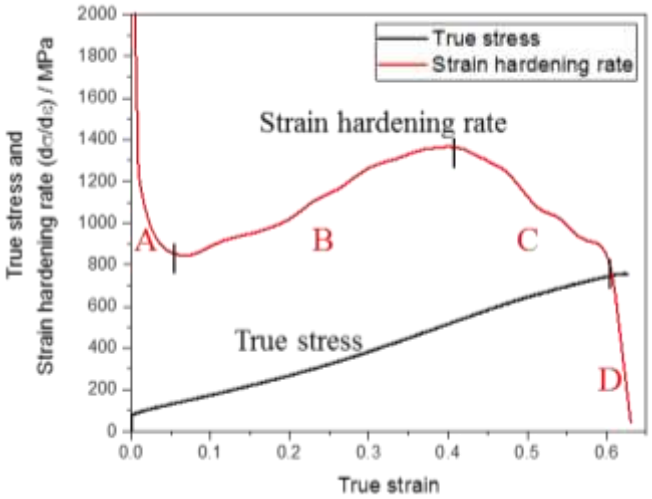

Fig. 2.2. True stress-strain curve and strain hardening rate of the as-annealed Cu-15at%Al sheet

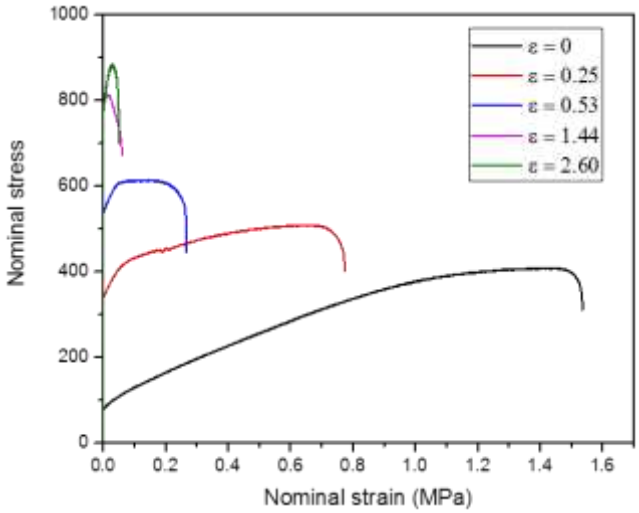

Fig. 2.3. S-S curve of cold-rolled Cu-15Al at various rolling strain

On the other hand, Considére criterion is the equations to give onset of the plastic instability such as necking or shear band.

$$\frac{d\sigma}{d\varepsilon} \leq \sigma \tag{2.2}$$

In the case of the initial material, uniform deformation is expected to continue until the true strain of 0.6. The necking takes place above strain of 0.6. In other word, the material has excellent uniform elongation and ductility.

Figure 2.3 shows nominal stress – strain curves obtained by the tensile test. Initial materials show excellent total elongation of 91% and ultimate tensile strength (UTS) of 409MPa. With strain increasing, strength increased while elongation decreased. In case of equivalent strain of 2.60, UTS was 881MPa while total elongation was limited to 4.6%.

2.3.2 Microstructure observation

Fig. 2.4 shows optical microstructure on longitudinal section of the cold rolled specimens. Fig. 2.5 shows inverse pole figure (IPF) map by EBSD analysis. At equivalent strain of 0.25, elongated grains and annealing twins were observed (Figs. 2.4a, 2.5a). Deformation twins with narrow width appeared locally. With strain increasing, deformation twinning was observed in selected grains (Figs. 2.4b, 2.5b). In the

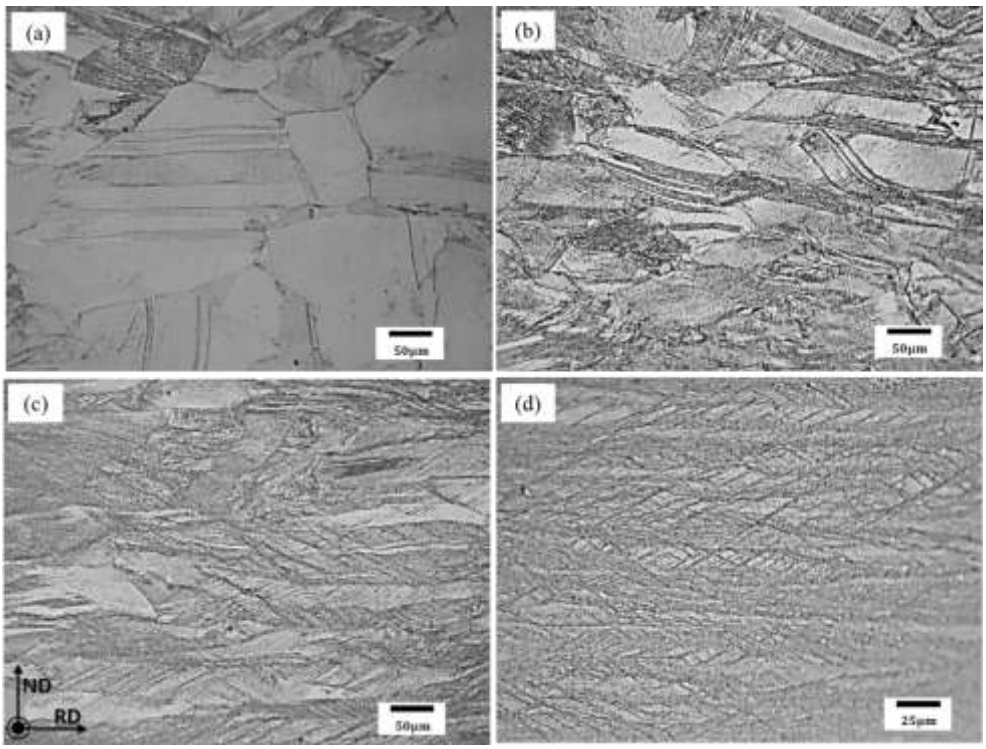

Fig. 2.4. Optical microscopy at equivalent strain of (a) 0.25, (b) 0.53, (c) 1.13 and (d) 2.60 of cold-rolled Cu-15at%Al.

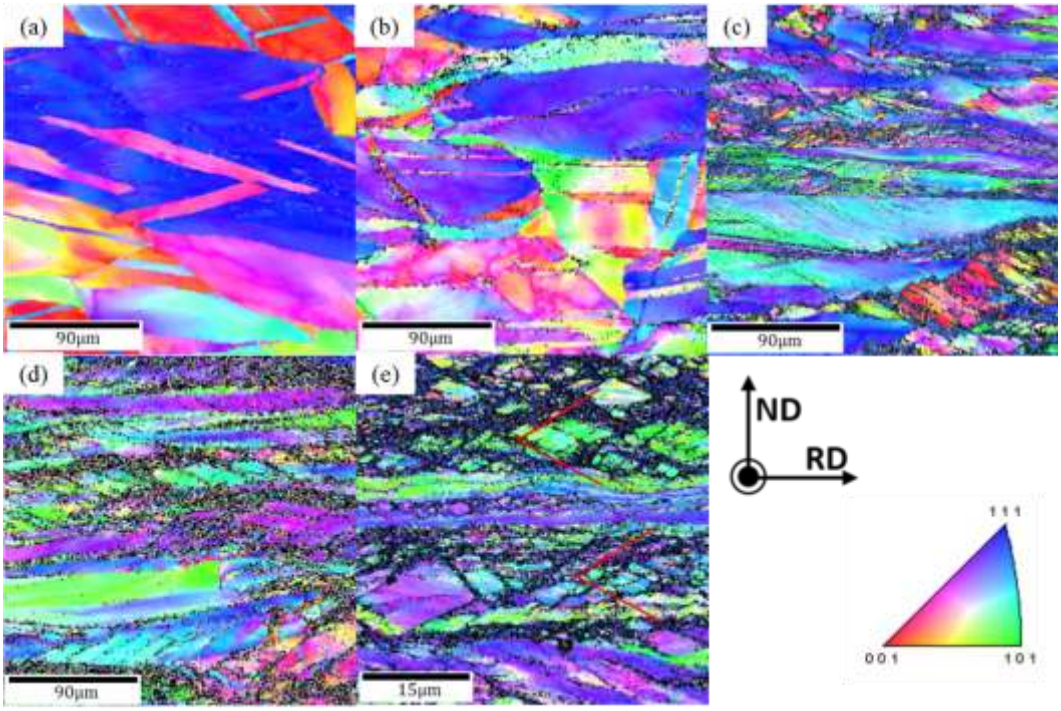

Fig. 2.5. EBSD Inverse pole figure map at the equivalent strain of (a) 0.25, (b) 0.53, (c) 1.13, (d) 1.44 and (e) 2.60, confidence index (CI) < 0.1 is not shown on the maps

case of equivalent strain of 1.13, shear bands appeared near the grains where the deformation twinning was occurred. The fraction of shear bands increased and intersections were observed (Figs. 2.4c, 2.5c). The fragmentation of grains by shear bands increased with increasing reduction in thickness. At the strain of 2.60, intersections of shear bands turns into rhomboidal prisms observed as shown in Figs. 2.4d and 2.5e.

2.3.3 Hardness test

The hardness increased with increasing reduction, while the slope, i.e., strain hardening rate, gradually decreased as seen in Fig. 2.6. The hardness of the specimen at $\varepsilon = 2.60$, which was measured to HV271, was 2.6 times higher than that of the initial specimen (HV107).

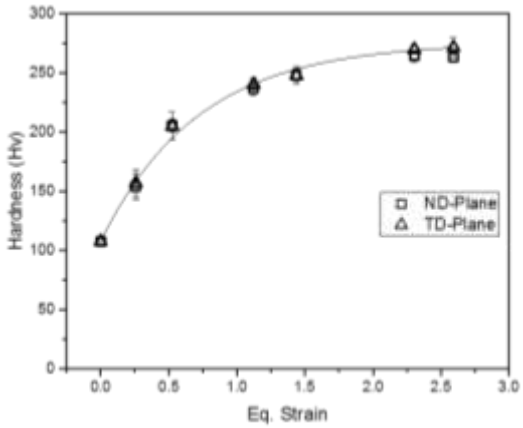

Fig. 2.6. Change in Vickers hardness as a function of equivalent strain of multi-pass rolled Cu-15at%Al (square) ND-plane, (triangle) TD-plane

2.4 Discussion

Fig. 2.7 shows distribution of misorientation angle of grain boundaries with increasing equivalent strain. The initial material showed a high fraction of annealing twins (misorientation angle = 60°) more than 30 percent, which resulted in a relatively high average misorientation angle of 40.8°. The increase in low angle grain boundaries (LAGB, misorientation angle < 15°) resulted in a decrease in average misorientation angle. On the other hand, fraction of LAGB tended to decrease with increasing strain to 1.13, and it was confirmed that formation of a high angle grain boundary (HAGB) angle occurred. Thereafter, the average misorientation angle tended to increase with increasing strain and was 21.4° at equivalent strain of 2.60.

Fig. 2.8 shows strengths and mean grain size as a function of equivalent strain. The grain size showed considerable decrease until the strain of 0.5. This is because mechanical twinning occurred actively at the

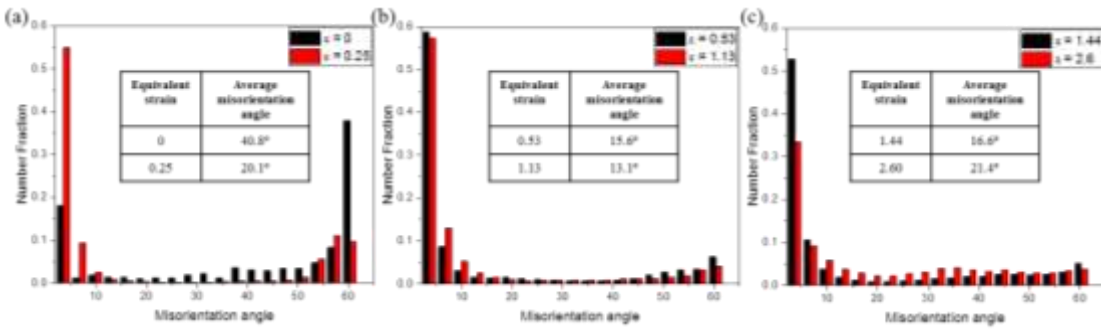

Fig. 2.7. Number fraction and average of misorientation angle of Cu-15at%Al as a function of equivalent strain, (a) 0 and 0.25, (b) 0.53 and 1.13, and (c) 1.44 and 2.60

beginning of rolling process. According to references [2.9, 2.10], deformation twinning depends on the crystallographic orientations of grains. Selective deformation twinning is considered to increase the standard deviation of the grain size. On the other hand, collaborations between slip and twinning continue to occur during deformation. Twinning in grains which were predominated is saturated. After this stage, twins do not increase further even strain still increases. According to the results shown in Fig. 2.2, it is predicted that inhomogeneous deformation occurs at the strain greater than 0.6, shear bands are initiated. C.S Hong et al [2.11] found that shear band in Cu-Al alloy initiate in twin / matrix lamellar structure and it increases with increasing shear strain. As the stain increases further, grain fragmentation by intersection of shear bands resulted in grain refinement and accumulated dislocations increase misorientation between subgrains leading to form nano-sized structure, as illustrated in Fig. 2.9.

Since the SFE of the alloy used is lower than 7, shear bands can be formed even at small strain. It is considered that deformation twinning is superior deformation mode, which leads to shear banding at lower accumulated strain. These shear bands intersect, so ultrafine grains are formed.

The results of this experiment, which was only cold rolling, were compared with the severely deformed and annealed references as shown in Fig. 2.10. Fig 2.10a shows the relationship between 0.2% proof stress and uniform elongation. It is found the balance between uniform elongation and 0.2% proof stress is

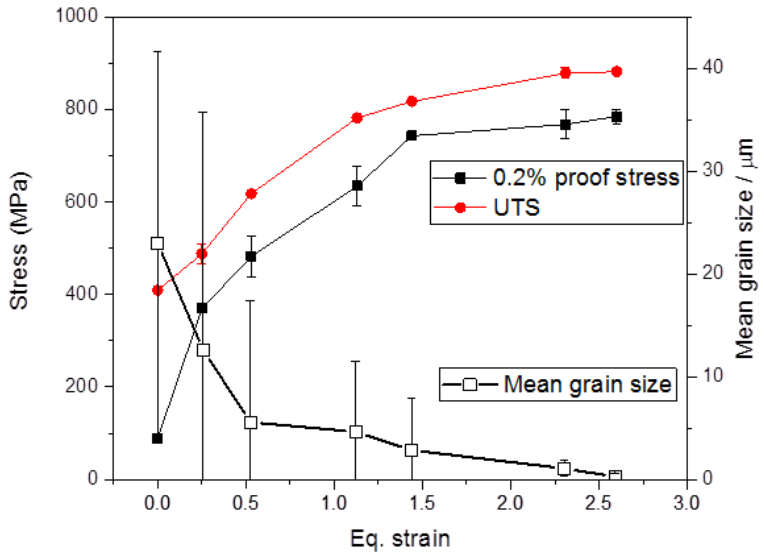

Fig. 2.8. 0.2% proof stress, UTS and mean grain size of Cu-15at%Al as a function of equivalent strain by multi-pass rolling

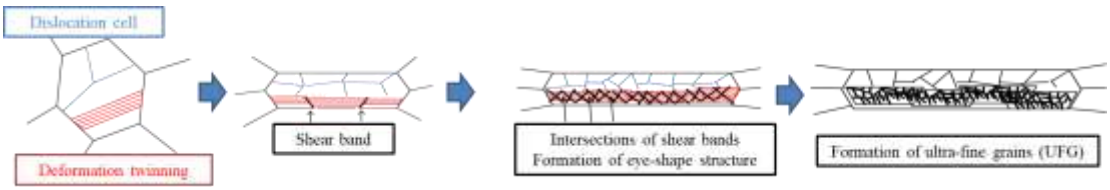

Fig. 2.9. Illustration of microstructure evolution in twinning-based Cu-15 at.% Al during rolling

very similar to those of references [2.2, 2.5]. Fig 2.10b shows the relationship between UTS and total elongation. It is found that the balance between strength and total elongation of this study is comparable to the results by high pressure torsion (HPT) followed by annealing [2.2] and 96% rolling followed by annealing [2.5]. The balances are much higher than that of 70:30 brass sheets [2.6]. It means that Cu-Al alloy by normal multi-pass rolling shows excellent tensile properties without heat treatment.

It is known that deformation twinning tend to occur more easily when grains of matrix are coarser [2.7]. At the early stage of deformation, it is considered that the balance between strength and elongation is improved by the formation of deformation twins. However, once shear bands formed and their intersections took place, as the deformation progresses further, the effect of deformation twinning was suppressed due to change in crystallographic orientations and finer grain size.

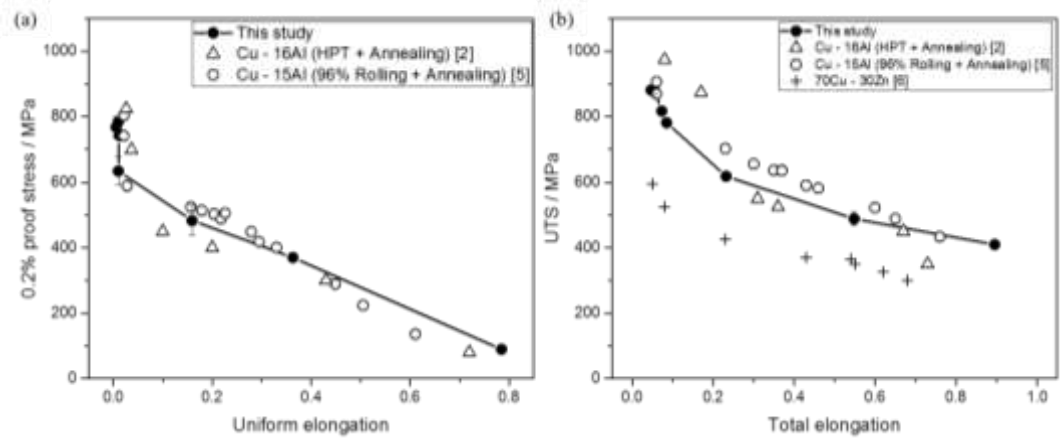

Fig. 2.10. Balance between strength and elongation, (a) 0.2% proof stress against uniform elongation, (b) UTS against total elongation

2.4 Conclusions

Multi-pass cold rolling of the Cu-15at%Al was carried out to observe microstructure evolutions and to measure change in mechanical properties. The remarks obtained in this study are as follows,

1. Microstructure evolution in rolling process can be subdivided into 3 stages. Deformation twinning, shear banding, and intersection of shear bands.
2. Ultrafine grains are formed by intersections of shear bands which are introduced by deformation twinning.
3. The balance between strength and elongation of this alloy without annealing was similar to those in literature by severe plastic deformation and annealing.

References

[2.1] R. Liu, Z. J. Zhang, L. L. Li, X. H. An and Z. F. Zhang, Scientific Reports, 5 (2015) 9550

[2.2] X. H. An, S. D. Wu, Z. F. Zhang, R. B. Figueiredo, N. Gao and T. G. Langdon, Scripta Materialia 66 (2012) 227-230

[2.3] X. H. An, S. Qu, S. D. Wu and Z. F. Zhang, Journal of Materials Research 26 (2011) 407-415,

[2.4] H. Miura, Y. Iwama and M. Kobayashi, Proc. 57th Meeting of Japan Copper Society (2017) 53-54 (In Japanese)

[2.5] Y. Z. Tian, L. J. Zhao, S. Chen, D. Terada, A. Shibata and N. Tsuji, Journal of Materials Science 49 (2014) 6629-6639

[2.6] ASM Metals Handbook (10th edition), Vol. 2, (1992) ASM International, Metals park, Ohio.

[2.7] E. El-Danaf, S. R. Kalidindi and R. D. Doherty, Metallurgical and Materials Transactions A 30 (1999) 1223-1233

[2.8] S.J. Lee, J. Han, S. Lee, S.H. Kang, S.M. Lee and Y.K. Lee, Scientific Reports, 7 (2017) 3573

[2.9] I. Gutierrez-Urrutia, S. Zaefferer, D. Raabe, Material Science and Engineering A 527 (2010) 3552–3560

[2.10] A. Gazder, A. Saleh, E. V. Pereloma, Scripta Materialia 68 (2013) 436–439

[2.11] C. S. Hong, N. R. Tao, X. Huang and K. Lu, Acta Materialia 58 (2010) 3103-3116

Chapter 3

Proposal of cryogenic high-speed rolling

3.1 Introduction

According to the previous chapter 2, it was confirmed that the deformation twinning occurred even in the conventional cold rolling in the case of Cu-15at%Al with very low stacking fault energy, thereby improvement in the balance of strength and ductility of the material due to deformation twinning and grain refinement was observed.

However, deformation twinning typically occurred when the low SFE material is plastically deformed. In the case of high SFE copper alloys, the twinning does not occur in the conventional rolling process, so that it is difficult to improve the strength and the ductility of the material by this technique. Moreover, adding a high amount of alloying elements decreases the electrical conductivity and ductility, and induces high cost. Therefore, after adding the least amount of alloying elements to balance the basic strength and electrical conductivity of the material, a method to generate deformation twins through metal forming is required.

Deformation mode is mainly determined by SFE of material, but it also varies with deformation temperature, and strain rate [3.1, 3.2]. The effects of these extrinsic factors are not significant, but if they have huge changes, deformation mode can be made enough to change from crystallographic slip to deformation twinning.

Severe operating conditions with cryogenic temperature and very high strain rate may form deformation twins during rolling. It is known that an increase in strain rate during deformation is thought to have an equivalent effect to that of a decrease in deformation temperature and vice versa. The combined effects of strain rate and deformation temperature (T) are often represented by a single parameter, the Zener-Hollomon parameter (Z), which is defined by the following equation,

$$\mathrm{Z} = \dot{\varepsilon} \exp(\frac{Q}{RT}) \tag{3.1}$$

where $\dot{\varepsilon}$ is the equivalent strain rate, Q is the activation energy, R is the gas constant, and T is the temperature, as mentioned in Section 1.1.6.

In this study, the high Z parameter rolling of copper alloys with high stacking fault energy was carried out to realize microstructure control. First, ranges of temperature and strain rate that can change deformation mode on copper were investigated. Subsequently, a novel rolling method is proposed, which can realize a high Z parameter which is able to change microstructure evolution and can be more applied in industries. Next, the Z parameter in the actual rolling process was calculated to predict a applicable temperature and strain rate, according to the rolling reduction rate, the rolling speed, and the temperature change.

3.2 Strain rate and temperature range to change the deformation mode

In first, a range of strain rate and temperature were investigated enough to change deformation mode from crystallographic slip to twinning to design the rolling process with a high Z parameter to expect microstructure control. Fig. 3.1 shows the ln Z contouring with the deformation mode map [3.3 ~ 3.8] of pure copper. In this calculation, activation energy, Q, was assumed to 72.5kJ/mol [3.9].

Three regions can be differentiated according to the deformation mode and microstructure [3.3]. In Region I, deformation is dominated by dislocation slip, and microstructure is characterized by elongated grains. In region II, crystallographic slip and deformation twinning compete with each other, forming a mixed microstructure. The proportion of twins increases with increasing ln Z. In Region III, deformation occurs mainly by deformation twinning. The microstructure is mainly composed of fine and dense twins.

On the other hand, if the SFE decreases by the addition of alloying elements, as in Fig. 3.1(b) and (c), the region II or III were simply reached even at the conventional strain rate and room temperature.

To realize deformation twinning in pure Cu (or high SFE Cu alloys), at least 30 of ln Z is required to activate deformation twinning. In addition, ln Z greater than 57 would be required if microstructure evolution is similar to that of Cu-15at% Al, which was shown in chapter 2. In order to reach 30 of ln Z at

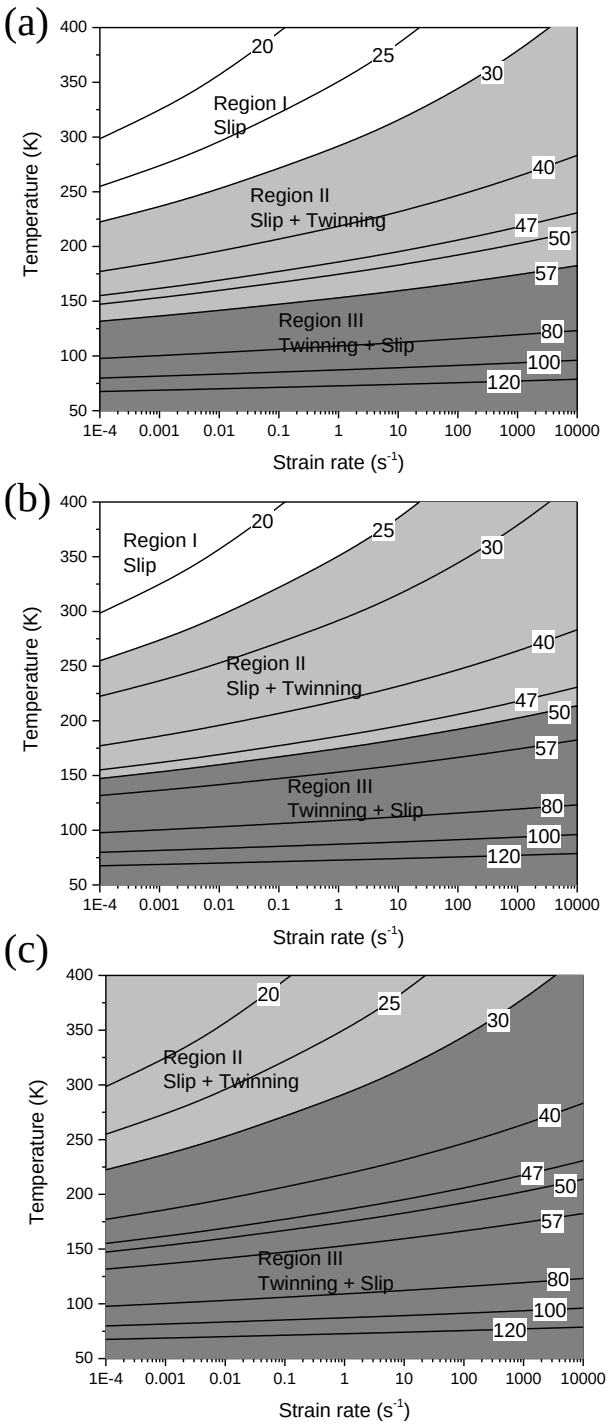

Fig. 3.1. Ln Z contouring map as a function of strain rate and temperature (a) pure Cu at SFE=78mJ/m^2, (b) Cu-5Zn at SFE=50 mJ/m^2, (c) Cu-20Zn at SFE=20 mJ/m^2 [3-3 ~ 3-9]

room temperature (298.15 K), the strain rate should be faster than 10 s^{-1}. However, reaching for the 57 of ln Z to accomplish to region III at room temperature, the strain rate is required by the eq. (3.1) to over 10^{12}

s^{-1}, which is impossible in realistic metalworking processes. Therefore, the rolling process at cryogenic temperature is necessary to accomplish to attain region III.

3.3 Proposal of cryogenic high-speed rolling (C-HSR)

Rolling at cryogenic temperature was gradually studied, as referred to in chapter 1.1.7. However, realizing the cryogenic rolling in industries is not practical. It is necessary for all equipments such as rolling rolls, tables, guides as well as the specimens to be cooled to cryogenic temperature because the specimen temperature may increase due to deformation and frictional heats generated by the rolling and the heat flow from rolls and atmosphere.

The idea of the combination of high-speed rolling and cryogenic rolling developed to satisfy the rolling conditions to increasing the Z parameter and reducing contact duration. Cryogenic high-speed rolling (C-HSR) was proposed as the rolling method where the specimen only cooled in liquid nitrogen with rolls at room temperature and supplied to high-speed rolling, as shown in Fig. 3.2. C-HSR will be employed to reduce contact duration with rolls so that the specimen is kept under room temperature even after rolling. In addition, the exceptional increase of the Z parameter due to the high strain rate and low temperature, leading to the contributing to the microstructure control. Therefore, it can be expected that C-HSR is not just a combination of the two processes, but a novel rolling process that can produce synergistic effects. Next, the implementation of the actual rolling process was carried out

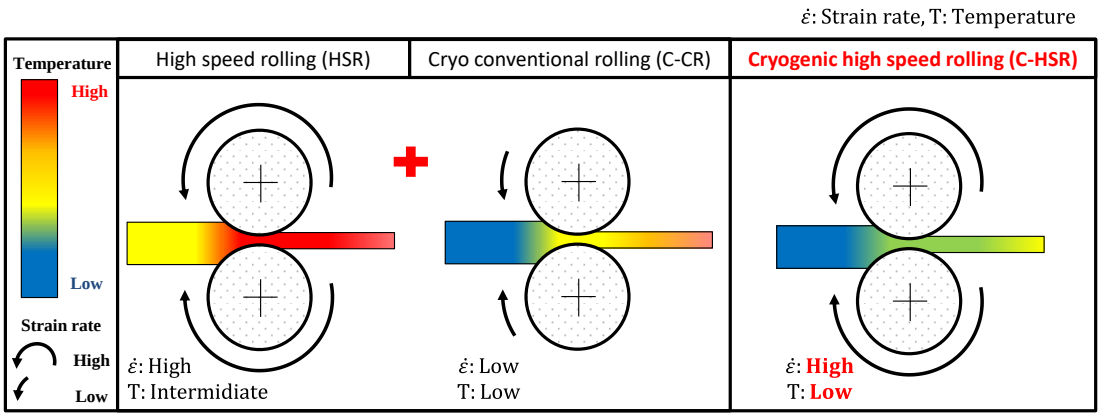

Fig. 3.2. Concept of the cryogenic high-speed rolling (C-HSR)

3.4 Design of the cryogenic high-speed rolling (C-HSR)

The laboratory, where is affiliated to the author, had been gradually studied high-speed rolling research since the 1980s [3.10 ~ 3.14]. However, the researches on high-speed rolling had been only conducted on high-temperature high-speed rolling of Fe alloys and improvement of workability of magnesium alloys. The same rolling mill was used to apply high rolling speed. The rolling mill was consisted of pinch roll, main roll (ϕ530mm), water quencher, and stopper, as shown in Fig. 3.3. The details referred to the ref. [3.10 ~ 3.12]. After the C-HSR, the temperature of the sheet is expected under room temperature, so that the water quencher is only used as the guide from rolls to the stopper.

In addition, the sheets to supply to the rolls were designed to soak in liquid nitrogen for 900s and then supplied to the rolls within 5s to realize the cryogenic temperature. On the other hand, the specimen was subtracted from the liquid nitrogen within a few seconds before supplying it to the rolls. In other words, the specimen contacted with air at room temperature, which caused the rises of temperature. To confirm the temperature increasing due to the atmosphere of room temperature, the temperature profile after subtracting from liquid nitrogen was established.

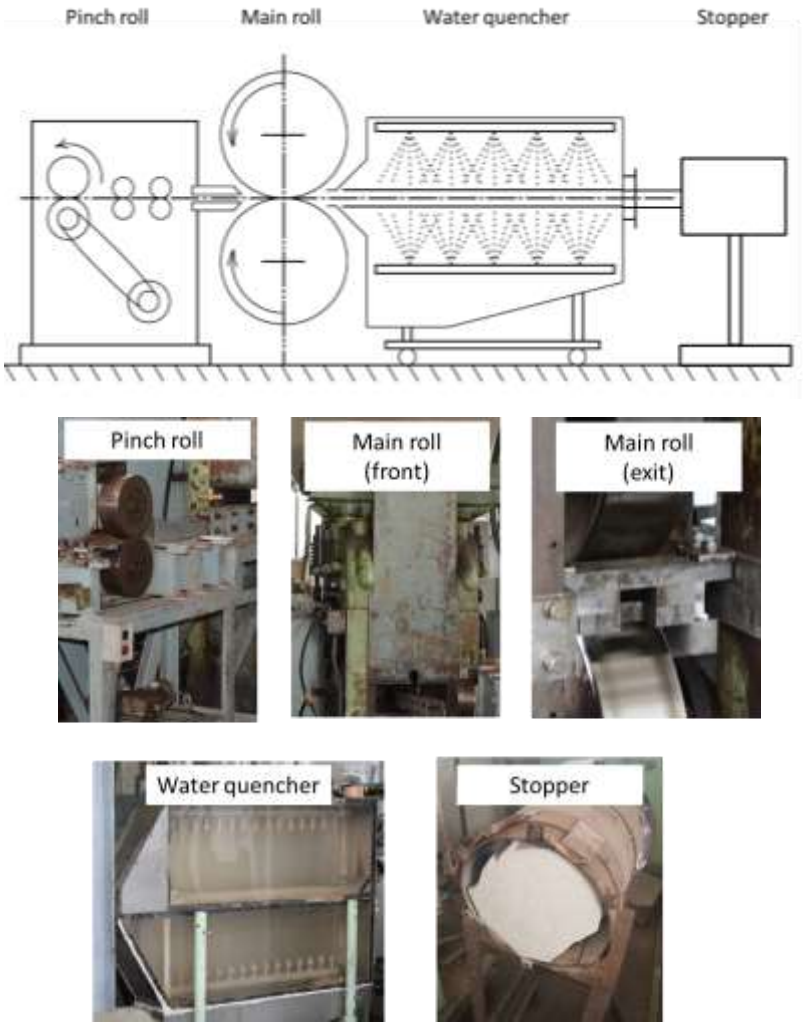

Fig. 3.3. Schematics and photographs of high-speed rolling mill

Fig. 3.4 shows the temperature profile of the specimen after subtracting from liquid nitrogen within 10min. The temperature rapidly increased around 60K within 10s after the subtracting. After the rapid increase, the temperature increased slowly. To maintain cryogenic (or very low) temperature, the rolling should be accomplished within 5s after the subtracting from liquid nitrogen. And the initial temperature of cryogenic high-speed rolling was determined to 100K.

Next, the calculation of the Z parameter in the rolling process was investigated to the feasibility study of the C-HSR

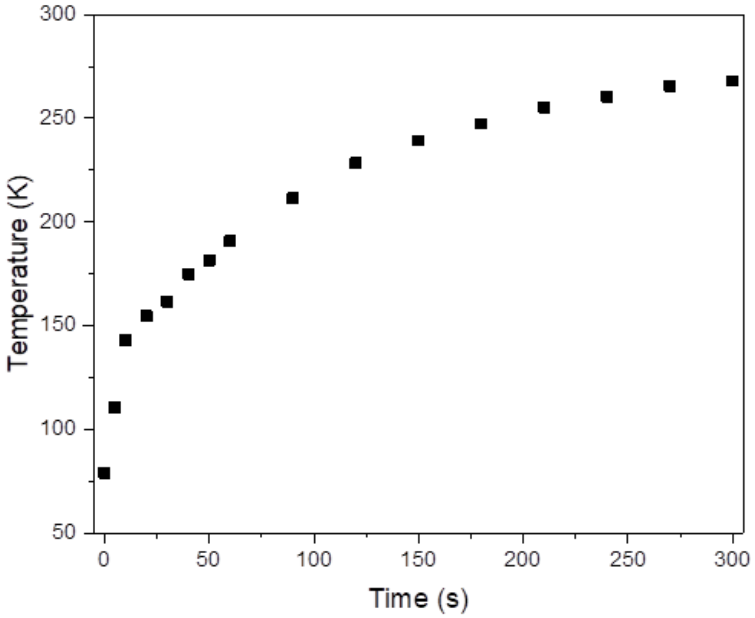

Fig. 3.4. Temperature profile of Cu-5mass% Zn sheet after subtracting from liquid nitrogen, as a function of time

3.5 Calculation of the Z parameter in the rolling process

3.5.1 Strain rate

There are several variables to determine the strain rate in the real rolling process. The mean strain rate during rolling is known to be given by the following equation.

$$\dot{\varepsilon} = \frac{2}{\sqrt{3}} \ln\left(\frac{h_0}{h_1}\right) \frac{v}{\sqrt{R(h_0 - h_1)}} \tag{3.2}$$

where $\dot{\varepsilon}$ is the mean strain rate, h_0 is the initial sheet thickness, h_1 is the sheet thickness after rolling, R is the radius of rolls, and v is the peripheral speed of rolls.

The mean strain rate as a function of the reduction in thickness and rolling speed is shown in Fig. 3.5. The initial sheet thickness h_0 and the radius of roll R were assumed to be 3mm and 265mm, respectively.

In order to accomplish the higher strain rate, the higher rolling speed, as well as the higher reduction in thickness are required because the strain rate is getting larger due to both h_0/h_0 and (h_0-h_1) in Eq. (3.2).

According to Fig. 3.1, a rolling speed of 11m/min is required to achieve the strain rate of 10 s^{-1} in the case of the reduction in thickness of 67% with an initial thickness of 3mm in order to change the deformation mode from the Region I to Region II. On the other hand, the 47m/min of rolling speed is required in order to achieve the same strain rate if the reduction is 10%. In addition, the higher strain rate is needed to the higher ln Z, which will accomplish the higher microstructure control.

To top it all off, the temperature of the sheet increases during the actual plastic working. The typical example of increasing temperature is deformation heat, which causes a decrease in the Z parameter. For example, if the temperature increases by only 25 K during rolling, the strain rate required for the transition becomes 40 s^{-1}, and rolling speed of 180 m/min is required to achieve this strain rate under the condition of 10% rolling reduction. Moreover, it is impossible to modify the deformation mode to region III at room temperature, as mentioned in the Chapter. 3.2. Therefore, the rolling process at the low-temperature rolling is essential to change microstructure control.

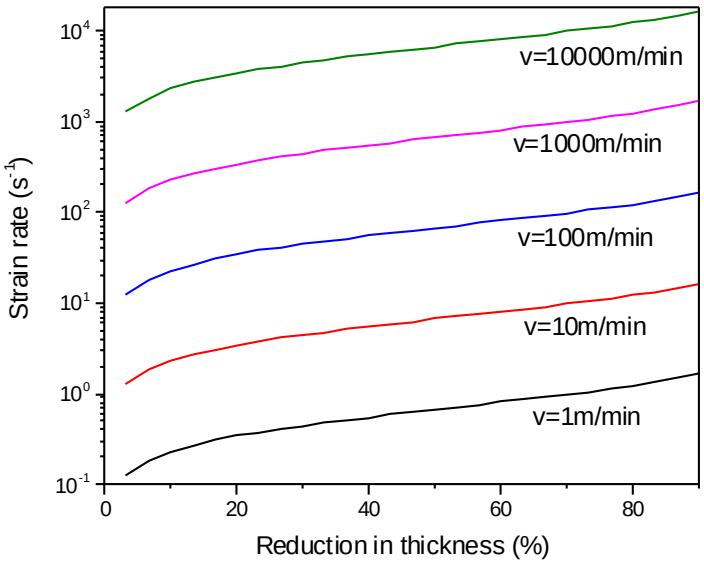

Fig. 3.5. Change in the strain rate at the different rolling speed as a function of the reduction in thickness (The initial sheet thickness h_0 and the radius of roll R were assumed to 3mm and 265mm)

3.5.2 Temperature

During the actual cold and cryogenic rolling process, the sheet experiences various temperature increasing. The heat that can change the temperature during rolling could be classified into three types; the contact heat between the rolling rolls and sheet, the deformation heat due to plastic deformation during rolling, and the friction heat between the sheet and rolls.

Heat balance was considered to estimate sheet temperature in order to calculate the Z parameter in the actual rolling process. Temperature change by rolling can be estimated using the following equation [3.15],

$$T_{\text{fin.}} = T_{\text{ini.}} + \Delta T_p + \Delta T_f - \Delta T_r \tag{3.3}$$

where, $T_{\text{ini.}}$ and $T_{\text{fin.}}$ are the initial and the final temperature of the specimen in rolling.

In this case, deformation heat in rolling (ΔT_p) is estimated by the following equation,

$$\Delta T_p = \frac{Q_p}{\rho_s c_s} = \frac{\eta_p k \ln(h_0/h_1)}{\rho_s c_s} \tag{3.4}$$

where ρ is the density c is the specific heat of sheet, h_0 and h_1 is the thickness before and after rolling, Q is the heat, W is the plastic work, k is the mean flow stress and η_p is the conversion efficiency of deformation work to heat, which is generally considered to be 0.9 [3.16].

Then, the temperature rise due to friction on the interfaces between the roll and the specimen (ΔT_f) is estimated by the following equation,

$$\Delta T_f = \frac{2\eta_f Q_f}{(h_0+h_1)\rho_s c_s/2} = \frac{4\eta_f \mu k v_r t_r}{(h_0+h_1)\rho_s c_s} \tag{3.5}$$

where η_f is the conversion efficiency of frictional work to the specimen, which is assumed 0.5 [3.16].

And then, the temperature change due to heat transfer between the rolls and the specimen (ΔT_R) is

Table 3.1. Selected material constants used for temperature calculation

	unit	**Specimen**	**Roll**
		Cu	Steel
Density	g/cm^3	8.94	7.87
Thermal conductivity	W/mK	386	73.3
Specific heat	J/gK	0.386	0.444
Friction coefficient		0.2	
	unit	**value**	
Temp. (sheet)	K	77	
Temp. (roll)	K	298.15	
Roll radius	m	0.265	
Mean flow stress	MPa	200	

given as follows,

$$\Delta T_R = \frac{2\eta_R Q_R}{(h_0+h_1)\rho_s c_s} = \frac{8\eta_R \lambda_s \sqrt{t_r}(T_{so}-T_m)}{(h_0+h_1)\rho_s c_s \sqrt{\alpha_s \pi}} \tag{4.5}$$

where α is $\lambda/\rho c$, λ is the thermal conductivity, t_r is the contact time, T_{so} is the specimen temperature, and T_m is the Laplace temperature constant between specimen and roll. η_R is the modification factor to consider the oxide layer and contact heat resistivity between roll and specimen, assumed 0.65 [3.16].

Materials constants for the estimation of temperature during rolling is shown in Table 3.1 [3.15 – 3.17]. For simplicity of calculation, the flow stress and the coefficient of friction were assumed to be equal under all conditions. Cryogenic temperature is assumed to 77K, which is liquid nitrogen temperature. Figs. 3.6 and 3.7 show the estimated temperature after the rolling using the eq. (3.3) to (3.5) and Table 3.1. Fig. 3.6 shows the calculated temperature as a function of the rolling speed at the reduction in thickness of 20%. The contact heat significantly decreased with increasing rolling speed. Therefore, contact duration between the rolls at room temperature and the sheet at cryogenic temperature should be recommended as short as possible.

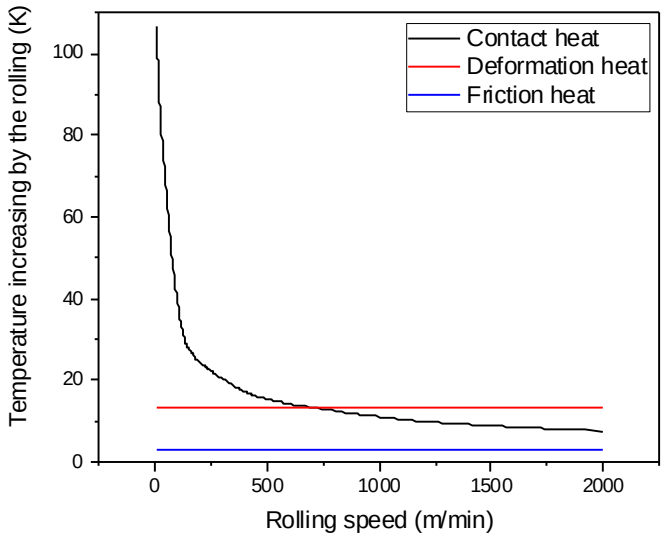

Fig. 3.6. The temperature estimation as a function of the rolling speed at the reduction in thickness of 20%

On the other hand, Fig. 3.6 shows the calculated temperature as a function of the reduction in thickness at the rolling speed of 1000m/min. All parameters show the tendency, which increased with the increasing reduction in thickness. Under the conditions of more than 15% of the reduction, the deformation heat increased most rapidly. Above the rolling reduction of 53%, the friction heat was calculated to be greater than the contact heat. Therefore, the low reduction in thickness in a rolling-pass is required to suppress the temperature increasing.

3.5 Feasibility study of C-HSR

According to the above estimation, the temperature changes before and after rolling in cryogenic (low speed) rolling and cryogenic high speed rolling are shown in Fig. 3.8, and compared with the measured temperature [3.3, 3.18].

At the rolling speed of 2 m/min, the temperature of 77 K before rolling increased to 246 K after the rolling. On the other hand, the C-HSR condition was predicted to be 148K at 1000 m/min of rolling speed. The measured temperature results are indicated by triangle symbols in Fig. 3.8. The experimental results

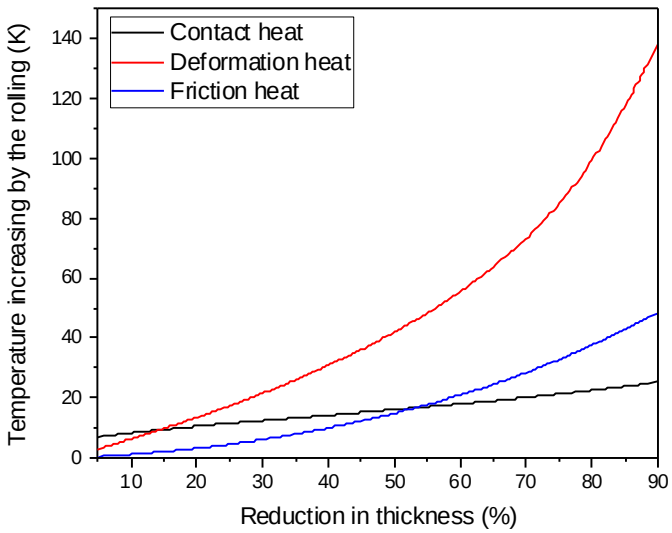

Fig. 3.7. The calculated temperature as a function of the reduction in thickness at the rolling speed of 1000m/min

were slightly higher than the prediction result, but it was confirmed that the estimated temperature change showed good agreement with the measured temperature [3.18].

On the other hand, when the reduction in thickness increases, the effect of cryogenic high-speed rolling becomes more pronounced. The temperature rises estimation at different rolling speeds after the 60% rolling is shown in Fig. 3.9. At the rolling speed of 10m/min, the strain rate is calculated to be about 6 s^{-1}, and the temperature after the rolling is estimated to exceed 300K. This increase in temperature will occur in the transition of the deformation mode from twinning to slip (Region III to Region I). In other words, the cryogenic temperature would be useless because the microstructure evolution would not be significantly different from rolling at room temperature. On the other hand, in the high-speed rolling conditions of 1500m/min, the strain rate of about 500 s^{-1} was exhibited, and the deformation mode was thought as the boundary between Region II and III.

Based on Figs. 3.8 and 3.9, the cryogenic high-speed rolling method proposed in this Chapter is considered to be an effective rolling method that maintains a high ln Z condition before the rolling, is a practical and cost-reasonable process compared to other cryogenic rolling processes.

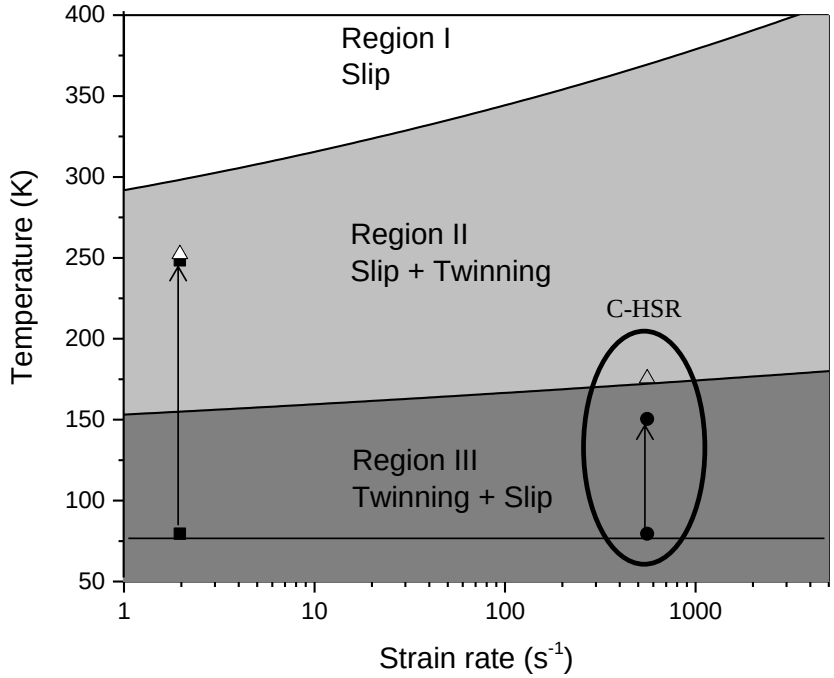

Fig. 3.8. Comparison between cryogenic rolling at different strain rate. Ln Z contour map of pure Cu [3.3] with (Square) Reduction in thickness of 20% at rolling speed of 2 and 1000m/min, (circle) Reduction in thickness of 20% at rolling speed of 1000m/min, (triangle) temperature after the rolling obtained by the experiment [3.18]

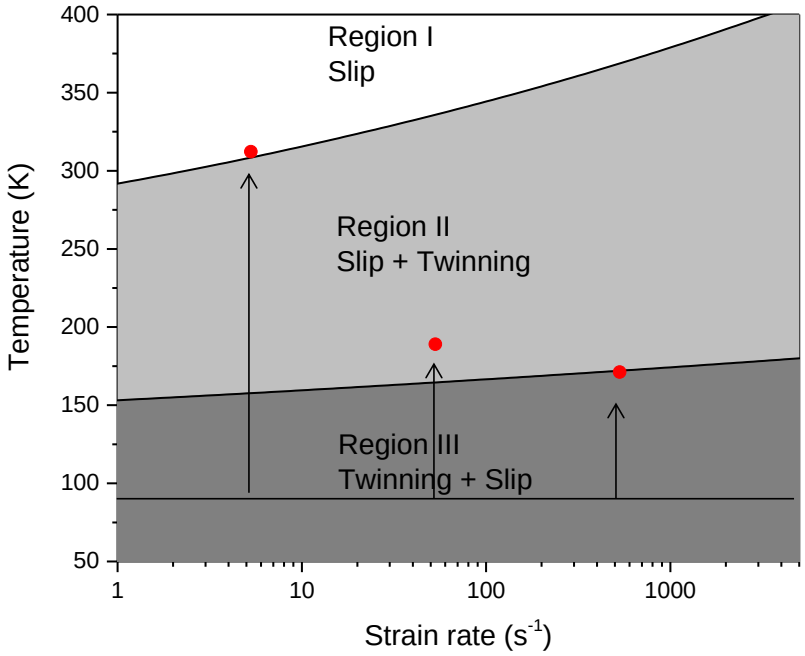

Fig. 3.9. Comparison between cryogenic rolling at the rolling speed of 10, 100 and 1000m/min, reduction in thickness is 60% with ln Z contouring map of pure Cu [3.3]

3.6 Conclusions

In this chapter, a novel rolling process was proposed, named “cryogenic high-speed rolling (C-HSR)”, where the specimen only cooled in liquid nitrogen with rolls at room temperature and supplied to high speed rolling. It is expected that high rolling speed is employed to reduce contact duration with rolls so that the specimen is kept under room temperature even after rolling. In addition, an exceptional increase of the Z parameter due to the high strain rate also could be contributing to the microstructure control.

The change in ln Z (Z: Zener-Hollomon parameter) was theoretically estimated through changes in temperature and strain rate during rolling. As a result, it was confirmed that the C-HSR could maintain a high ln Z even at a high rolling reduction. In the case of the specimen at cryogenic temperature and the rolls at room temperature, a high rolling speed (750 m/min) not only contributes to the improvement of ln Z, but also reduces the contact heat, so that a synergistic effect can be expected to reduce the temperature increasing due to less contact duration during C-HSR.

References

[3.1] X.H. An, S.D. Wu, Z.G. Wang, and Z.F. Zhang, Progress in Materials Science, 101 (2019) 1-45

[3.2] P. Wang, J. Jie, C. Liu, L. Guo, and T. Li, Mater. Sci. Eng. A, 715 (2018) 236-242

[3.3] Y. Zhang, N. R. Tao, and K. Lu, Acta Mater. 59 (2011) 6048-6058

[3.4] T. L. Brown, C. Saldana, T. G. Murthy, J. B Mann, Y. Guo, L. F. Allard et al., Acta Mater. 57 (2009) 5491

[3.5] Y. M. Wang, T. Jiao, and E. Ma, Mater. Trans. 44 (2003) 1926

[3.6] M. Hatherly, J. Inst. Met. 8 (1960) 60

[3.7] J. D. Embury, A. S. Keh, and R. M. Fisher, Trans. Metall. Soc. AIME, 236 (1966) 1252

[3.8] J. Gryzieckl, and A. Latkowski, Mater. Sci. Eng. A, 104 (1988) 15

[3.9] A. Mishra, B.K. Kad, F. Gregori, M.A. Meyers, Acta Mater. 55 (2007) 13–28

[3.10] T. Sakai, Y. Saito, K. Hirano, and K. Kato, Trans. ISIJ. 28 (1988) 1028-1035

[3.11] T. Sakai, Y. Saito, and K. Kato, Trans. ISIJ. 27 (1987) 520-525

[3.12] T. Sakai, Y. Watanabe, and H. Utsunomiya, Mater. Sci. Forum 618-619 (2009) 483-486

[3.13] H. Koh, T. Sakai, H. Utsunomiya, and S. Minamiguchi, Mater. Trans. 48 (2007) 2023

[3.14] J. Su, M. Sanjari, A. S. H. Kabir, I. –H. Jung, J. J. Jonas, S. Yue, and H. Utsunomiya, Mater. Sci. Eng. A. 636 (2015) 582

[3.15] Rolling theory committee ed., Theory and Practice of Flat Rolling, ISIJ, Japan, 1984. [In Japanese]

[3.16] J. Kokado, J. Jpn. Soc. Tech. Plasticity, 11 (1970) 816-824. [In Japanese]

[3.17] ASM International Handbook Committee, ASM Handbook, vol. 2: Properties and Selection: Nonferrous Alloys and Special-Purpose Materials, ASM International, Materials Park, 1990

[3.18] Y. Mochizuki, Bachelor's Thesis, Osaka University (2020)

Chapter 4

Mechanical properties and electrical resistivity of Cu - 5mass% Zn by cryogenic high-speed rolling

4.1 Introduction

Enhancement of strength and ductility of materials is one of the most important aspects of alloy design and materials engineering. In copper alloys, excellent electrical conductivity is also required for many applications. However, it is known that most strengthening mechanisms cause the lattice distortion, leading to a decrease in electrical conductivity due to electron scattering.

It was reported in the last few years that cryogenic rolling is effective to promote deformation twinning and to improve the mechanical properties. Bahmanpour et al. [4.1] reported that dynamic recovery and recrystallization are suppressed, grain refinement and deformation twinning are apparently promoted in cryo-rolling of pure copper and Cu-Al-Zn alloy. Even the dislocations rearranged themselves into dislocation cells, improvement in the ductility was observed. Roy et al. [4.2] reported that dislocation density of α-brass accumulated pass by pass at cryogenic temperature. Wang et al. [4.3] proposed a cryogenic rolling using a specially designed liquid nitrogen cooling system that deformation twinning and shear banding were the primary deformation mechanisms of Cu-35%Zn alloy, which realized improvement in balance between strength and ductility. According to these researches, it is found that rolling at cryogenic temperature improves mechanical properties due to deformation twinning. Deformation twinning can be activated not only at cryogenic temperature, but also under high strain rate conditions.

However, realizing the cryogenic rolling in industries is not practical. It is necessary for all equipments such as rolling rolls, tables, guides as well as the specimens to be cooled to cryogenic temperature because the specimen temperature may increase due to deformation and frictional heats generated by the rolling and the heat flow from rolls and atmosphere.

In previous chapter, cryogenic high-speed rolling was proposed as the rolling method where the

specimen only cooled in liquid nitrogen with rolls at room temperature and supplied to high speed rolling. It is expected that high rolling speed is employed to reduce contact duration with rolls, so that the specimen is kept under room temperature even after rolling, leading to the high Z parameter.

In this chapter 4, cryogenic high-speed rolling was applied to the Cu-5Zn alloy which has a low strength but a relatively high electrical conductivity; because plastic deformation process can increase the strength, however decrease the conductivity so that initial material with high conductivity is preferable.

In order to evaluate the process, comparison with conventional cold (and low-speed) rolling, cryogenic low-speed rolling and high-speed (room temperature) rolling were performed and microstructure, texture, mechanical properties and electrical conductivity were investigated.

4.2 Experimental procedure

Cu- 5 mass% Zn - 0.02 mass% Si alloy sheets with width × length × thickness = 30 × 300 × 2.5mm were used. Before the rolling, heat treatment was carried out at 773K for 7200s, to form equiaxed microstructure with mean grain size of 13.5μm. Four rolling methods were performed; (1) cryogenic high-speed rolling (C-HSR), (2) high-speed cold rolling (HSR), (3) cryogenic low-speed rolling (C-LSR), and (4) low-speed cold rolling (LSR). The rolling speed was at either 1500m/min [high-speed, (1), (2)] or 5m/min [low-speed, (3), (4)]. The details are shown in Table 1.

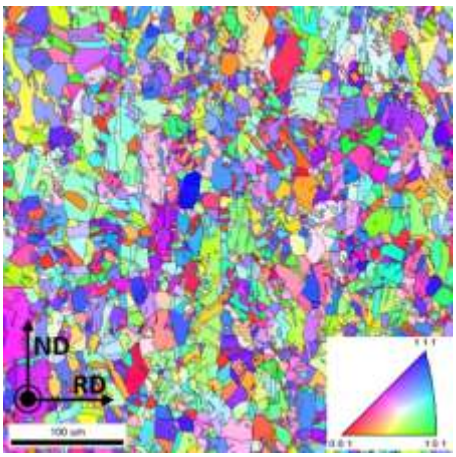

Fig. 4.1. Initial microstructure of Cu-5 mass% Zn alloy sheet

Table 4.1. Rolling conditions on this study

	Low speed rolling (LSR)	High speed rolling (HSR)	Cryogenic low speed rolling (C-LSR)	Cryogenic high speed rolling (C-HSR)
Roll diameter	Ø 310mm	Ø 530mm	Ø 310mm	Ø 530mm
Rolling speed	5m/min	1500m/min	5m/min	1500m/min
Initial temp.	RT	RT	77K	77K
Strain rate	1st pass : 1.1 x 10^1 s^{-1} (LSR), 1.3 x 10^3 s^{-1} (HSR) 2nd pass : 5.8 x 10^0 s^{-1} (LSR), 1.7 x 10^3 s^{-1} (HSR)			

The roll diameter was 530mm for the high-speed rolling [(1) C-HSR and (2) HSR] and was 310mm for the low-speed rolling [(3) C-LSR and (4) LSR]. Reduction in thickness of 60% was applied at the first pass, and then reduction was applied at the 2nd pass so that the total reduction in thickness was 80%. In the case of the two cryogenic rollings (C-LSR and C-HSR), the specimens were soaked in liquid nitrogen at 77K for 900s to cool before the rolling and applied to rolls within 3s.

In order to identify the temperature reaching cryogenic temperature, the temperature profile was prepared using the k-type thermocouple. The thermocouple was attached to the specimen by the spot-welding. According to the result, the temperature reached at the liquid nitrogen temperature (77K) within the 60s. However, the soaking time was determined to 900s to guarantee the maintaining cryogenic temperature.

The strain rate, estimated with the contact length and the rolling duration using the following equation,

$$\dot{\varepsilon} = \frac{2}{\sqrt{3}} \ln\left(\frac{h_0}{h_1}\right) \frac{v}{\sqrt{R(h_0 - h_1)}} \tag{4.1}$$

where h_0 is the initial thickness (2.5mm), h_1 is the thickness of the rolled specimen, R is radius of roll and v is peripheral speed of rolls, was 1.3-1.7 x 10^3 s^{-1} for high speed rolling while 5.8-11 s^{-1} for low speed rolling.

After the rolling, scanning electron microscopy with electron backscatter diffraction (SEM-EBSD) analysis was carried out and microstructural information, e.g., mean grain size, distribution of misorientation and fraction of twin boundaries, were obtained by TSL-OIM Analysis 7.3 software.

Specimens were prepared by mechanical polishing until #4000 of SiC paper and 1μm and 0.3μm of Al_2O_3 powder, followed by electro-polishing in a solution (H_3PO_4 : C_2H_5OH : H_2O = 50ml : 50ml : 100ml), with a voltage of 5V at 273K. The operation voltage of the SEM was 15 kV, the step size in the Kikuchi-pattern scanning was 0.15μm. In addition, to reduce topographic effects, points with confidence index (CI) less than 0.1 were excluded.

Tensile test were performed with an initial strain rate of 1.67×10^{-3} s^{-1}. The specimens with the gauge length of 10mm and the width of 5mm were used. Electrical conductivity was measured using the four-probe method and expressed as percent of International Annealed Copper Standard (%IACS) which is related back to conductivity of annealed copper (5.8×10^7 S/m). Specimen for the tensile test and the four-probe method was prepared to be parallel to the rolling direction; i.e. sampling was carried out in the good way. In addition, heat balance during rolling was estimated using the simplified method to calculate the average temperature considering the deformation heat, frictional heat and contact heat transfer [4.4].

4.3 Results

4.3.1 Mechanical properties and conductivity

Fig. 2 shows ultimate tensile strength (UTS) and total elongation of the rolled sheet as a function of total reduction in thickness by rolling. In all the rolling methods, tensile strength increased and elongation decreased with increasing total rolling reduction. C-HSRed specimens showed higher tensile strength than those by other rolling methods. In the case of 1-pass rolling (60% reduction), LSRed specimen presented tensile strength of 446MPa and total elongation of 9.1% while C-HSRed specimen was 503MPa and 11.9%. The UTS was measured to 576MPa with 5.3% of total elongation after 80% of cryogenic high-speed rolling. The LSRed specimen showed the similar UTS with HSR at 1-pass rolling, otherwise showed similar value with C-LSR at 2-pass rolling.

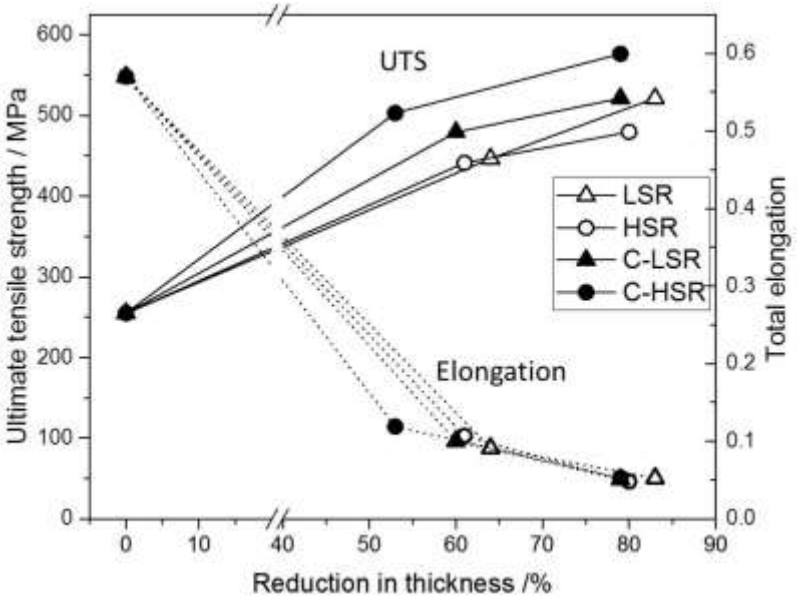

Fig. 4.2. Tensile strength and total elongation as a function of reduction in thickness

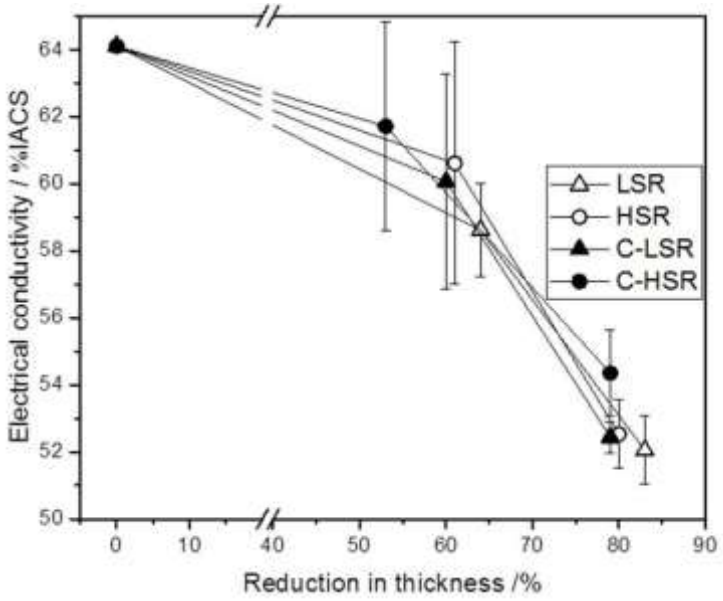

Fig. 4.3. Change in electrical conductivity as a function of reduction in thickness

Fig. 3 shows relationship between %IACS conductivity and reduction in thickness. Although conductivity decreased with increasing reduction in thickness, C-HSR specimen showed higher %IACS than LSR. Electrical conductivity of the C-HSRed specimen showed 62%IACS, while LSRed one showed 59%IACS after the 1-pass rolling. LSR showed the lowest conductivity.

4.3.2 Microstructure and texture

Fig. 4.4 and 4.5 show the inverse pole figure (IPF) map on the longitudinal section of the rolled sheets showing ND orientation, and the superimposing of the high angle grain boundary (HAGB, misorientation angle > 15°) and Σ3 boundary map, respectively. Grains elongated in the rolling direction were observed. Deformation twins were formed in the inlined direction about 35 degree to the rolling direction. Remnant grains are coarse and elongated in the rolling direction showing the ND//<110> orientation, while inlined and twinned grain showed ND//<111> orientation. C-HSR showed the highest fraction of ND//<111> orientation while LSR rarely showed that orientation.

Mean grain size and fraction of Σ3 twin boundaries over total boundaries ($f_{\Sigma 3}$) were shown in Table.4. 2. C-HSRed specimen showed $f_{\Sigma 3}$ = 0.17 whereas conventionally cold-rolled one (LSR) showed $f_{\Sigma 3}$ = 0.05. However, $f_{\Sigma 3}$ were not much different after the 2-pass rolling. It is considered that transition from twin boundaries to shear band, decreased the fraction of twin boundaries [4.5].

Formation of shear bands during rolling is clearly related with evolution of the rolling texture [4.6]. To

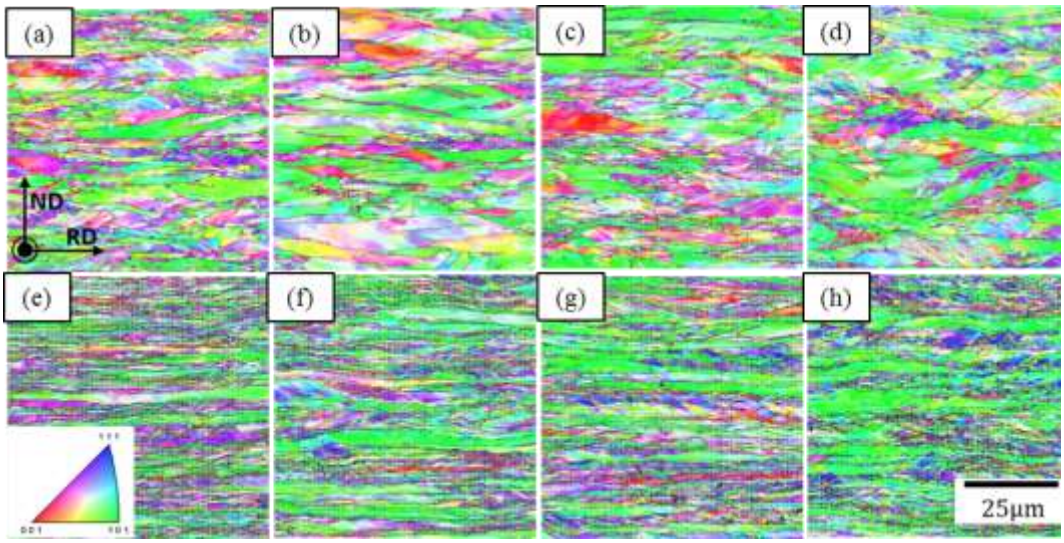

Fig. 4.4. Inverse pole figure maps showing ND orientation after various methods (a-d) *r*=60%, (e-h) *r*=80%, (a) and (e) : low speed cold rolling (LSR), (b) and (f) : high-speed cold rolling (HSR), (c) and (g) : cryogenic low-speed rolling (C-LSR), (d) and (h) : cryogenic high-speed rolling (C-HSR)

investigate the rolling texture of sheets processed by various rolling methods, {111} pole figures were drawn based on EBSD data, and shown in Fig. 5. After the 2nd pass, the textures showed a difference; The LSRed specimen showed typical copper-type rolling texture, while the C-HSRed specimen showed typical brass-type rolling texture. The HSRed and C-LSRed specimen showed the intermediate rolling texture with mixed copper and brass type components.

It is known that deformation twinning is activated at cryogenic temperature and/or high strain rates [4.7]. The transition to the brass-type texture is due to the deformation twinning and shear banding.

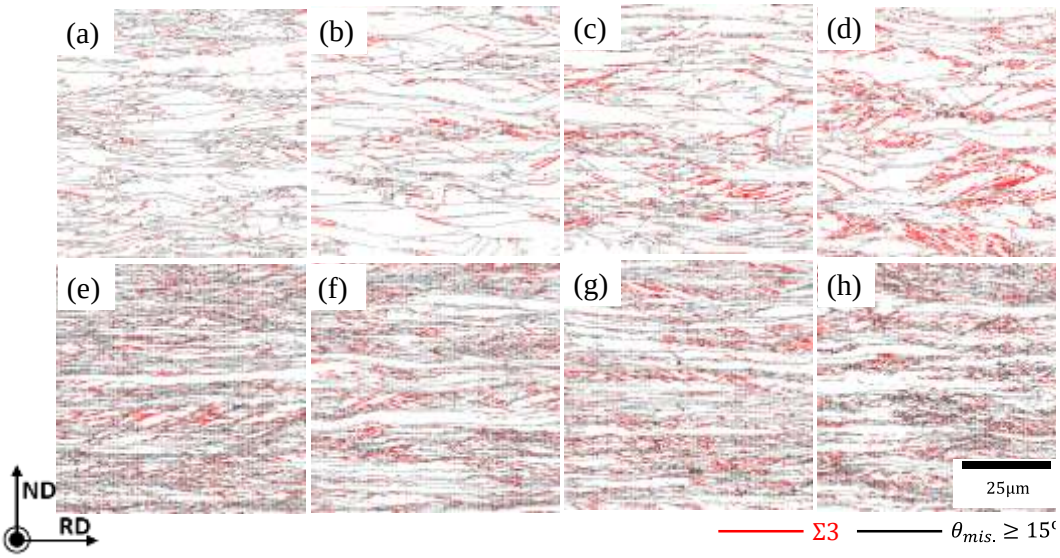

Fig. 4.5. High angle grain boundary (HAGB) map and Σ3 boundary map (a-d) *r*=60%, (e-h) *r*=80%, (a) and (e) : low speed cold rolling (LSR), (b) and (f) : high-speed cold rolling (HSR), (c) and (g) : cryogenic low-speed rolling (C-LSR), (d) and (h) : cryogenic high-speed rolling (C-HSR)

Table 4.2. Mean grain size and fraction of Σ3 boundaries of various rolling conditions

Pass		**LSR**	**HSR**	**C-LSR**	**C-HSR**
1-pass (*r*=~60%)	Mean grain size (μm)	1.68 ±9.32	2.91 ±15.6	1.39 ±7.91	1.54 ±8.93
	Σ3 fraction	0.049	0.076	0.083	0.171
2-pass (*r*=~80%)	Mean grain size (μm)	0.55 ±2.93	0.53 ±3.89	0.57 ±3.21	0.30 ±2.53
	Σ3 fraction	0.059	0.059	0.072	0.067

Although high rolling speed increases frictional heat, in the case of metals and alloys with high thermal conductivity, the decrease in contact heat transfer due to shorter contact duration is considered to have less total temperature increase. If the rolling method is applied to the specimen only with liquid nitrogen at a sufficiently high rolling speed to be negligible the contact heat flow, it can be cost-reasonable and be possible to obtain additional effects due to the high strain rate.

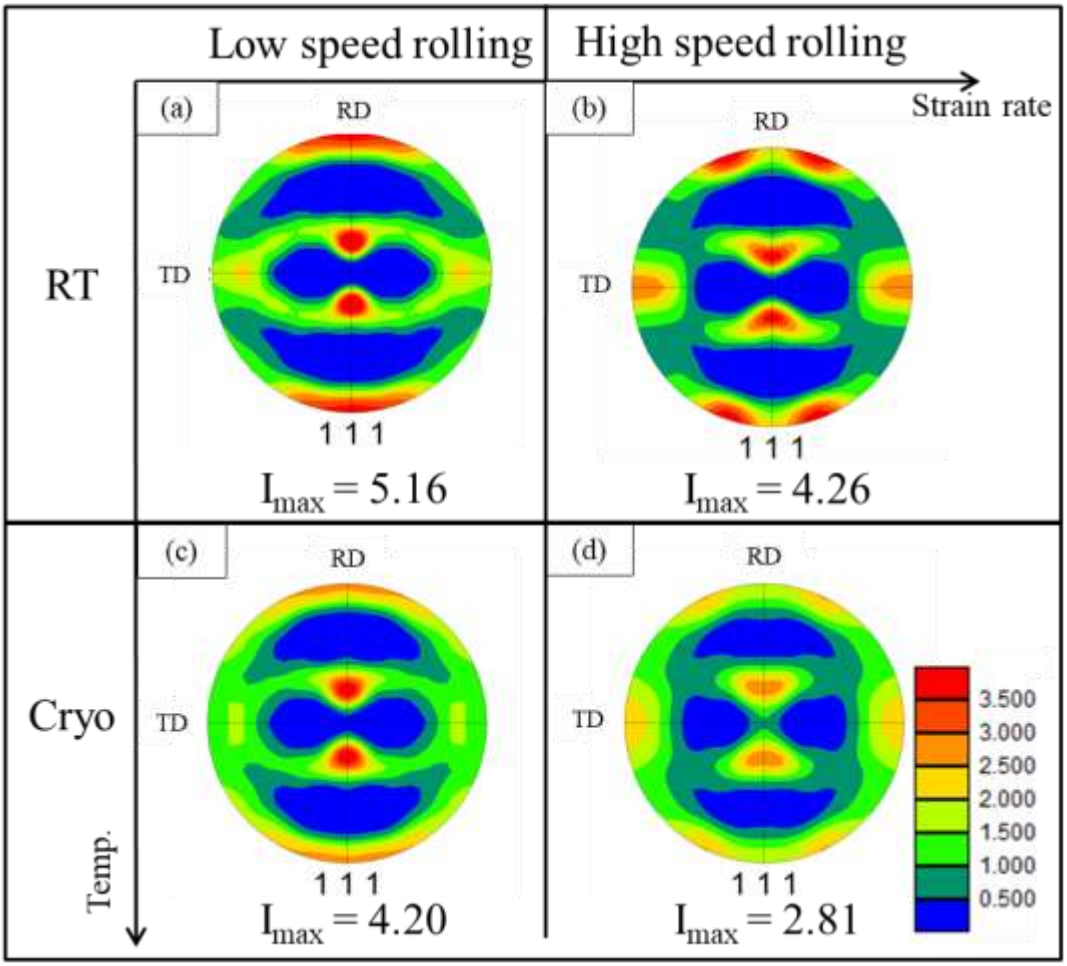

Fig. 4.5. {111} pole figure maps after various rolling methods (r=80%), (a) low-speed cold rolling (LSR), (b) high-speed cold rolling (HSR), (c) cryogenic low-speed rolling (C-LSR) and (d) cryogenic high-speed rolling (C-HSR)

4. Discussion

4.4.1 Estimation of temperature during rolling

Table 4.3. Selected material constants used for temperature calculation

	unit	**Specimen**	**Roll**
		Cu-5%Zn	Steel
Density	g/cm^3	8.86	7.87
Thermal conductivity	W/mK	234	73.3
Specific heat	J/gK	0.38	0.444
Friction coefficient		0.2	
	unit	**value**	
Rolling speed	m/min	1500 (HSR), 10 (LSR)	
Temp. (specimen)	K	100.00 (Cryo.), 298.15 (RT)	
Temp. (roll)	K	298.15	
Roll radius	m	0.265 (HSR), 0.185 (LSR)	
Thickness (initial)	mm	2.5	
Thickness (after)	mm	1.0	
Reduction in thickness		60%	
Mean flow stress	MPa	200	

In the cryogenic rolling methods, the specimen temperature increased after taking out from liquid nitrogen before the rolling. In other words, the sheet contacted with air at room temperature, which occurred rises of temperature. Initial temperature was assumed to 100K based on the result from chapter 3. The temperature estimation was carried out based on the calculation written in Chapter 3 [4.4, 4.13]. It was assumed that friction coefficient was 0.2 and that the mean flow stress was 200MPa for all the cases. Other material constants were shown in Table 3. Fig. 6 shows the estimated temperature after 60% single-pass rolling with various rolling methods. HSRed specimen results in the highest final temperature among four rolling methods. During the cryogenic rolling, the rolls at room temperature contacted with cryogenic specimen, heat transferred from the rolls to the specimen. The temperature of the C-LSRed sheet increased to 226 K during rolling resulted in temperature higher than RT due to relatively long contact duration in the rolling process. On the other hand, the specimen temperature increased by only 92K in C-HSR process, so the final temperature was 192K, which was the lowest temperature among the rolling methods and 105 K lower than the room temperature.

According to the estimation, the final temperature decreases with increasing the rolling speed. If the rolling speed was 100m/min, the temperature is estimated at 234K. Meanwhile, the temperature decreased

to 197K in the case of the rolling speed was 1000m/min. On the other hand, the final temperature showed the linear function relationship with the initial temperature. For instance, if the initial temperature was 200K, the final temperature was estimated to be about 286K. Therefore, in order to realize C-HSR, the rolling speed should be faster than 1000m/min and that the specimen should be cooled to temperature below 200K.

4.4.2 Effect of cryogenic high-speed rolling on microstructure evolution

Stacking fault energy (SFE) of the used alloy was approximately 50 mJ/m^2 where dislocation slip was primary deformation mode rather than twinning [4.7]. However, the lower deformation temperature induces deformation twinning. So it is regarded as the decrease in apparent SFE. This change in microstructural evolution was supposed to be responsible for the improvement in mechanical properties and electrical conductivity. When the SFE is below a critical value, the primary deformation mechanism is

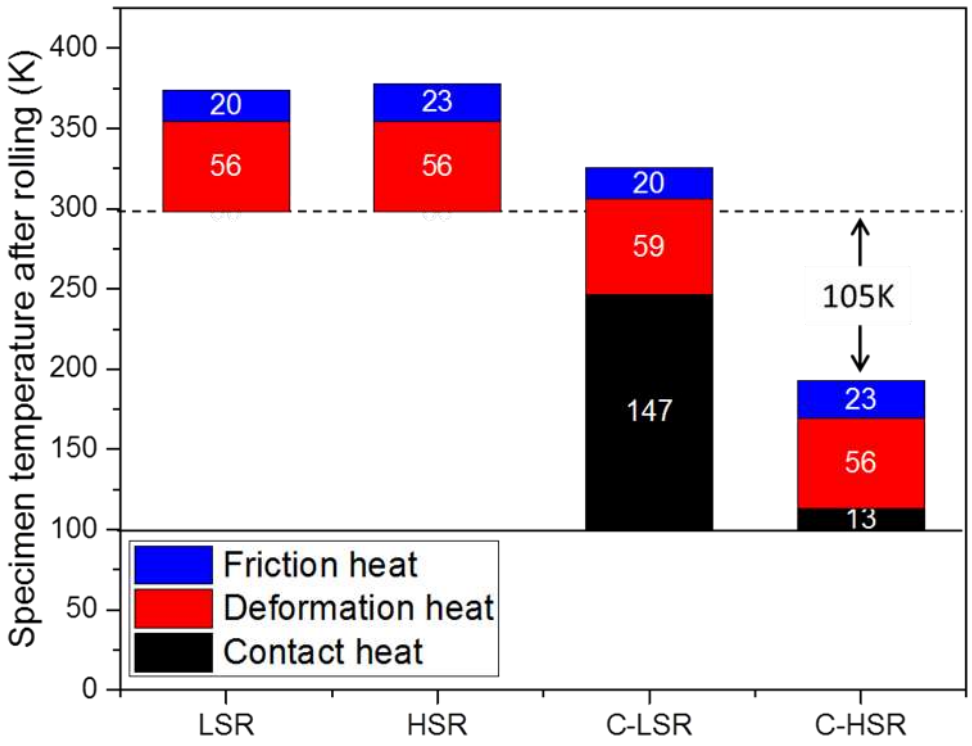

Fig. 4.6. Estimated temperature of specimen after 60% single-pass rolling in various rolling methods

twinning at room temperature and at a low strain rate. In contrast, twinning stress slightly depends on strain rate and deformation temperature, whereas slip stress is highly sensitive to strain rate and temperature [4.8].

An et al. [4.9] systemically reviewed about effects of external loading conditions on deformation mode on Cu and Cu alloys. The activation of a deformation mechanism shows a significantly high sensitivity to the ln Z value in materials with medium SFE [4.6, 4.7]. Plastic deformation under fairly mild conditions with low ln Z as a result of relatively strong dislocation activities, the microstructure is quite similar to that of a high-SFE material. Instead, the microstructures induced by the deformation under high ln Z conditions exhibit similar dislocation motions and features to those of low-SFE materials. According to Fig. 6 and Table 1, ln Z of each rolling process was 20.6 at LSR, 25.3 at HSR, 23.6 at C-LSR and 42.7 at C-HSR, respectively, if activation energy is assumed to 57kJ/mol [4.11].

It was reported that SFE and ln Z had a mutual effects on the deformation mode and deformation-induced microstructure in various Cu alloys [4.9, 4.12]. About 25 of ln Z was boundary line of slip and slip + twinning in case of SFE = 50mJ/m^2. Only C-HSR exceed the line which the deformation mode activated the deformation twinning. Therefore it is found that high Z value of C-HSR developed the features similar to those of low-SFE materials which were activation of deformation twinning in microstructural and brass-type texture and calculated ln Z had a good agreement with above references.

Generally, it can be easily considered combination of high strain rate and low temperature was incompatible because deformation heat was considerable under high strain rate, leading to the temperature increasing. However, according to the above results, although high strain rate increases deformation heat, the heat balance consequently showed that the lowest temperature can be realized by HSR due to low contact heat. Moreover, realizing the cryogenic rolling in industries, it is necessary for all equipment such as rolling rolls and guide as well as the specimens to decrease temperature because conducting materials could increase the temperature intensely due to deformation and friction heat generated by their high thermal conductivity. Therefore, the proposed rolling method in this study, where the specimen is only cooled with liquid nitrogen and immediately rolled at a sufficiently high rolling speed, which is leading to high Zener-Hollomon parameter to promote deformation twins, can be cost-reasonable and be feasible technique to attain Cu alloy sheets with well-balanced tensile strength and electrical conductivity.

4.5 Conclusions

1. Cryogenic high-speed rolling (C-HSR) process enabled simultaneous improvement in strength and electrical conductivity of Cu-5mass%Zn sheets.
2. The 60/80% low-speed rolled (LSR) sheet showed the tensile strength of 440/520MPa and the electrical conductivity of 59/52%IACS, respectively. On the other hand, the C-HSR showed improved properties with 503/580MPa and 62/54%IACS, respectively.
3. Deformation twins were most frequently formed in the C-HSRed specimen. The processed sheet showed typical brass-type rolling texture.
4. Heat balance showed only the C-HSR was able to keep the sheet temperature below the room temperature throughout the rolling process.

References

[4.1] H. Bahmanpour, A. Kauffmann, M.S. Khoshkhoo, Mater. Sci. Eng. A, 529 (2011) 230-236.

[4.2] B. Roy, N.K. Kumar, P.M.G. Nambissan, J. Das, AIP Adv., 4, (2014) 067101-8.

[4.3] P. Wang, J. Jie, C. Liu, L. Guo, T. Li, Mater. Sci. Eng. A, 715 (2018) 236-242

[4.4] Rolling theory committee ed., Theory and Practice of Flat Rolling, ISIJ, Japan, 1984. [In Japanese]

[4.5] S. Lee, Y. D. Im, R. Matsumoto, H. Utsunomiya, Mater. Sci. Forum, 941 (2018) 1523-1528

[4.6] Y.S. Li, N.R. Tao, K. Lu, Acta Mater., 56 (2008) 230-241.

[4.7] F.J. Humphreys and M. Hatherly, Recrystallization and Related Annealing Phenomena 2nd edition, Elsevier, 2004.

[4.8] A.H. Cottrell, Dislocations and Plastic Flow in Crystals. Oxford University Press, UK, 1953.

[4.9] X.H. An, S.D. Wu, Z.G. Wang, Z.F. Zhang, Progress in Materials Science, 101 (2019) 1-45.

[4.10] Y.S. Li, Y. Zhang, N.R. Tao, K. Lu, Acta Mater., 57 (2009) 761-772.

[4.11] A. Gangulee, J. Appl. Phys., 45 (1974) 3749-3756

[4.12] Y. Zhang, N.R. Tao, K. Lu, Acta Mater., 59 (2011) 6048-6058.

[4.13] J. Kokado, J. Jpn. Soc. Tech. Plasticity, 11 (1970) 816-824. [In Japanese]

Chapter 5

Strength and Electrical Conductivity of Cu-Al Alloy Sheets by Cryogenic High-Speed Rolling

5.1 Introduction

In face-centered cubic (FCC) materials with high stacking fault energy (SFE), dislocations move actively with cross slip, so that excellent ductility is observed and that low energy cellular structures are formed by mutual trapping, rearrangement, and annihilation with low piling up at grain boundaries [5.1-5.4]. On the other hand, FCC materials with low SFE show a rapid increase in dislocation density with plastic deformation, which leads to higher strength with less ductility [5.1,5.2]. This is because dislocations in low SFE materials are decomposed into partials. The very wide stacking fault ribbons between the partials make them difficult for cross-slip. Therefore, deformation twinning and shear banding are more frequently observed in the later stage of the deformation, leading to the grain refinement.

Deformation twins contribute to the strengthening of materials, which can be understood as the apparent grain refinement because twin boundaries act as obstacles for dislocation movement. Deformation twinning improves the work hardening ability, which increases the deformation homogeneity and delays the occurrence of necking and further contributes to a larger uniform elongation [5.6]. The twinning makes the increase in ductility. In addition, an increase in the electrical resistivity by twin boundaries is about one order of magnitude lower than that by the grain boundaries [5.6,5.7]. Therefore, if the material contains a high density of twin boundaries, the material is supposed to be effectively strengthened without losing conductivity much. The facts are practically crucial for electrical conductors.

Copper and copper alloys were studied to investigate the effects of SFE on the deformation of FCC metals because twinning is known to the dominant deformation mode when SFE is less

than 25mJ/m^2 [5.8]. SFE of Cu (=78mJ/m^2) decreases with the addition of alloy components, such as Si, Zn, and Al. Significantly decrease in SFE is observed when alloyed with Al, where SFE of Cu-7mass% Al is 6mJ/m^2 [5.9]. Cu-Al is a single-phase solid solution alloy unless the alloying amount excesses the stable solubility limit of Al in Cu (≈ 8 mass% in room temperature). The high strength is deserved from the finer grain size and limited dislocation recovery process, whereas the improved ductility is attributed to the higher work hardening, which is also due to the difficulty of dynamic recovery. It was reported that both the strength and ductility of Cu-Al alloy were improved with increasing Al contents by severe plastic deformation (SPD) and annealing [5.6, 5.10-5.12]. This phenomenon was reported as twinning induced plasticity (TWIP) [5.6]. Besides, the authors reported that cold-rolled Cu-Al alloy showed that a similar balance without annealing due to deformation twinning [5.13].

Twinning and dislocation are competitive deformation modes, depending on the SFE of the material. The deformation mode also depends on the processing conditions, especially the strain rate and deformation temperature [5.14-5.17]. For example, twinning is not observed in pure copper at moderate strain under room temperature; however, twins are readily formed when pure copper is shock deformed under high pressures [5.16], or deformed at cryogenic temperature [5.17].

In Chapter 4, it showed C-HSR promoted deformation twinning in relatively high SFE Cu alloy (Cu-5mass%Zn, SFE=50mJ/m^2), and the balance of strength and conductivity was improved [5.18]. However, C-HSR has not been confirmed with Cu alloys with intermediate and low SFE.

In Chapter 5, C-HSR was carried out with Cu-3Al (SFE = 25mJ/m^2) and Cu-7Al (SFE = 7mJ/m^2) to investigate the effects of rolling conditions and SFE. For comparison, low-speed rolling (LSR) was also carried out at room temperature. Mechanical properties and electrical conductivity of the rolled specimens were measured. EBSD analysis was conducted to investigate the microstructure evolution and during the rollings. In order to discuss the mechanism why C-HSR improves the properties, the modified Hall-Petch equation [5.9] and the Mayadas-Shatzkes (MS) model [5.19] were applied to estimate the contributions of deformation

Table 5.1. Chemical compositions of the alloys used (mass%)

Alloy	Al	Fe	Ni	Si	Cu
3Al	3.11	0.31	0.001	0.01	bal.
7Al	6.79	0.03	0.001	0.006	bal.

twinning, grain refinement, and dislocation density, separately.

5.2 Experimental procedure

Cast and cold-rolled 3mm-thick sheets were used. The chemical compositions of the sheets were Cu- *X* mass% Al (*X* = 3.1, 6.8, referred to as '3Al' and '7Al'), as shown in Table 1. To obtain similar mean grain sizes and to eliminate casting defects, the sheets were treated at 973K for 1800s and cooled in air. The heat-treated materials are referred to as 'initial material'. Microstructures of the initial materials are shown in Fig. 5.1. Annealing twins were observed in equiaxed grains. The mean grain size was 19.9μm in 3Al and 23.7μm in 7Al, respectively.

Cryogenic high-speed rolling (C-HSR) was carried out on a 2-high, high-speed rolling mill with a roll diameter of 530mm at 1500m/min. Before the C-HSR, specimens were soaked in liquid nitrogen for 900s and then supplied to the rolls within 3s. The sheet temperature before the C-HSR was around 100K, while that after the C-HSR was still under room temperature. Conventional low-speed cold rolling (LSR) with a roll diameter of 310mm at 5m/min was also carried out at room temperature as the control group. The thickness was reduced up to 60-70% by 2-pass rolling; the reduction at the first rolling pass was up to 30%, and the total reduction at the second rolling pass up to 60-70%. The total reduction in thickness *r* was estimated using the following equations,

$$r = \frac{h_0 - h_1}{h_0} \tag{5.1}$$

where *r* is the reduction in thickness, h_0 is the initial thickness (=3mm), h_1 is the thickness of the

Table 5.2. Rolling conditions on this study

	Low speed cold rolling (LSR)	Cryogenic high-speed rolling (C-HSR)
Roll diameter	∅ 310	∅ 530
Rolling speed	5m/min	1500m/min
Rolling temperature	RT	100K
Number of rolling passes	2	2
Pass schedule (total reduction)	First pass : 30% (Cu-3Al), 30% (Cu-7Al) Second pass : 67% (Cu-3Al), 60% (Cu-7Al)	
Equivalent strain rate	First pass : $1.1 \times 10^{1}\ s^{-1}$ Second pass : $5.8 \times 10^{0}\ s^{-1}$	$1.3 \times 10^{3}\ s^{-1}$ $1.7 \times 10^{3}\ s^{-1}$

rolled specimen. Meanwhile, the mean strain rate $\dot{\varepsilon}$ is estimated using the following equations,

$$\dot{\varepsilon} = \frac{2}{\sqrt{3}} \ln\left(\frac{h_0}{h_1}\right) \frac{v}{\sqrt{R(h_0 - h_1)}} \tag{5.2}$$

where R is the radius of rolls, and v is the peripheral speed of rolls. The mean strain rate of C-HSR and LSR was 0.7-1.2 × 10^3 s^{-1} and 3.5-5.2 × 10^0 s^{-1}, respectively.

After each rolling pass, the tensile test was performed at an initial strain rate of $1.67 \times 10^{-3}\ s^{-1}$ by Shimadzu Autograph AGI – 100kN. The specimens with a gauge length of 20mm and a width of 4.7mm were sampled from the rolled sheet by a wire-cutting machine. The electrical conductivity of the specimen was measured using the four-probe method and expressed as a percent of International Annealed Copper Standard (%IACS) which is following,

$$\%\text{IACS} = \frac{\kappa_{specimen}}{\kappa_{annealed\ Cu}} = \frac{R_{annealed\ Cu}}{R_{specimen}} \tag{5.3}$$

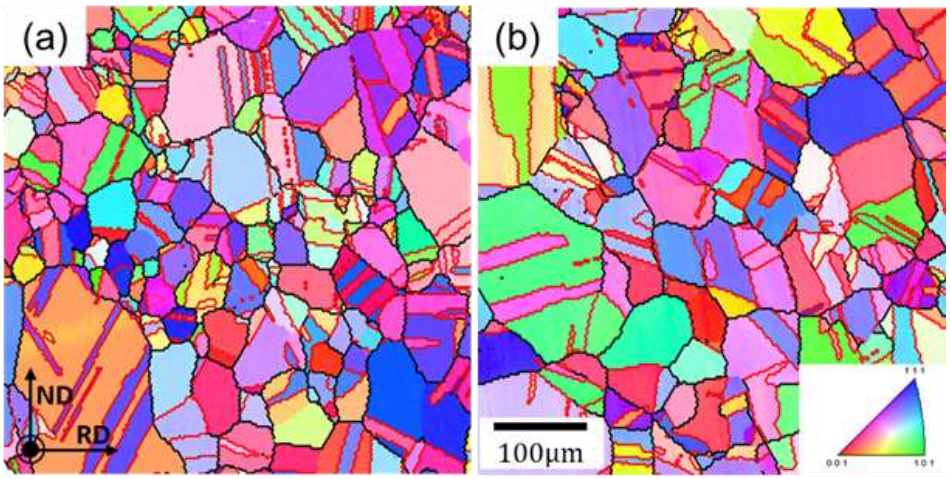

Fig. 5.1. Microstructure of initial Cu-Al alloy sheets (a) Cu-3Al, (b) Cu-7Al, the red line shows Σ3 boundaries and the black line shows high angle grain boundaries

where $\kappa_{specimen}$ and $\kappa_{annealed\ Cu}$ is the conductivity of the specimen and that of the standard annealed copper, respectively. $R_{specimen}$ is the electrical resistivity of the specimen measured by the four-probe method, and $R_{annealed\ Cu}$ is the electrical resistivity of the annealed copper (=1.7241 × 10^{-8} Ωm, ASTM standard B193-02), respectively. The tensile axis and electric current were parallel to the rolling direction.

Microstructures were observed on the plane perpendicular to the transverse direction (TD) by a Scanning Electron Microscope with electron backscatter diffraction (SEM-EBSD) analysis. Microstructural information, e.g., statistic distributions of grain size, misorientation, and Σ3 twin boundaries, were obtained by TSL-OIM analysis software Ver. 4. The specimens were prepared by mechanical polishing until #4000 of SiC paper, 1μm, and 0.3μm of Al_2O_3 powder, followed by electro-polishing in a solution (H_3PO_4 : C_2H_5OH : H_2O = 50ml : 50ml : 100ml), with a voltage of 5V at 0^oC. The operation voltage of the SEM was 15 kV. The step size in the Kikuchi-pattern scanning was 0.15μm. The points with confidence index (CI) less than 0.1 were excluded in the analysis.

Quantitative X-ray diffraction (XRD) analyses of the samples were carried out using a diffractometer with Cu K_α radiation, operating at 1.2kW by Rigaku SmartlabSE. A series of

θ-2θ scans were performed to the XRD patterns at room temperature. An annealed pure copper sheet after full grain growth was used as a reference to remove the instrumental broadening of XRD peak for calculating both the microstrain and the crystallite size. The scans were implemented at room temperature to measure the dislocation density after the rolling.

5. 3. Results

5.3.1 Mechanical and electrical properties

Fig. 5.2 shows the nominal stress-strain curves of the rolled sheets obtained by the tensile test. Tensile strength increased with increasing number of rolling passes. In the case of 3Al, C-HSRed specimens showed higher 0.2% proof stress and tensile strength than those of the LSRed ones. The 1-passed LSRed specimen presented 0.2% proof stress of 371MPa and tensile strength of 416MPa, while the C-HSRed specimen presented 442 and 524MPa, respectively. Increased strength by the C-HSR was also observed after the 2-pass rolling. 0.2% proof stress and tensile strength after the 2-pass C-HSR were 568 and 665MPa, respectively. Meanwhile, those were 518 and 605MPa in the case after LSR, respectively.

In comparison with 3Al, the simultaneous increase in strength, as well as ductility, was

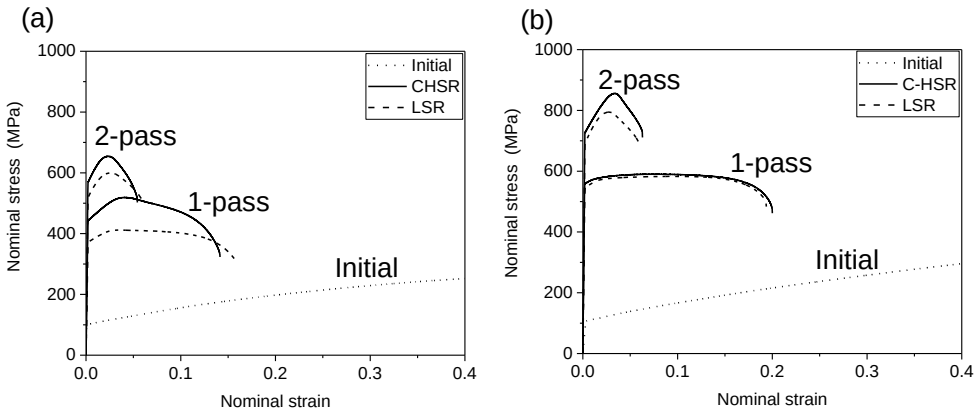

Fig. 5.2. Nominal stress-strain curve of rolled Cu-Al sheets by tensile test, (a) Cu-3Al and (b) Cu-7Al

observed in 7Al. Meanwhile, the C-HSR showed a less strengthening effect with 7Al than that with 3Al. The flow curves of 1-pass C-HSR and LSR 7Al were not so different. The C-HSR specimen after 1-pass rolling showed the 0.2% proof stress of 558MPa and the tensile strength of 590MPa, while the LSR showed 523MPa and 580MPa, respectively. However, the tensile strength of the 2-pass C-HSR was higher than that of the LSR. It was 841MPa, which was 40MPa higher than that of LSR.

Zhang et al. [5.20] reported that dynamic plastic deformation with high strain rate ($\dot{\varepsilon} = \sim 10^3\ s^{-1}$) at liquid nitrogen temperature (LNT-DPD) of Cu-Al alloy improved yield strength compare to deformation with low strain rate at room temperature (RT-QSC). This strengthening was obviously observed with SFE exceeding 25mJ/m^2. However, yield strengths of Cu-4.5wt%Al (SFE=12mJ/m^2) were similar in the case of both of the LNT-DPD and the RT-QSC. In other words, a similar trend of strength was shown between the LSR and C-HSR with very low SFE.

Ordinarily, the strengths both of the LSR and the C-HSR specimens are improved with increasing Al amount. However, the elongation of the rolled 7Al was higher than those of the 3Al. This trend can not be explained by the traditional trade-off relationship. Liu et al. [5.6] and An et al. [5.11] also reported that the simultaneous improvement in strength and ductility in Cu-Al alloys. This mechanism is related to “twinning induced plasticity (TWIP)” phenomena, which is due to the deformation twinning during the tensile test.

5.3.2 Electrical conductivity

Electrical conductivities after the two rolling methods are not much different. The conductivity decreased slightly with an increasing reduction in thickness, as shown in Fig. 5.3. Increasing Al contents decreased conductivity remarkably. The conductivity was 20.9%IACS at the initial state of Cu-3Al while it was 16.2%IACS of Cu-7Al. Although the C-HSRed Cu-3Al decreased to 20.8%IACS after 1-pass rolling and 19.6%IACS after 2-pass rolling, they were slightly higher than those of the LSRed specimens, which were 20.4 and 19.4%IACS,

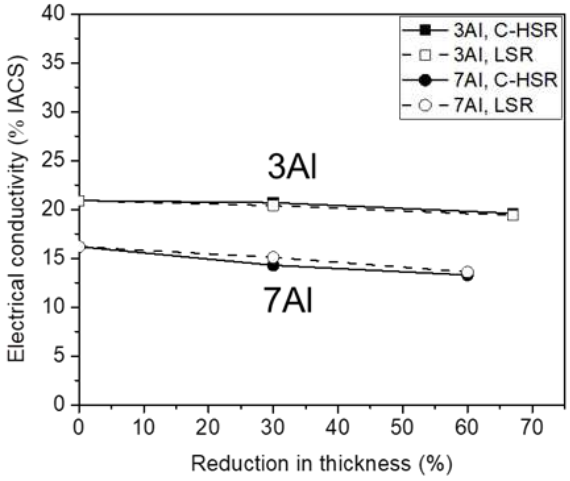

Fig. 5.3. Electrical conductivity of rolled specimens as a function of rolling reduction in thickness

respectively. Meanwhile, a decrease in the conductivity by rolling was larger in 7Al. The electrical conductivity of C-HSRed 3Al decreased to 14.3 and 13.3%IACS, while LSRed 3Al decreased to 15.1 and 13.6%IACS, respectively. Although it was reported that the electrical conductivities of copper alloys are more affected by plastic deformation than aluminum alloys due to work hardening [5.21]. However, it is a notable even though C-HSR increased the strength more than that of LSR, the electrical conductivities of the two are not much different.

5.3.3 Microstructures

Fig. 5.4 shows the microstructures of the rolled Cu-3Al obtained by the EBSD analysis. Deformation twins appeared locally with a narrow width in elongated grains in the 1-passed 3Al, as shown in Fig. 5.4(a). Compared to the LSR, the C-HSR showed higher fractions of Σ3 boundaries, i.e., twin boundaries (Fig 5.4b). After the second pass, shear bands appeared near the grains where the deformation twinning has occurred. Similar microstructural evolution during plastic deformation was observed in [5.22]. The C-HSRed specimen showed a higher fraction of shear bands than that of the LSR, as shown in Fig. 5.4(c) and (d). The fragmentation of grains by shear banding was also observed after the second pass, which contributes to the

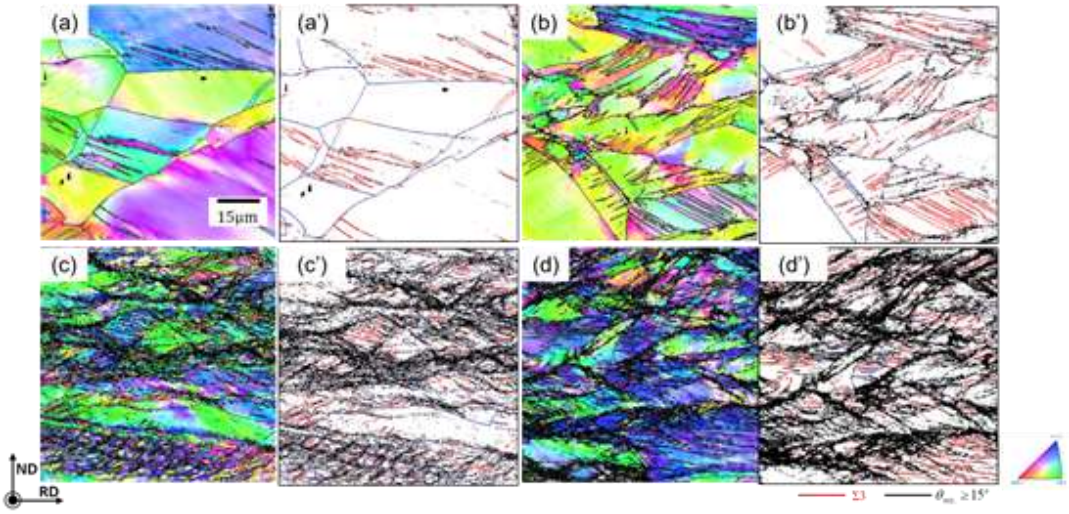

Fig. 5.4. Microstructure of Cu-3Al sheets after (a) 1-pass LSR, (b) 1-pass C-HSR, (c) 2-pass LSR, (d) 2-pass C-HSR, (a) to (d) inverse pole figure map showing ND orientation, (a') to (d') showing the Σ3 boundaries (red) and high angle grain boundaries (black)

grain refinement. In the case of C-HSR, the intersections of shear bands turn into rhomboidal prisms observed in the microstructure.

Fig. 5.5 showed the EBSD maps of the 7Al. In contrast to the 3Al, LSR and C-HSR showed similar microstructures in the 7Al. After the 2-pass rolling, the deformation twins and shear bands appeared within selected elongated grains, which were more narrower than those of 3Al. It is supposed to be thought that deformation twins were not developed in the case of C-HSRed 7Al with very low SFE.

Statistical distributions of the misorientation angle in the rolled sheet were compared in Fig 5.6. C-HSR increased misorientation angle under 15 degrees, i.e., low angle grain boundaries and 60^{o} of Σ3 twin boundaries in the case of 3Al. On the other hand, 7Al showed similar low angle grain boundary (LAGB, 2^{o} < misorientation angle < 15^{o}) distribution both with LSR and C-HSR, though the increasing fraction of Σ3 boundary was observed.

Fig. 5.7 shows the summary of EBSD analysis, which were (a) Σ3 twin boundary density, (b) LAGB density, and (c) mean intercept length (a reciprocal of the mean grain size). The boundary density is estimated as the total length of grain boundaries within a unit area, which is evaluated using the following equation. [5.23,5.24]

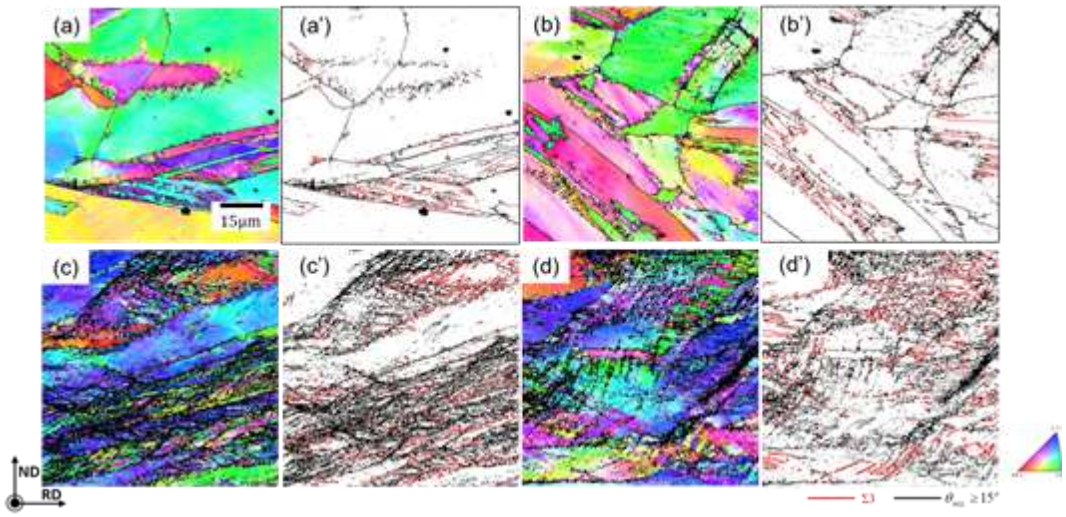

Fig. 5.5. Microstructure of Cu-7Al sheets after (a) 1-pass LSR, (b) 1-pass C-HSR, (c) 2-pass LSR, (d) 2-pass C-HSR, (a) to (d) inverse pole figure map showing ND orientation, (a') to (d') showing the Σ3 boundaries (red) and high angle grain boundaries

$$S_v = \frac{l_B}{A} \tag{5.4}$$

where S_v is the boundary density, l_B is the total length of grain boundaries obtained by EBSD, and A is the measured area. Therefore Σ3 twin boundary density ($S_v^{\Sigma 3}$), and LAGB density (S_v^{LAGB}), can be expressed as follows,

$$S_v^{\Sigma 3} = \frac{l_B^{\Sigma 3}}{A} \tag{5.5}$$

$$S_v^{LAGB} = \frac{l_B^{LAGB}}{A} \tag{5.6}$$

where $l_B^{\Sigma 3}$ is the total length of Σ3 boundaries, l_B^{LAGB} is the LAGB length. Each boundary lengthes were obtained by Fig. 5.1, 5.4 and 5.5.

At first, Fig. 5.7(a) showed the Σ3 twin boundary density. In 3Al, it increased at the 1st pass then decreased at the second pass. Ths C-HSRed specimen showed higher twin density than the

LSRed one. In 7Al, both rolling methods showed a similar twin density after the 1st pass, and then the C-HSRed specimen showed more increase than the LSR. C-HSR showed higher LAGB density than that of LSR, both of 3Al and 7Al, as shown in Fig. 5.7(b). Moreover, it was observed that the LAGB density was gradually improved with rolling passes. At last, it was observed that the mean intercept length increased with the number of rolling passes, as shown in Fig. 5.7(c). The mean intercept length was measured by the linear intercept method in *TSL OIM Analysis 7* software. The C-HSR showed longer intercept length than the LSR in all cases. SFE dependence of grain size is observed in the Cu-Al alloys consistent with previous investigations

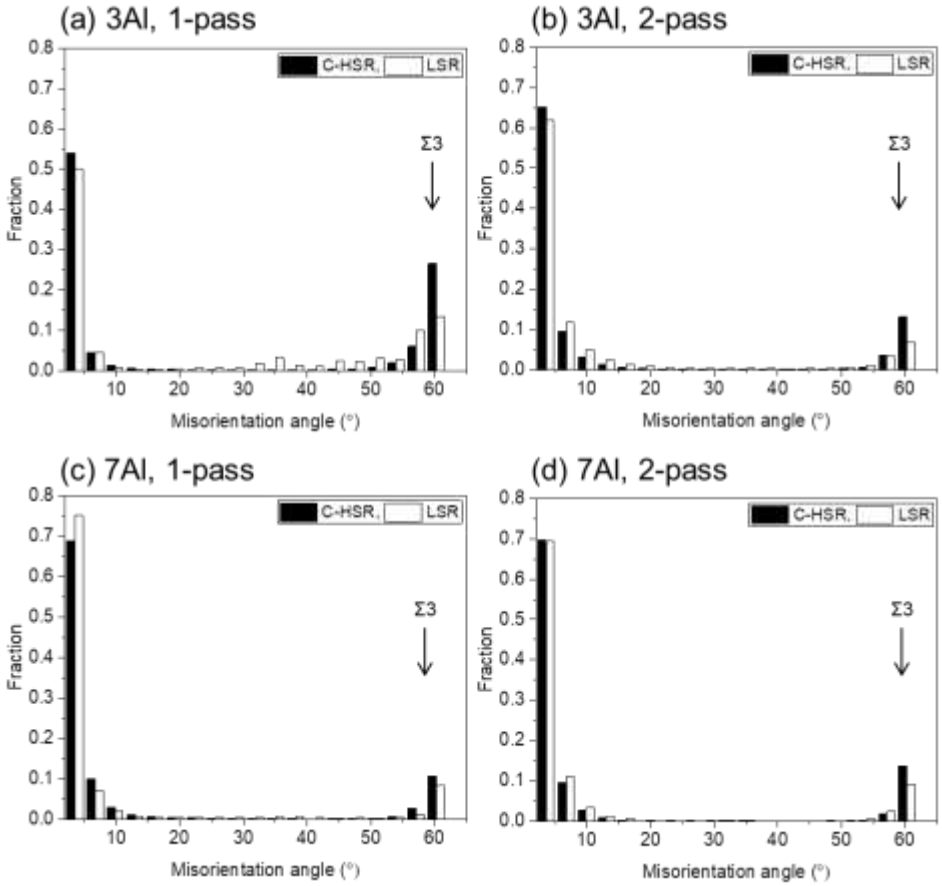

Fig. 5.6. Histograms of misorientation angle of rolled sheets, (a) Cu-3Al, 1-pass, (b) Cu-3Al, 2-pass, (c) Cu-7Al, 1-pass and (d) Cu-7Al, 2-pass, (open column) C-HSR, (closed column) LSR

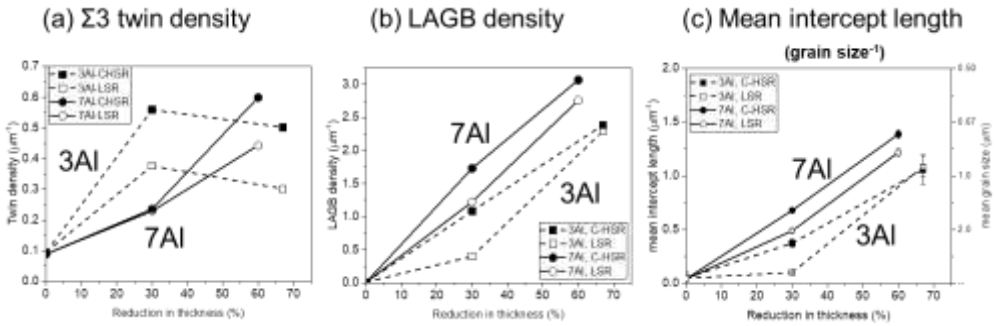

Fig. 5.7. Summary of EBSD analysis, (a) Σ3 twin boundary density , (b) Low angle grain boundary (LAGB), and (c) Mean intercept length

[5.1,5.25,5.26] that decreasing SFE leads to finer grains in the HPT Cu-Zn alloys and ECAP Cu-Al alloys.

Zhang et al. [5.20] found that the cryogenic temperature deformation of Cu-Al alloy mainly developed the deformation twinning due to suppression of dislocation movement. Nanoscale deformation twinning dominates the plastic deformation process. With decreasing SFE, the twinning tendency is enhanced and is accompanied by a decreasing twin/matrix lamella thickness and a reduction in grain sizes in cryogenic temperature deformation. Meanwhile, deformation at room temperature occurs mainly by twinning, and the resultant microstructure is similar to that at low temperature when SFE is below 25mJ/m^2. The similar results were comparable to those of the above reference, in which the C-HSR was attributed to grain refinement and deformation twinning at 3Al, but less sensitive at 7Al.

In materials of low SFE, shear bands develop within a highly twinned microstructure characterized by thin twin/matrix lamellae that are formed at the early stage of deformation [5.27-5.29]. Hong et al. [5.30] found that the development of shear bands in a Cu-4.5wt%Al alloy processed utilizing dynamic plastic deformation (DPD) with strain rate in the range of 10^2 – 10^3 s^{-1}. The shear bands is known to develop until the maximum shear strain $\gamma_{max} < 4$; (1) Deformation twins were formed inside many grains at low strains. (2) The density of deformation twins increases, and then bending, necking, and detwinning of original twin/matrix lamellae have occurred ($\gamma_{max} < 2$). (3) The twin lamellae are changed to the de-twinned

dislocation structure ($2 < \gamma_{max} < 4$).

Based on these observations, it is concluded that the decreasing of Σ3 twin boundary density of 3Al after the second rolling pass is due to the shear banding during the second pass. Meanwhile, in 7Al, extra-low SFE induces the deformation twinning even after the 2-pass rolling, leading to the increasing of twin density.

5.3.4 X-ray diffraction analysis

The XRD peaks of the rolled specimens are presented in Fig. 5.8, indicating an increased peak broadening with an increasing number of rolling passes. After the rolling, the intensity of 111 peak emphasized, which is a similar trend with EBSD results. In addition, C-HSR showed a higher intensity of 220 peak than that of LSR at the same rolling pass regardless of the Al component. It is thought that the brass component was more evolved after the C-HSR [5.31].
The dislocation density ρ can also be measured by XRD analysis. The average crystallite size

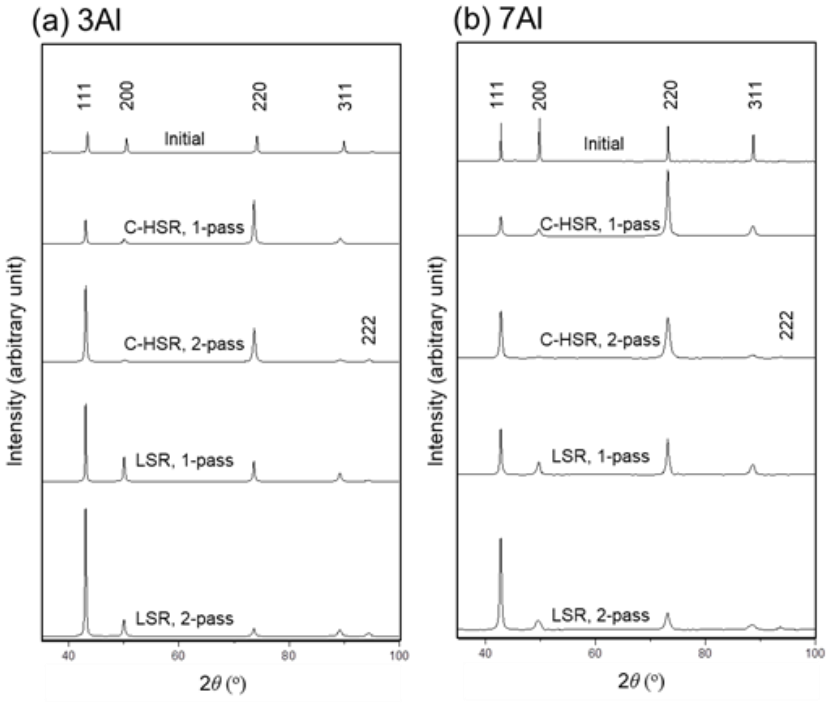

Fig. 5.8. XRD patterns of rolled Cu-Al alloy sheets, (a) Cu-3Al, (b) Cu-7Al

Table 5.3. The measured crystallite size and dislocation density of the rolled sheets

	Rolling method	Initial	LSR-1pass	C-HSR-1pass	LSR-2pass	C-HSR-2pass
3Al	**Crystallite size (nm)**	362	181	206	90	42
	Dislocation density ($x10^{14}$ /m^2)	0.189	0.560	1.14	2.43	3.49
7Al	**Crystallite size (nm)**	69	50	35	35	13
	Dislocation density ($x10^{14}$ /m^2)	0.245	3.65	5.45	7.07	7.83

d_{XRD} and the microstrain $<\varepsilon^2>^{1/2}$ can be estimated from the Scherrer-Wilson method through the peaks by the XRD peak broadening, which was following relationship [5.32,5.33],

$$\rho = \frac{2\sqrt{3}<\varepsilon^2>^{\frac{1}{2}}}{d_{XRD}b} \quad (5.7)$$

where b is the Burgers vector which is $2\sqrt{3}a$, and a is the lattice parameter of the specimen.

Table 5.3 shows the dislocation density of the rolled sheets. The C-HSRed specimen showed higher dislocation density than the LSR regardless of the rolling passes and alloying amount. The accumulation of dislocation density was higher in 7Al than 3Al due to lower stacking fault energy [5.34]. After the 2-pass of C-HSR, the dislocation density of 7Al was 7.8×10^{14} /m^2, while 3Al was 3.5×10^{14} /m^2.

5. 4. Discussion

5.4.1 Modified Hall-Petch equation

In order to understand the strengthening mechanisms of the rolled samples, yield stress was calculated based on the characteristics of deformation microstructures. For the calculation of yield stress, it is assumed that strengthening contributions from dislocation grain boundaries and deformation twin boundaries could be involved. Thus, the yield stress of materials can be written as,

$$\sigma_y = \sigma_0 + \sigma_{dis} + \sigma_{gb} + \sigma_{dt} \quad (8)$$

where σ_0 is the friction stress of Cu-Al alloys, σ_{dis} is the contribution of dislocations, σ_{gb} is the contribution of grain boundaries, and σ_{dt} is the contribution of the deformation twin boundaries.

According to Rohatgi et al. [5.9], friction stress, σ_0 of Cu-Al alloys showed a straight-line fit with at % of Al contents, which was following equation,

$$\sigma_0 = 1.4 + 6.0(\mathrm{C}_{Al})^{2/3} \ \text{[MPa]} \quad (5.9)$$

where C_{Al} is Al concentration (at.%). Thus, the frictional stress was assumed 23.4MPa at Cu-3Al and 37.1MPa at Cu-7Al, respectively.

Meanwhile, the work-hardening effect by rolling also contributes to the flow stress using the Taylor equation [5.35], which relates the flow stress of a material to its dislocation density.

$$\sigma_{dis} = M\alpha Gb\sqrt{\rho} \quad (5.10)$$

where M is the Taylor factor (3.04), α is a material constant (0.42) [5.36,5.37], G is the shear modulus (=43GPa), b is the Burgers vector (0.256nm), ρ is the dislocation density.

The strengthening due to grain boundaries and deformation twins can be estimated by modifying the Hall-Petch relationship and writing as a linear sum of the strength due to the untwinned and twinned grains [5.9] :

$$\sigma_{gb} + \sigma_{dt} = \left(kd^{-1/2}\right) \times (1 - f_t) + \left(kD^{-1/2}\right) \times f_t \tag{5.11}$$

where d is the grain size neglecting twins, D is the intertwin spacing of deformation twins [5.53,5.54], f_t is the twin boundary fraction in the HAGB, and k is the Hall-Petch parameter which is 0.34 at Cu-3Al and 0.48 at Cu-7Al [5.9], respectively. In this calculation, the values of f_t, D, and d were used those shown in Fig. 5.6, 5.7(a) and 5.7(c), respectively. In addition, the twin density of the initial specimen was counted out in the calculation, so that the effect of annealing twins were excluded in the strengthening of deformation twins (σ_{dt}).

Fig. 5.9 shows the yield stresses of the extrapolated based on the modified Hall-Petch equation and by experiment. In the case of 1-passed Cu-3Al, strengthening by the dislocation density and Hall-Petch effect (GB+twin) showed almost equivalent. Comparing to LSR, the increased strength of C-HSR could be considered due to the increase of dislocation density and deformation twin boundaries. After the 2-pass rolling, the contribution of dislocation density significantly increased, while the effect of the twin boundary decreases, and the effect of grain boundary increased. This effect was more clear in C-HSR than LSR.

In the case of Cu-7Al, it was calculated the strengthening by dislocation density was more effective than that of 3Al in all rolling pass. 1-pass Cu-7Al was shown that the contribution by deformation twins was slightly smaller, while the contribution by grain boundary was higher

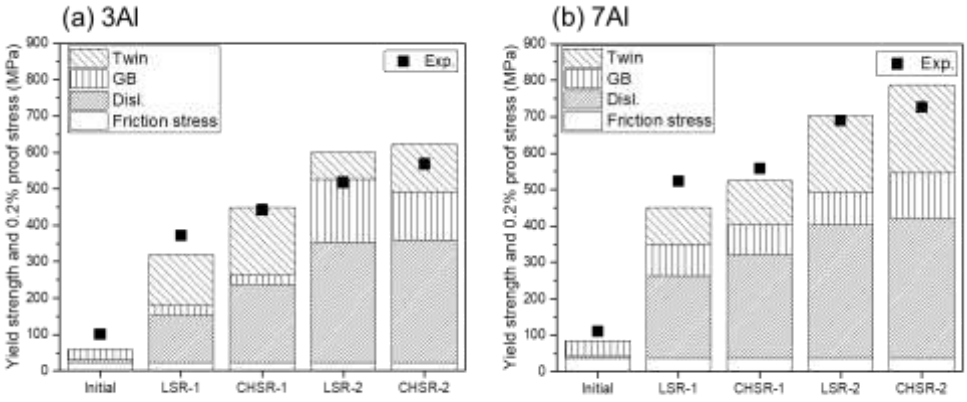

Fig. 5.9. Calculated yield strength and experimental 0.2% proof stress (a) Cu-3Al, (b) Cu-7Al, (Twin) contribution for deformation twin boundaries

than that of Cu-3Al.

The Cu-32%Zn alloy with the SFE of 14 mJ/m^2 was subjected to the dynamic plastic deformation (DPD) at liquid nitrogen temperature, during which the deformation process was classified into three stages: the planar dislocation activities (ε = 0-0.2), deformation twinning (ε=0.2-0.8) and shear banding (ε= 0.8-1.6) [5.34]. In addition, very low SFE in Cu-15 at%Al takes place the shear banding from the true strain of 0.4 at the RT [5.13]. The SFEs of the Cu-3Al and Cu-7Al alloys are 25 mJ/m^2 and 6 mJ/m^2, respectively. The equivalent strain is 0.4 at 1-pass rolling then, 0.9 of the stain is supplied after the 2-pass rolling (the total equivalent strain is 1.3). Therefore even in the case of 1-passed Cu-7Al, deformation twinning induced shear banding was already initiated to generate high angle grain boundaries, owing to the increase in the contribution of grain boundaries. However, the contribution of deformation twins increased after 2-pass rolling. It could also be thought due to very low SFE maintaining both of deformation twinning and shear banding. Enhanced strength in Cu-Al alloys by C-HSR is due to the finer mean grain size, twin density, and the higher dislocation density.

5.4.2 Electrical resistivity change after rolling

According to Matthiessen's rule. The electrical resistivity of metallic materials can increase as

$$R = R_0 + R_{gb} + R_d + \cdots \tag{5.12}$$

where R_0 is the bulk resistivity, R_{gb} is the resistivity induced by the grain boundaries, and R_d is the electron scattering by dislocation.

It is generally accepted [5.38] that there are two major contributions to the increase of resistivity in the size-effect regime: electron scattering at external surfaces or interfaces of the copper film and internal grain boundaries. In 1970, Mayadas and Shatzkes (MS) [5.19] proposed a model for the resistivity, *R*, of the polycrystalline film:

$$R_0 + R_{gb} = R_0 \left[1 - \frac{3}{2}\alpha + 3\alpha^2 - 3\alpha^3 \ln\left(1 + \frac{1}{\alpha}\right)\right]^{-1} \quad (5.13)$$

where α is defined as,

$$\alpha = \left(\frac{\beta}{1-\beta}\right)\frac{\lambda}{d} \quad (5.14)$$

where λ is the electron mean path (39nm [5.39]), d is the mean grain size, and β is the GB reflection coefficient, which varies from 0 for total transmission to 1 for total reflection. M-S equation was suggested to explain the rapid increase of electrical resistivity of the thin film. However, this relation is reported to be well-matched in the case of plastic deformed bulk materials [5.52].

In order to classify the effect of two different grain boundaries, which were twin and conventional grain boundary, the value of β=0.0164 for Σ3 CSL boundaries [5.40] and β=0.5 for other random grain boundaries was used within the range of values found in the literature [5.19, 5.39, 5.40].

Typically, the primary reason for increasing electrical resistivity was used to be considered by the dislocation density during plastic deformation [5.49-5.51]. For the simplification, the resistivity contributed by dislocation density, R_d, was assumed as the remained resistivity of the experimental resistivity (R_{exp}), minus the resistivity of grain and twin boundaries ($R_0 + R_{gb}$), which is following,

$$R_d = R_{exp} - \left(R_0 + R_{gb}\right) = R_{exp} - R_0 \left[1 - \frac{3}{2}\alpha + 3\alpha^2 - 3\alpha^3 \ln\left(1 + \frac{1}{\alpha}\right)\right]^{-1} \quad (5.15)$$

And then, the increment of electrical resistivity by dislocations (R_d), is calculated by $\rho * \Delta^{disl}$, where ρ is once again dislocation density and Δ^{disl} is the specific dislocation resistivity [5.50, 5.51].

In contrast to the yield strength, the electrical conductivity, which is usually referred to as the counterpart of the strength, is reduced by the addition of alloying elements. It is conceivable that the effect of dislocation density to increase electrical resistivity will be significant, as the effect of dislocation density on increasing the strength.

Fig. 5.10 shows the comparison between the predicted and the measured electrical resistivity. As opposed to the yield strength, most of the contribution to electrical resistivity was determined by dislocation density. Of course, the contribution by GB and TB increased with the increasing rolling pass or Al contents; however, those were considered minor changes were comparing to the effect of dislocation density.

Fitted $\Delta^{disl.}$ is 4.14×10^{-24} for Cu-3Al and 1.58×10^{-23} Ωm for Cu-7Al, respectively. Although these results are much higher than that of pure copper, it is valid when compared with other studies [5.6, 5.10, 5.11] that are known to decrease the electrical conductivity by increasing strain as work hardening increases. This increase of the resistivity with increasing strain was similar to reference [5.49].

Based on the eq. (5.13) and ref. [5.48], mean grain size is less dependent on the electrical conductivity if the mean grain size is in micrometer scales, then the conductivity intensely rises when the size reached below the nanocrystalline. A principal reason to make ultrafine grain

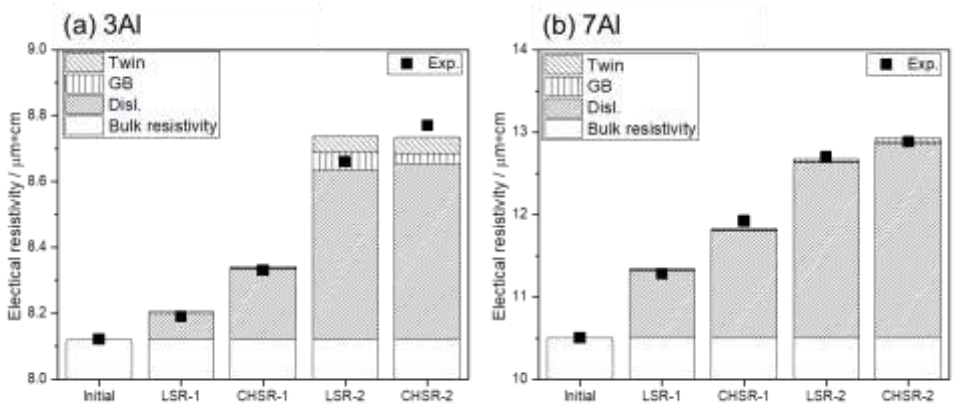

Fig. 5.10. Measured electrical resistivity (Exp.) and predicted resistivity with components (bar), (a) Cu-3Al, (b) Cu-7Al

(UFG) during plastic deformation was absolute an amount of strain. It was reported that the required rolling strain to form the nano-sized grain was 80% in the case of Cu-35Zn alloy [5.55, 5.56]. Since the reduction in thickness at this study was up to 70% (equivalent true strain = 1.1), it was not enough to reach for the evolution of UFG microstructure. Therefore, it could be concluded that the increase in the electrical resistivity dominantly resulted from the dislocation density when the grain/twin is not evolved to submicron or nano-size.

5.4.3 Effect of C-HSR and Al contents

The balance of strength, ductility, and electrical conductivity is shown in Fig. 5.11. It was observed that the strength-elongation balance and the strength-conductivity balance of C-HSRed Cu-3Al was improved comparing to that of LSR. On the other hand, the results of Cu-7Al showed a similar balance with both (strength – elongation) and (strength – conductivity).

Electrical conductivity by both the rolling methods was increased with increasing rolling pass. Increasing Al contents increased the resistivity remarkably and decreasing slope with rolling. However, even though C-HSR increased the strength than that of LSR, though the electrical

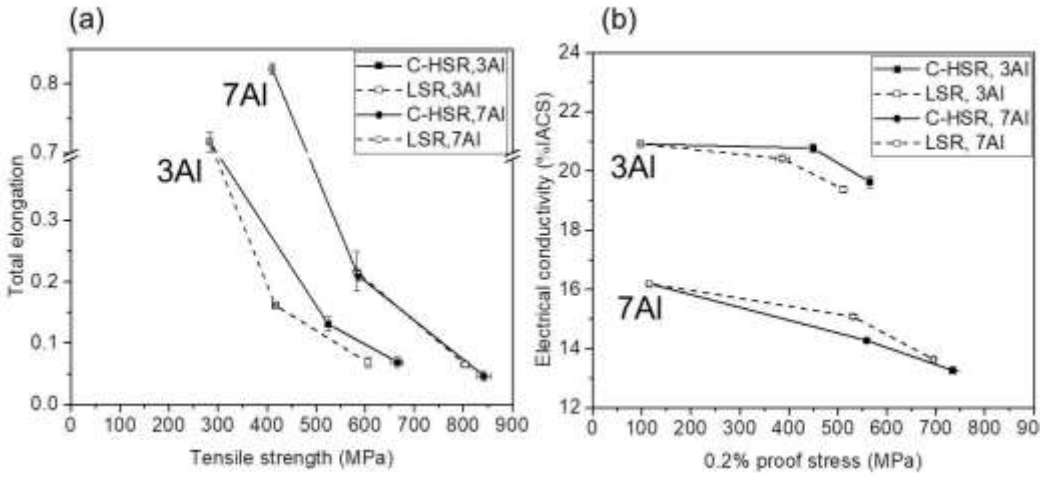

Fig. 5.11. Balance of strength, elongation and electrical conductivity, (a) tensile strength – total elongation, (b) 0.2 proof stress - %IACS conductivity

Table 5.4. Estimated temperature and ln Z of during the rolling

	Rolling method	LSR-1pass	C-HSR-1pass	LSR-2pass	C-HSR-2pass
3Al	**Temperature prior to rolling (K)**	100	100	298	298
	Temperature after rolling (K)*	330	140	396	216
	Ln Z	28 ~ 30	69 ~ 94	24 ~ 31	48 ~ 94
7Al	**Temperature prior to rolling (K)**	100	100	298	298
	Temperature after rolling (K)*	341	152	435	258
	Ln Z	21 ~ 24	52 ~ 75	17 ~ 25	34 ~ 76

***Temperature after the rolling was estimated with considerations of deformation heat, friction heat, and contact heat between the specimen and roll. The details are refered in chapter 4.

conductivities of the two are not much different.

It was reported that SFE and ln Z had a mutual effect on the deformation mode and deformation-induced microstructure in various Cu alloys where Z is the Zener-Hollomon parameter, which is following as [5.47]

$$\ln Z = \ln \dot{\varepsilon} + \frac{Q}{RT} \tag{16}$$

where $\dot{\varepsilon}$ is the strain rate, Q is the activation energy for diffusion, R is the gas constant, and T is the deformation temperature. Table 5.4 shows the estimated temperature before and after the rolling and ln Z if the activation energy is assumed to 72.5 kJ/mol [5.57]. Temperature after the rolling was estimated with considerations of deformation heat, friction heat, and contact heat between the specimen and roll. Other details of the estimation are given in previous section

Table 5.5. Material constants for estimation of temperature change

	unit	**Specimen**		**Roll**
		Cu-3Al	Cu-7Al	AISI E 52100
Density	g/cm^3	8.43	7.98	7.81
Thermal conductivity	W/mK	86.5	74.0	46.6
Specific heat	J/gK	0.383	0.377	0.475
Friction coefficient		0.2		
Rolling speed	m/min	1500(C-HSR) , 5(LSR)		
Temp. (specimen)	K	100.00(C-HSR). 298.15(LSR)		
Temp. (roll)	K	298.15		
Roll radius	m	0.265(C-HSR), 0.185(LSR)		
Thickness (Ini)	mm	3mm		
Thickness (aft)	mm	1mm		
Rolling step	mm	3->2->1mm		
Mean flow stress	MPa	Cu-3Al, 1-pass : 200, 2-pass : 330 Cu-7Al, 1-pass : 250, 2-pass : 430		

4.4.1. The used material constants and the estimated temperature is shown in Table 5.5 and Fig. 5.12, respectively. According to Zhang et al. [5.20], the deformation mode and microstructure characteristics of the Cu alloys were summarized in an SFE – ln Z space using a few dozen literatures. In the case of SFE = $25mJ/m^2$, mixed microstructure with ultrafine grains (UFG) + nano-twins (NT) + nano-grains (NG) were evolved by slip and twinning when ln Z is less than approximately 32. Then, NT + NG microstructure were evolved if ln Z exceeds the 32. However, there is no boundary line if the SFE is less than $14mJ/m^2$. NT + NG microstructure by twinning is mainly evolved regardless of ln Z, which could be the reason why C-HSR showed similar properties with LSR in the case of Cu-7Al.

In other words, the sensitivity of the deformation mechanism to ln Z is related to SFE of Cu alloys. It is reported that the evolution of the microstructure is less dependent on ln Z for high SFE and extremely low SFE. Meanwhile, the activation of a deformation mechanism shows a significantly high sensitivity to the ln *Z* value in Cu alloys with medium SFE [5.15, 5.20, 5.45,

5.46]. These are founded on the improved balance after the C-HSR in the case of Cu-5%Zn [5.18] with relative high SFE and Cu-3Al with intermediate SFE Cu alloy, but comparable balance in the case of 7Al compared to conventional cold rolling. Therefore, for the effective application of C-HSR,-extra-low SFE Cu alloy should be avoided.

As this results, cryogenic high-speed rolling (C-HSR) in this study, where the specimen only in cooled with liquid nitrogen and immediately rolled at a sufficiently high rolling speed, which is leading to high Zener-Hollomon parameter to promote deformation twin and dislocation density, can be cost-reasonable (compared to other cryogenic processes) and attain the improved balance of (strength - electrical conductivity) and (strength – total elongation) in the case of Cu-3Al, but this process was less sensitive to the improvement in the case of Cu-7Al due to extra low SFE.

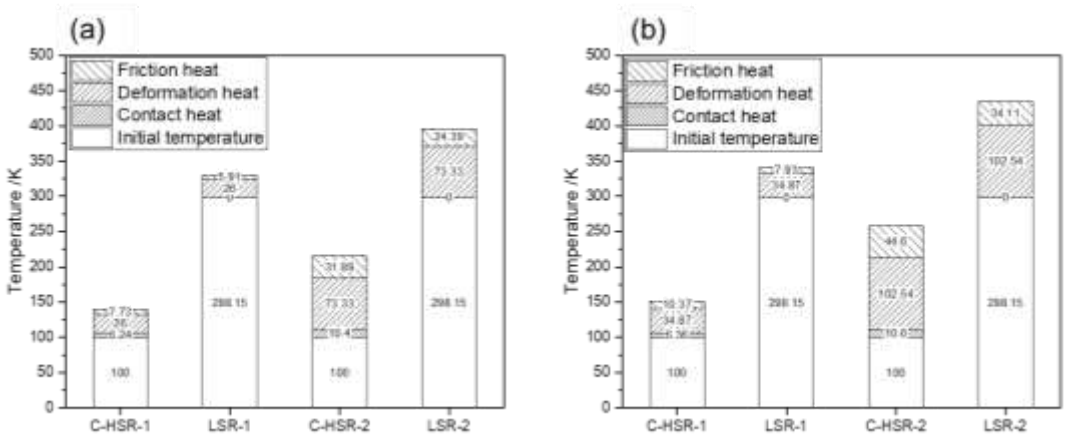

Fig. 5.12. Estimated temperature of specimen in rolling process, (a) Cu-3Al and (b) Cu-7Al

5.5 Conclusions

Cryogenic high-speed rolling (C-HSR), where the specimen is cooled in liquid nitrogen and supplied to high speed rolling with rolls at room temperature, of the Cu- *x* Al (*x* = 3.1, 6.7 mass %, referred as 3Al and 7Al, respectively) was carried out to investigate mechanical and electrical properties. The remarks obtained are as follows,

1. C-HSR showed a more strengthening effect than LSR. 2-pass rolled (0.2% proof stress/tensile strength) were (568/665MPa) for Cu-3Al and (726/841MPa) for Cu-7Al with comparable elongation.
2. C-HSR is more effective to the Cu-3Al with higher SFE in balance both of (strength – ductility) and (strength – conductivity). However, it is less sensitive in the case of Cu-7Al due to its extremely low SFE. For improvement of the balance by C-HSR, extra-low SFE Cu alloy is less effective.
3. Yield strength and electrical conductivity were predicted using the modified Hall-Petch equation and modified MS model. The experimental results were in agreement; dislocation density, as well as grain boundaries and deformation twins, were contributed to yield strength; meanwhile, only dislocation density was dominant to increase electrical resistivity.

References

[5.1] S. Qu, X.H. An, H. J. Yang, C. X. Huang, G. Yang, Q. S. Zang, Z. G. Wang, S. D. Wu, Z. F. Zhang, Acta Mater., 57 (2009) 1586

[5.2] N. R. Tao, Z. B. Wang, W. P. Tong, M. L. Sui, J. Lu, K. Lu K, Acta Mater., 50 (2002) 4603

[5.3] D. A. Hughes, N. Hansen, Acta Mater., 45 (1997) 3871

[5.4] N. R. Tao, K. Lu, Scripta Mater., 60 (2009) 1039

[5.5] D. Kuhlmann-Wilsdorf, Materials Science and Engineering A, 113 (1989) 1

[5.6] R. Liu, Z. J. Zhang, L. L. Li, X. H.An, Z. F. Zhang, Scientific Report, 5 (2015) 9550

[5.7] L. Lu, Y. Shen, X. Chen, L. Qian, K. Lu, Science, 304 (2004) 422

[5.8] F. J. Humphreys, M. Hatherly, Recrystallization and related annealing phenomena, 2nd edition, Elsevier, (2004), pp. 35

[5.9] A. Rohatgi, K. S. Vecchio, G. T. Gray III, Metall. Mater. Trans., A 32 (2001) 138

[5.10] X. H. An, S. Qu, S. D. Wu, Z. F. Zhang, J. Mater. Res., 26 (2011) 407

[5.11] X. H. An, S. Qu, S. D. Wu, Z. F. Zhang, R. B. Figueiredo, N. Gao, T. G. Langdon, Scripta Mater, 66 (2012) 227

[5.12] Y. Z. Tian, L. J. Zhao, S. Chen, D. Terada, A. Shibata, N. Tsuji, J. Mater. Sci., 49 (2014) 6629

[5.13] S. Lee, Y. D. Im, R. Matsumoto, H. Utsunomiya, Mater. Sci. Forum, 941 (2018) 1523

[5.14] D. H. Warner, W. A. Curtin, S. Qu, Nat. Mater., 6 (2007) 876

[5.15] Y. S. Li, Y. Zhang, N. R. Tao, K. Lu, Acta Mater., 57 (2009) 761

[5.16] D. H. Lassila, T. Shen, B. Y. Cao, M. A. Meyers, Metall. Mater. Trans. A, 35 (2004) 2729

[5.17] T. H. Blewitt, R. R. Coltman, J. K. Redman, Journal of Applied Physics, 28 (1957)

651

[5.18] S. Lee, R. Matsumoto, H. Utsunomiya H. Fujiwara, J. Jpn. Inst. Copper, 58-1 (2019) 52

[5.19] A. F. Mayadas, M. Schatzkes, Phys. Rev. B, 1 (1970) 1382

[5.20] Y. Zhang, N.R. Tao, K. Lu, Acta Mater. 59 (2011) 6048

[5.21] C.S. Çetinarslan, Mater. Des. 30 (2009) 671

[5.22] G.H. Xiao, N.R. Tao, K. Lu, Mater. Sci. Eng. A. 513–514 (2009) 13

[5.23] Y. Miyajima, S.-Y. Komatsu, M. Mitsuhara, S. Hata, H. Nakashima, N. Tsuji, Philosophical Magazine, 90 (2010) 4475

[5.24] M. Detrois, R. L Goetz, R. C. Helmik, S. Tin, Materials Science and Engineering A, 647 (2015) 157

[5.25] Y.H. Zhao, Z. Horita, T.G. Langdon, Y.T. Zhu, Mater. Sci. Eng. A. 474 (2008) 342

[5.26] L. Balogh, T. Ungár, Y. Zhao, Y.T. Zhu, Z. Horita, C. Xu, T.G. Langdon, Acta Mater. 56 (2008) 809

[5.27] Y. Nakayama, K. Morii, Trans. Jpn. Ins. Metals 7 (1982) 422

[5.28] K. Morii, Y. Nakayama, Trans. Jpn. Ins. Metals 22 (1981) 857

[5.29] M. Hatherly, A. S. Malin, Scripta Metallurgica 18 (1984) 449

[5.30] C.S. Hong, N.R. Tao, X. Huang, K. Lu, Acta Mater. 58 (2010) 3103

[5.31] J.A. Jiménez, M. Carsí, O.A. Ruano, F. Peñalba, Steel Res. Int. 80 (2009) 50

[5.32] G. K. Williamson, R. E. Smallman, III. Philos. Mag. 1 (1956) 34

[5.33] R. E. Smallman and K. H. Westmacott, Philos. Mag. 2 (1957) 669

[5.34] Y. Pang, P. Li, H. S. Kim, Y. Gong, Y. Shen, L. Sun, X. Zhu, Mater. Trans. 56 (2015) 1658

[5.35] G. I. Taylor, Proc. R. Soc. London. Ser. A, 145 (1934) 362

[5.36] F. F Lavrentev, Mater. Sci. Eng. 46 (1980) 191

[5.37] I. Bailey and P. B. Hirsch, Philos. Mag. B 5 (1960) 485

[5.38] D. Josell, S.H. Brongersma, and Z. Tőkei, Annu. Rev. Mater. Res. 39, (2009) 231

[5.39] S.M. Rossnagel and T.S. Kuan, J. Vac. Sci. Technol. B 22 (2004) 240

[5.40] C. Mathieu, L. Dongping, G. Daniel, G. Hong, Phys. Rev. Appl. 2 (2014) 044007.

[5.41] W. Steinhogl, G. Schindler, G. Steinlesberger, M. Engelhardt, Phys Rev. B. 66 (2002) 075414.

[5.42] G. Ramaswamy, A.K. Raychaudhuri, J. Goswami and S. A. Shiveshankar, J. Phys. D 30 L5 (1997)

[5.43] C. Hull, International Critical Tables, 6 (1930) McGraw-Hill, p.167

[5.44] L. M. Clarebrough, M. E. Hargreaves, M. H. Loretto, Philos. Mag. 7 (1962) 73.

[5.45] W. S. Zhao, N. R. Tao, J. Y. Guo, Q. H. Lu, K. Lu, Scripta Mater. 53 (2005) 745-749.

[5.46] Y. S. Li, N. R. Tao, and K. Lu, Acta Mater. 56 (2008) 230

[5.47] C. Zener, J. H. Hollomon, Journal of Applied Physics, 15 (1944) 22

[5.48] M. Shimada, M. Moriyama, K. Ito, S. Tsukimoto, M. Murakami, J. Vac. Sci. Technol. B Microelectron. Nanom. Struct. 24 (2006) 190.

[5.49] V.S. Sarma, J. Wang, W.W. Jian, A. Kauffmann, H. Conrad, J. Freudenberger, Y.T. Zhu, Mater. Sci. Eng. A. 527 (2010) 7624

[5.50] Z.S. Basinski, J.S. Dugdale, A. Howie, Philos. Mag. 8 (1963) 1989

[5.51] R.A. Brown, J. Phys. F Met. Phys. 7 (1977) 1477

[5.52] T.S. Orlova, A.M. Mavlyutov, A.S. Bondarenko, I.A. Kasatkin, M.Y. Murashkin, R.Z. Valiev, Philos. Mag. 96 (2016) 2429

[5.53] R.L. Fullman, JOM. 5 (1953) 447

[5.54] Y. Zhang, N.R. Tao, K. Lu, Scr. Mater. 60 (2009) 211

[5.55] C. Kobayashi, T. Sakai, A. Belyakov, H. Miura, Philos. Mag. Lett. 87 (2007) 751

[5.56] H. Miura, H. Nakao, T. Sakai, Trans. Mater. 48 (2007) 2539

[5.57] A. Mishra, B.K. Kad, F. Gregori, M.A. Meyers, Acta Mater. 55 (2007) 13

Chapter 6

Applications of cryogenic high-speed rolling

6.1 Introduction

According to previous chapters, it has been confirmed that the cryogenic high-speed rolling changes the microstructure evolution of the copper alloy, which leads to improved mechanical and electrical properties. This is because the deformation mode due to the increase of the Z parameter has shifted. However, this process is expected to be possible with other metals and alloys. In this chapter, other metals and alloys have been investigated for their application to cryogenic high-speed rolling. It was predicted how it would be applied to other materials, including other materials, including other Cu, Al, Fe, Mg, and high entropy alloy (HEA).

6.2 Cryogenic high-speed rolling for other materials

6.2.1 Other Cu alloys and FCC materials

Cu-Ni-Si-based alloy series is a precipitation hardening type alloy, and mechanical properties are determined by Ni_2Si precipitates, which leads to the high strength. When this alloy is solution heat treatment, SFE is expected to be very low due to the alloy component of Ni and Si. However, if the precipitation occurs, the matrix will remain only of Cu, which leads to increasing of SFE.

Muchime et al. including the author reported [6.1] that Cu–2.3％Ni–0.55％Si mass% sheets, which had been aged at 723K after solution treatment at 1173K or 1273K, were subsequently processed by either low–speed rolling (LSR) with a rolling speed of 5 m/min at RT, or C-HSR with a rolling speed of 1500m/min. The total reduction in thickness of 78％ was applied in 3-pass operation. Mechanical properties, electrical conductivity, and microstructure of the

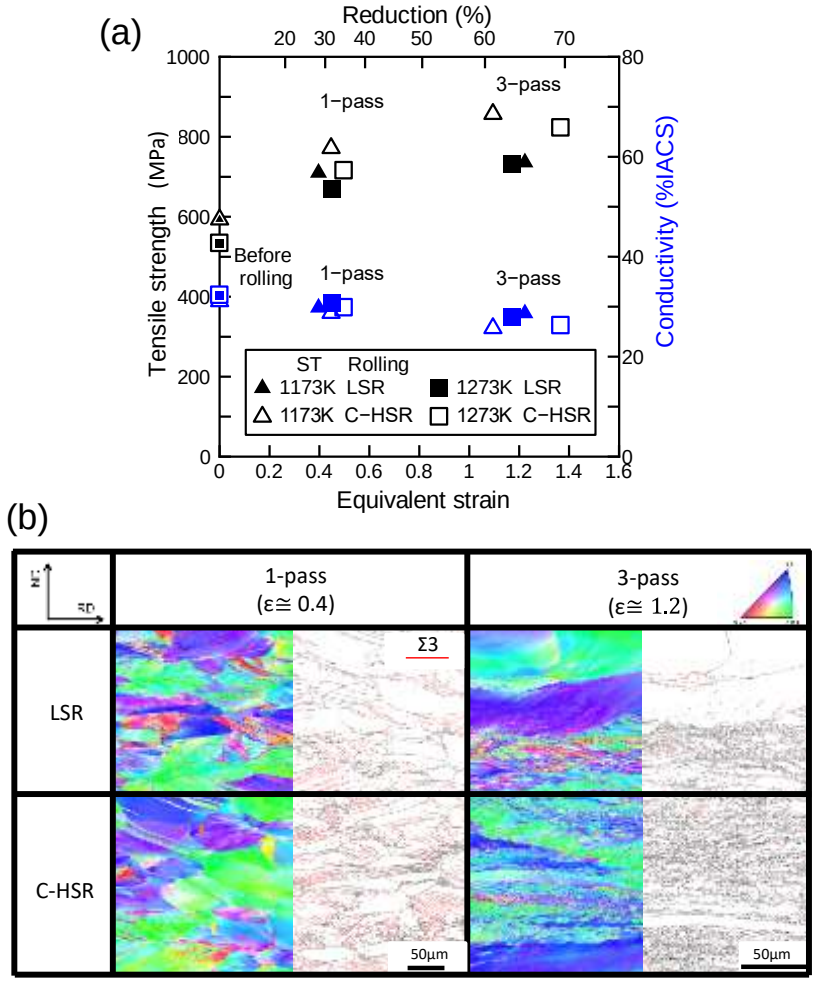

Fig. 6.1 (a) Change in tensile strength and electrical conductivity of Cu–Ni–Si sheet after solution treatment at 1173 K or 1273 K as a function of equivalent strain of rolling. (b) IPF map showing ND orientation（left） and twin grain boundary map (right) of Cu–Ni–Si sheet rolled after solution treatment at 1273 K [6.1].

as-rolled sheets were investigated. The LSRed sheet showed the tensile strength of 731 MPa and electrical conductivity of 27.9％IACS, while the C-HSRed sheet showed 822 MPa and 26.2％IACS. The C-HSRed sheet contains more deformation twins and shear bands in the microstructure than the LSRed sheet, as shown in Fig 6.1.

Lee et al. [6.2] reported that the application of cryo-rolling to the commercial Al alloys is anticipated to refine their grains to the sub-micrometer level with less plastic deformation than the SPD processes, as shown in Fig. 6.2(a) to (c). The cryo-rolling was more effective in enhancing both tensile strength and yield strength of the 5083 Al alloy, as shown in Fig. 6.2(d),

at least 10% increase than those of the alloy rolled at room temperature with the same reduction ratio, mainly due to the suppression of dynamic recovery during deformation at cryogenic temperature. According to this study, if the C-HSR is applied to Al alloys, more improvement of mechanical property is expected due to the higher Z parameter.

Tao et al. [6.3] reported that texture evolution during strain-induced BCC and HCP phase transformation in 304L stainless steel at cryogenic temperature. The BCC {100} planes are mostly oriented with their plane-normal parallel to the loading direction at the beginning of the

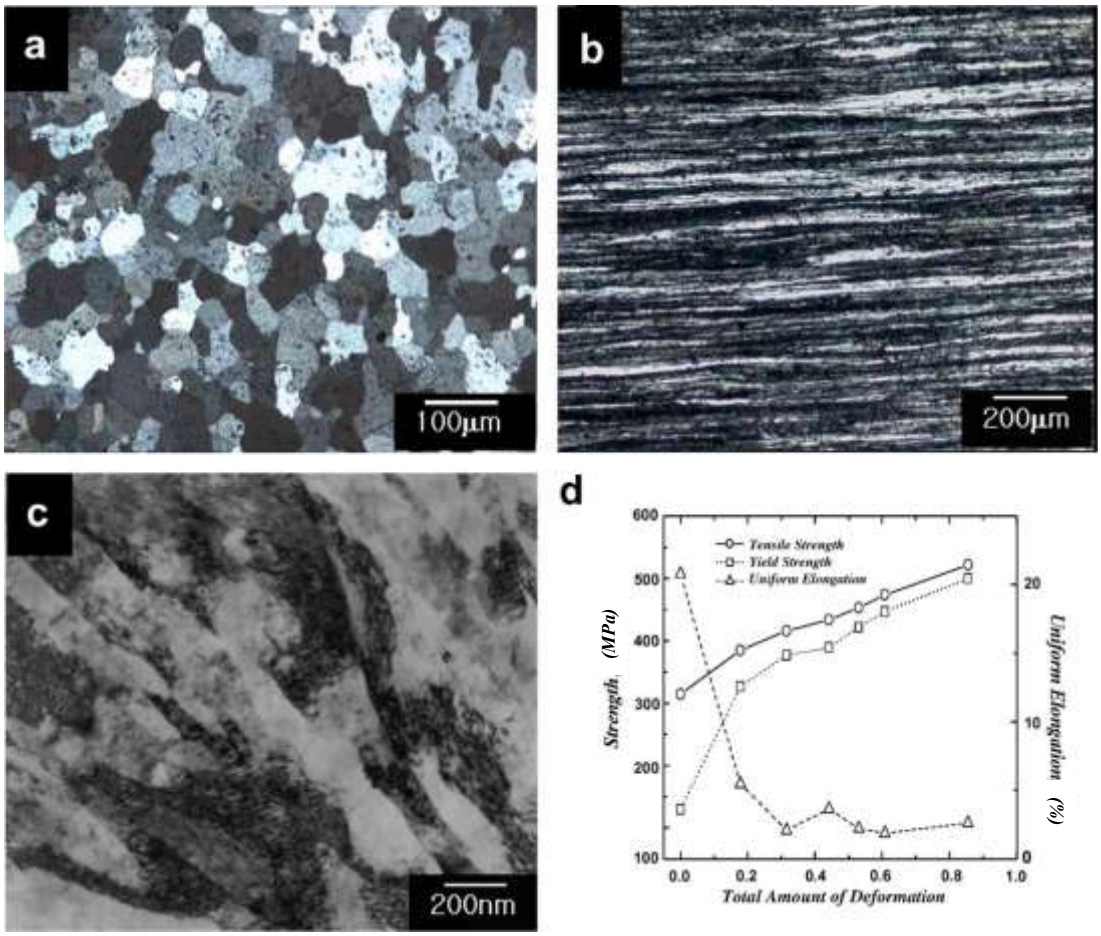

Fig. 6.2. Microstructures and tensile properties of the 5083 Al alloy with the amount of deformation at cryogenic temperature: (a) optical micrograph of the starting material, annealed at 540 C for 2 h; (b) optical micrograph, deformed 85% at cryogenic temperature; (c) TEM micrograph, deformed 85% at cryogenic temperature, and (d) tensile properties as a function of the total amount of deformation at cryogenic temperature [Lee et al., 6.2].

phase transformation, and this texture is weakened during the subsequent compressive deformation. In the case of FCC to HCP transformation, it is less dependent on the grain orientation, although the FCC grains with {111} plane-normal at an angle close to 40^{o} to the loading direction transform and the {0001} plane-normal of the newly formed HCP phase tends to rotate toward the loading direction during the texture evolution.

The martensitic phase transformation is the most representative strengthening method of iron, and it will lead to the improvement of strength through cryogenic deformation. However, the cryogenic temperature in this study was only maintained to 203K. Cryogenic high-speed rolling needs to be guaranteed to maintain the lower temperature so that the larger fraction of the martensite phase transformation is achieved.

6.2.2 HCP materials

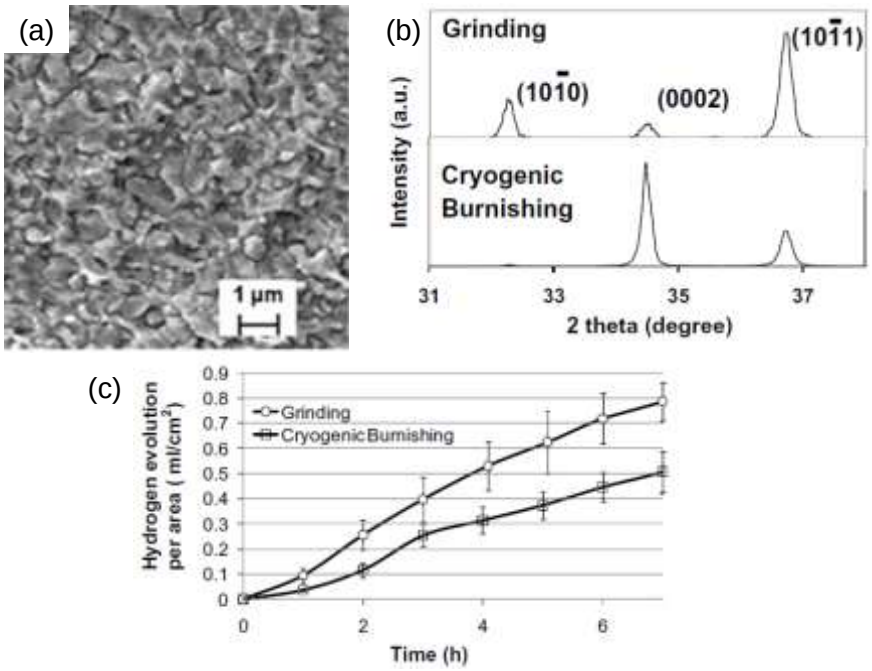

Fig. 6.3 (a) SEM photograph of the microstructure near the surface (b) X-ray diffraction spectra of surfaces after cryogenic machining (burnishing) and conventional grinding (c) Comparison of corrosion resistance of AZ31 Mg alloy in 5 wt.% NaCl after different treatments: hydrogen evolution [Pu et al., 6.4].

Pu et al. [6.4] reported that the cryogenic machining of Mg-Al-Zn alloy for enhanced corrosion resistance. Liquid nitrogen is sprayed onto the tool-workpiece interface during cryogenic machining of Mg alloy to suppress the increase in temperature. Fig. 6.3(a) shows an ultrafine-grained surface layer was produced on Mg-Al-Zn alloy. In addition, a strong basal texture was also created on the burnished surface, as shown in Fig. 6.3(b). The corrosion resistance, one of the most critical magnesium alloy properties, was remarkably improved, compared to the surface by a conventional grinding, as shown in Fig. 6.3(c).

Referring to the above study, it is believed that the improved corrosion resistance is due to the strong basal texture that occurred by cryogenic deformation. If the cryogenic high-speed rolling is applied to the magnesium alloy, the basal texture of the entire sheet also will be formed, not just the surface. Therefore, it is possible to expect not only the improvement of corrosion resistance but also increasing strength by grain refinement.

6.2.3 Other materials

High-entropy alloys (HEAs), referred to entropy-stabilized solid solution alloys with multi-principal elements having approximately equiatomic concentrations, have triggered substantial research interest in the last decade [6.5 – 6.7]. The heavy lattice distortion and the sluggish diffusion induced by mixing multiple elements enable HEAs to possess exceptionally high structural stability and excellent mechanical properties.

Lin et al. [6.8] reported that the cryogenic-deformation-induced phase transformation from the FCC to HCP structure in a FeCoCrNi HEA was observed. Atomic-scale investigation revealed that the HCP phase formed via the glide of Shockley partial dislocations on every other {111} FCC plane. In addition, Stepanov et al.[6.9] reported that the microstructure evolution in CoCrFeNiMn HEA during 77 and 293K. Although the deformation twins developed at both temperatures, it was confirmed that the case of cryogenic rolling was further formed. The improved yield strength was observed in the case of cryogenic rolling, which was 1500MPa; meanwhile, that of room temperature was 1200MPa, respectively.

These results show characteristics similar to the C-HSRed copper alloy in previous chapters. In order to apply microstructure control by cryogenic plastic deformation to actual metal forming, the C-HSR, proposed metalworking process in this study, is expected to be more practical. In addition, it is believed that C-HSR is applicable not only to correspond in copper alloys, but a wide selection of materials is also possible.

6.3 Conclusions

For various metallic materials, the possibilities have been confirmed that the cryogenic high-speed rolling could exhibit improved properties. In addition to commercial alloys such as Al, Fe, and Mg, as well as new types of metal materials such as high entropy alloy (HEA), the cryogenic high-speed rolling method is considered to be applicable.

References

[6.1] R. Muchime, S. Lee, R. Matsumoto, H. Utsunomiya, K. Mihara, H. Fujiwara, J. Japan Ins. Copper 59-1 (2020) [in press]

[6.2] Y. B. Lee, D. H. Shin, K.-T. P, and W. J. Nam, Scr. Mater. 51 (2004) 355-359

[6.3] K. Tao, D. W. Brown, S. C. Vogel, and H. Choo, Metall. Mater. Trans. A 37 (2006) 3469

[6.4] Z. Pu, S. Yang, G. –L. Song, O. W. Dillon Jr., D. A. Puleo, and I. S. Jawahir, Scr. Mater. 65 (2011) 520

[6.5] J. W. Yeh, S. K. Chen, S. J. Lin et al. Adv. Eng. Mater. 6 (2004) 299

[6.6] Y. Zhang, T. T. Zuo, Z. Tang et al. Prog. Mater. Sci. 61 (2014) 1

[6.7] D. B. Miracle, O. N. Senkov, Acta Mater. 122 (2017) 448

[6.8] Q. Lin, J. Liu, X. An, H. Wang, Y. Zhang, and X. Liao, Mater. Res. Lett. 6 (2018) 236

[6.9] N. Stepanov, M. Tikhonovsky, N. Yurchenko, D. Zyabkin et al. Intermetallics 59 (2015) 8

Chapter 7

Summary

In the present study, microstructure control of Cu alloy sheets by cryogenic high-speed rolling has been investigated. The following remarks are derived.

In Chapter 1, background, motivations, purpose, and outline of this research work are described.

In Chapter 2, multi-pass cold rolling of the Cu-15at%Al was carried out to observe microstructure evolutions and to measure the change in mechanical properties. Microstructure evolution in the rolling process can be subdivided into three stages: deformation twinning, shear banding, and the intersection of shear bands. Ultrafine grains are formed by intersections of shear bands, which are introduced by deformation twinning. The balance between strength and elongation of this alloy without annealing was similar to those in literature by severe plastic deformation and annealing.

In Chapter 3, a novel rolling process; cryogenic high-speed rolling (C-HSR) was proposed. The proposed rolling process where the specimen only cooled in liquid nitrogen are supplied to high-speed rolling with rolls at room temperature. The change in ln Z (Z: Zener-Hollomon parameter) was theoretically estimated through changes in temperature and strain rate during rolling. As a result, it was confirmed that the C-HSR could maintain a high ln Z even at a high rolling reduction. In the case of the specimen at cryogenic temperature and the rolls at room temperature, a high rolling speed (750 m/min) not only contributes to the improvement of ln Z, but also reduces the contact heat, so that a synergistic effect can be expected to reduce the temperature increasing due to less contact duration during C-HSR.

In Chapter 4, the cryogenic high-speed rolling (C-HSR) process enabled a simultaneous improvement in strength and electrical conductivity of Cu-5mass%Zn sheets. The low-speed rolled (LSR) sheet showed the tensile strength of 440/520MPa and electrical conductivity of 59/52%IACS after 60/80% rolling. On the other hand, the C-HSR showed improved properties

with 503/580MPa and 62/54%IACS, respectively. Deformation twins were most frequently formed in the C-HSRed specimen. The processed sheet showed the typical brass-type rolling texture. Heat balance showed only the C-HSR was able to keep the sheet temperature below the room temperature throughout the rolling process.

In Chapter 5, Cryogenic high-speed rolling (C-HSR) of the Cu- *x* Al (*x* = 3.1, 6.7 mass %, referred to as 3Al and 7Al, respectively) was carried out to investigate mechanical and electrical properties. C-HSR showed a more strengthening effect than LSR. 2-pass rolled (0.2% proof stress/tensile strength) were (568/665MPa) for Cu-3Al and (726/841MPa) for Cu-7Al with comparable elongation. C-HSR is more effective to the Cu-3Al with higher SFE in balance both of (strength – ductility) and (strength – conductivity). However, it is less sensitive in the case of Cu-7Al due to its extremely low SFE. For improvement of the balance by C-HSR, extra-low SFE Cu alloy is less effective. Yield strength and electrical conductivity were predicted using the modified Hall-Petch equation and modified MS model. The experimental results were in agreement; dislocation density, as well as grain boundaries and deformation twins, were contributed to yield strength; meanwhile, only dislocation density was dominant to increase electrical resistivity.

In Chapter 6, applications of cryogenic high-speed rolling for other materials were described

Summarizing these studies, the definition of proposed rolling, named cryogenic high-speed rolling (C-HSR), is the processing method in which only the sheet is only cooled in liquid nitrogen and supplied to high-speed rolling with rolls at room temperature. The low initial temperature (~100 K) and high strain rate (500 – 1500 s^{-1}) can realize the high Z ($\ln Z > 40$), leading to enable to change deformation mode, as shown in Fig. 7.1. C-HSR improved the balance of strength - conductivity and strength – elongation compared to the conventional cold-rolling, as shown in Fig. 7.2 and 7.3, respectively.

This research will expand the fundamental knowledge of the deformation behavior on Cu alloys with various ranges of SFEs, strain rate, and temperature. In addition, the microstructure evolution and its contribution to the mechanical and electrical properties were systemically described. Therefore, this thesis contributes establishment of metal forming technologies and

their industrial applications.

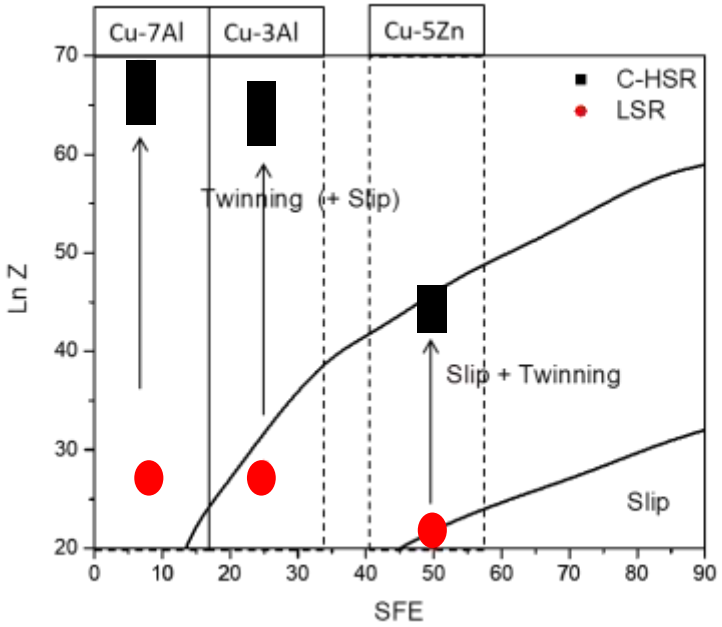

Fig. 7.1 The deformation mode map [7.1] in the SFE - ln Z (Zener-Hollomon) parameter space for the Cu alloys in this study. C-HSR means cryogenic high-speed rolling and LSR means conventional (low-speed) cold rolling

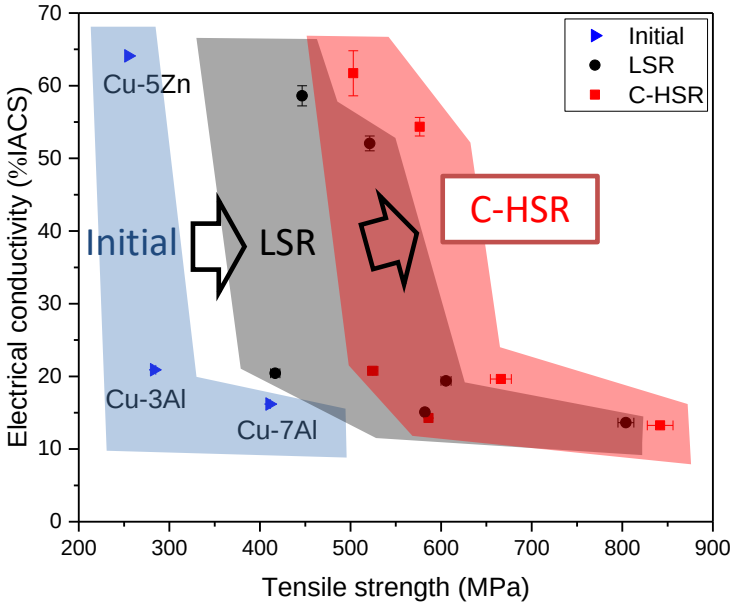

Fig. 7.2 Balance of tensile strength and electrical conductivity in various copper alloys. Initial : as-annealed, LSR : low-speed cold rolling, C-HSR : cryogenic high-speed rolling

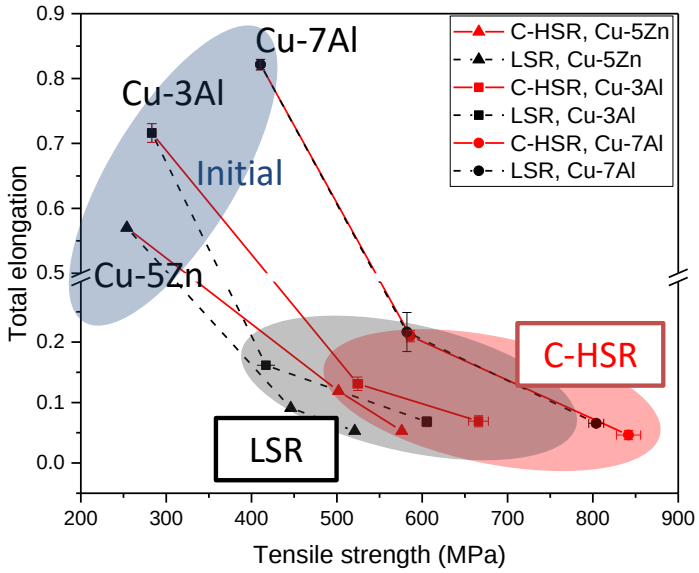

Fig. 7.2 Balance of tensile strength and total elongation in various copper alloys. Initial : as-annealed, LSR : low-speed cold rolling, C-HSR : cryogenic high-speed rolling

Reference

[7.1] Y. Zhang, N. R. Tao, and K. Lu, Acta Mater. 59 (2011) 6048-6058

Publications

Publications related to this thesis

1. Sangmin Lee, Yong-Deok Im, Ryo Matsumoto, and Hiroshi Utsunomiya
   Deformation twinning and change in mechanical properties of Cu-15at%Al in multi-pass cold rolling
   Material Science Forum, **941** (2018) 1523-1528

2. Sangmin Lee, Ryo Matsumoto, Hiroshi Utsunomiya, and Hidemichi Fujiwara
   Cryogenic high-speed rolling of Cu-5mass% Zn alloy sheet
   Journal of Japan Institute of Copper, **58** (2019) 52-57

3. Sangmin Lee, Yong-Deok Im, Ryo Matsumoto, and Hiroshi Utsunomiya
   Strength and electrical conductivity of Cu-Al alloy sheets by cryogenic high-speed rolling
   Material Science and Engineering A, (2020) (in press)

4. Ryunosuke Muchime, Sangmin Lee, Ryo Matsumoto, Hiroshi Utsunomiya, Kuniteru Mihara, and Hidemichi Fujiwara
   Influence of cryogenic high-speed rolling on tensile strength and electric conductivity of Cu-Ni-Si alloy sheet
   Journal of Japan Institute of Copper, **59** (2020) 213-218

5. Sangmin Lee, Ryunosuke Muchime, Ryo Matsumoto, and Hiroshi Utsunomiya
   Texture and mechanical properties of Cu alloys by cryogenic high-speed rolling
   IOP Conference, (2021) (to be submitted)

Other publications

1. Sang-Min Lee, Ji-Woon Lee, Hyun-Jin Choi, and Soong-Keun Hyun
   High temperature deformation and continuous dynamic recrystallization behavior of AA6082 using processing map
   Korean Journal of Metals and Materials, **54** (2016) 793-801

2. Youngkyu Kim, Gyeongwoo Kim, Jungsoo Park, Sangmin Lee, Dongjin Kim, and Kuk-hyun Song
   Implementation of exceptional microstructures and mechanical properties of structural carbon steel tubes by friction welding
   Journal of Manufacturing Processes, (2020) (under review)

3. Dongjin Kim, Sangmin Lee, Seung-Joon Lee, Shijo Nagao, Katsuraki Suganuma, and Chuantong Chen
   Cracking formation and fracture characteristics of a sintered porous Ag joint in a GaN device at different thermos-mechanical stresses during a thermal shock test
   (to be submitted)

4. S. Kaneko, S. Takeuchi, S. Lee, and H. Utsunomiya
   Evolution of mechanical properties and macro textures of AZ91D sheets by hot rolling and subsequent annealing
   IOP Conference, (2021) (to be submitted)

Acknowledgements

First of all, I would like to express my sincere appreciation to my advisor, *Dr. Hiroshi Utsunomiya*, Professor of Division of Materials and Manufacturing Science, in his continuous support, generous advice, encouragement, heartful guidance and abundant discussions during my years of graduate study at Osaka University.

The reader of this dissertation, *Dr. Hideki Araki*, Professor of Division of Materials and Manufacturing Science, and *Dr. Yuichiro Koizumi*, Professor of Division of Materials and Manufacturing Science, deserve sincere thanks for their careful and through review of the entire manuscript. Also, I wish to express my sincere gratitude to my Associate Professor *Ryo Matsumoto* for his continuous guidance, accurate criticism and encouragement during this research work.

I wish to great pay acknowledgement to *Dr. Hidemichi Fujiwara*, Chief Researcher in Furukawa Electric Co. Ltd., and *Dr. Yong-Deok Im*, Researcher in Hyundai Heavy Industries Co. Ltd., their helpful comments and valuable discussions for the work on this dissertation.

Special thanks are expressed to *Dr. Seung-Koon Hyun*, Professor of Inha University in Korea for his kind comments and supports for the work on this dissertation.

I would like to express my appreciation to *Mr. Jyoji Miyamoto*, Division of Materials and Manufacturing Science, for his kind discussion and advice. Thanks also to all members of Utsunomiya Lab. who are *Mr. Shugo Kameyama, Mr. Jinkan Kou, Mr. Shota Komaki, Mr. Shuhei Kondo, Mr. Tomohiro Uchibori, Mr. Takeshi Kayashima, Mr. Seiji Takatsuka, Mr. Masahiro Yamashita, Mr. Harutaka Sakaguchi, Mr. Sotaro Tanaka, Mr. Yohei Noguchi, Mr. Tomoya Fujimoto, Mr. Soichiro Maeda, Mr. Ryo Aizawa, Mr. Kazuki Takamoto, Mr. Kakeru Hashimoto, Mr. Ryohei Homi, Mr. Ryunosuke Muchime, Mr. Soichi Yamada, Mr. Toshifumi Yamamura, Mr. Yuji Iseka, Mr. Takashi Jinnouchi, Mr. Daisuke Taniguchi, Mr. Keisuke Tonomura, Mr. Yuma Mochizuki, Mr. Yuya Monda, Mr. Sosuke Yabuno, Mr. Yusaku Nakamura, Mr. Kota Ichikawa, Mr. Shusuke Kunisawa, Mr. Yoshimitsu Terada, Mr. Yohei Matsumoto, Mr. Tatsuya Motodamari, Mr. Ryuta Yamanishi, Mrs. Aiko Isonaga*, ex-secretary, and *Mrs. Mari Sasaki*, secretary for extending all the help. Among them, great

acknowledgement and thanks is given to *Mr. Dae-Jin Yoon* and *Dr. Woo-Young Kim* for kind support and advice.

Also, I would like to thank my friends at Osaka University, including *Dr. Seung-Joon Lee*, *Dr. Seung-Joon No*, *Dr. Dongjin Kim, Dr. Hyoseok Shi, Dr. Won-Rak Lee*, *Mr. Yong-Won Park, Mr. Sang-Kook Lee, Ms. Jungin Kim, Mr. Young-Joon Seo, Ms. Jae-Bong Yeon, Mr. Dong-Jo Kim, Mr. Sung-Cheol Kim, Mr. Young-Suk Im, Mr. Byeongho Park, Mr. Yonghyun Park, Mr. Hyun-Soo Park, Mr. Kyong-Tae Kim, Mr. Gi-Tack Jung, Mr. In-Sung Choi, Mr. Won-Joon Lee, Ms. Soo-Yeon Jung, Mr. Yeon-Bin Choi, Mr. Jae-Young Choi, Mr. Saso Dolinsek, and Mr. Kazuki Tanaka,* for their kind support and encouragement.

I am deeply appreciated to childhood friends of mine in Korea, especially to *Dr. Seung-Hoon Hong*, and *Mr. Moon-Young Bae*, for helpful advice and encouragement,

Finally, I greatly appreciate the patience of my family, especially my parents, my father *Song-Woo Lee*, my mother *Kyung-Mi Ko*, and my sister *Da-Young Lee*, for endure me during the completion of this dissertation. This thesis could not have been able to successfully complete without their dedication and sacrifice.

Sangmin Lee

2020